NASA/TM–2006–214145

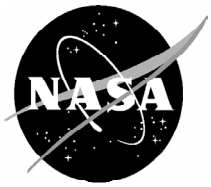

Remote Versus Local Forcing of Chlorophyll Variability in the South Atlantic Bight

Sergio R. Signorini and Charles R. McClain

December 2006

The NASA STI Program Office … in Profile

Since its founding, NASA has been dedicated to the advancement of aeronautics and space science. The NASA Scientific and Technical Information (STI) Program Office plays a key part in helping NASA maintain this important role.

The NASA STI Program Office is operated by Langley Research Center, the lead center for NASA's scientific and technical information. The NASA STI Program Office provides access to the NASA STI Database, the largest collection of aeronautical and space science STI in the world. The Program Office is also NASA's institutional mechanism for disseminating the results of its research and development activities. These results are published by NASA in the NASA STI Report Series, which includes the following report types:

- TECHNICAL PUBLICATION. Reports of completed research or a major significant phase of research that present the results of NASA programs and include extensive data or theoretical analysis. Includes compilations of significant scientific and technical data and information deemed to be of continuing reference value. NASA's counterpart of peer-reviewed formal professional papers but has less stringent limitations on manuscript length and extent of graphic presentations.
- TECHNICAL MEMORANDUM. Scientific and technical findings that are preliminary or of specialized interest, e.g., quick release reports, working papers, and bibliographies that contain minimal annotation. Does not contain extensive analysis.
- CONTRACTOR REPORT. Scientific and technical findings by NASA-sponsored contractors and grantees.
- CONFERENCE PUBLICATION. Collected papers from scientific and technical conferences, symposia, seminars, or other meetings sponsored or cosponsored by NASA.
- SPECIAL PUBLICATION. Scientific, technical, or historical information from NASA programs, projects, and mission, often concerned with subjects having substantial public interest.
- TECHNICAL TRANSLATION. English-language translations of foreign scientific and technical material pertinent to NASA's mission.

Specialized services that complement the STI Program Office's diverse offerings include creating custom thesauri, building customized databases, organizing and publishing research results . . . even providing videos.

For more information about the NASA STI Program Office, see the following:

- Access the NASA STI Program Home Page at http://www.sti.nasa.gov/STI-homepage.html
- E-mail your question via the Internet to help@sti.nasa.gov
- Fax your question to the NASA Access Help Desk at (301) 621-0134
- Telephone the NASA Access Help Desk at (301) 621-0390
- Write to:
  NASA Access Help Desk
  NASA Center for AeroSpace Information
  7115 Standard Drive
  Hanover, MD 21076–1320

NASA/TM–2006–214145

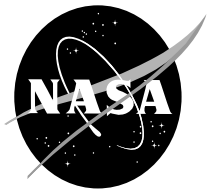

Remote Versus Local Forcing of Chlorophyll Variability in the South Atlantic Bight

Sergio R. Signorini
Science Applications International Corporation, Beltsville, Maryland

Charles R. McClain
NASA Goddard Space Flight Center, Greenbelt, Maryland

National Aeronautics and
Space Administration

Goddard Space Flight Center
Greenbelt, Maryland 20771

December 2006

Available from:

NASA Center for AeroSpace Information
7115 Standard Drive
Hanover, MD 21076–1320

National Technical Information Service
5285 Port Royal Road
Springfield, VA 22161

Table of Contents

Acknowledgments

This work was supported under a NASA Research Announcement 03-OES-03, Interdisciplinary Science in the NASA Earth Science Enterprise. The proposal title is "Eastern U.S. Continental Shelf Carbon Budget Modeling, Data Assimilation, and Analysis", Eileen Hofmann, Principal Investigator. We are thankful to Antonio Mannino for insightful comments and suggestions.

PROLOGUE

This TM documents results of analyses addressing the local versus remote forcing of chlorophyll variability on the shelf and slope regions of the South Atlantic Bight (SAB) based on satellite-derived products and a limited amount of in situ data. This study is part of a larger multi-disciplinary, multi-institutional effort to study the Eastern U.S. Continental Shelf carbon budget (U.S. Eastern Continental Shelf Carbon Budget: Modeling, Data Assimilation, and Analysis, U.S. ECoS), a project funded by the NASA Earth System Enterprise Interdisciplinary Science Program that started in the summer 2004. The SAB encompasses processes that bridge the gap between estuaries and the coastal ocean through exchanges of suspended and dissolved materials via river runoff, shelf circulation, and Gulf Stream variability.

Relatively high concentrations of chlorophyll-a (Chl-a) are observed on the inner and middle shelves throughout the year. North of 33^{o}N the highest nearshore chlorophyll concentrations are near the capes (Romain, Fear, and Lookout), in great part due to topographically enhanced wind-driven upwelling, but also due to point source coastal river discharge. South of that latitude the estuaries are marsh-dominated and the river discharges have a more diffuse effect on the nutrient loading and resulting chlorophyll concentrations.

There is a connection between the North Atlantic Subtropical Gyre (NASG) variability and the SAB shelf response via Gulf Stream forcing, which is the western branch of the NASG. The size and strength of the NASG, which is governed by the large-scale wind circulation and seasonal solar radiation, has an impact on the oceanographic processes of the SAB as a result of Gulf Stream onshore/offshore motion. The evolution of the Gulf Stream eastward deflection and the formation of the Charleston Gyre were analyzed using sea surface temperature, chlorophyll, and surface currents.

SeaWiFS-derived images of Chromophoric Dissolved Organic Material (CDOM) absorption coefficient were used to trace the riverine sources of DOM and the low salinity front on the inner and middle shelves, which are consistent with historical data. Long-term (9 years) upward trends in chlorophyll were found in the middle shelf, consistent with downward trends in salinity and upward trends in river discharge. Seasonal and episodic variations in heat flux have an impact on chlorophyll variability because they drive changes in vertical mixing and consequently nutrient renewal. Time series analysis of chlorophyll and surface heat flux show a strong seasonal anti-phase correlation in the SAB middle shelf.

1. Introduction

The physical and biological processes of the South Atlantic Bight (SAB) have been comprehensively studied in the past. Examples of these studies were published in the Coastal and Estuarine Sciences series [*Atkinson et al.*, 1985], and the special issue of the *Journal of Geophysical Research* [*J. Geophys. Res*., *88*, C8, May 30, 1983] which contain a collection of papers addressing the oceanography of the SAB and adjacent Gulf Stream based on *in situ* data analyses and numerical models. The SAB encompasses processes that bridge the gap between estuaries and the coastal ocean through exchanges of suspended and dissolved materials via river runoff, shelf circulation, and Gulf Stream variability [*Menzel*, 1993]. The complexity of the SAB circulation is shown in the seasonal surface current maps in Figure1. The currents were derived from the sum of Aviso geostrophic components and Ekman drift, as it will be described in subsection 2.2. The shelf surface currents depicted in Figure 1 are in agreement with the characterization of the seasonal mean circulation described in previous studies [*Lee et al.*, 1991].

The SAB has been the topic of a number of ocean color satellite analyses investigating processes ranging from specific events to interannual variability. Early studies of specific events used data from the Coastal Zone Color Scanner and were focused on Gulf Stream frontal eddies [*McClain*, 1985; *McClain et al.*, 1990; *McClain et al.*, 1984; *Yoder et al.*, 1981b]. The CZCS coverage was frequent enough in these cases to observe the propagation of these rapidly moving events which were difficult to map from ships. The high pigment concentrations in the cold cores of the eddies in contrast to the low concentrations of the Gulf Stream and the adjacent outer shelf waters make identification of the features straightforward even though the structures are fairly complex. The *in situ* versus satellite comparison of the absolute concentrations across one such eddy showed excellent agreement over a range of 0.1 to 8 mg/m^3. This was one of the first validations that quantitative pigment concentrations could be derived from a satellite sensor [*McClain et al.*, 1984]. Similarly, *McClain and Atkinson* [1985] showed an unusually clear manifestation of the Charleston Gyre using a CZCS pigment concentration image. More recently, *Li et al.* [2003] used MODIS data to describe a cross-shelf coastal water transport event in the Georgia Bight.

Aside from event scale phenomena, the CZCS data was used to describe the spatial and temporal distribution of pigments over seasonal [*McClain et al.*, 1988] and interannual timeframes [*Martins and Pelegri*, 2006; *Yoder et al.*, 2001]. *McClain et al.* [1988] `focused on time series of pigments and ancillary data, such as coastal winds and river discharge, to examine correlations between physical and biological processes using a one-year time series of SAB coverage. Seasonal pigment difference maps implied routes of coastal water transport offshore of Capes Fear and Romain. *Martins and Pelegrí* [2006] noted a mission-long decrease in October-May pigment concentrations throughout the

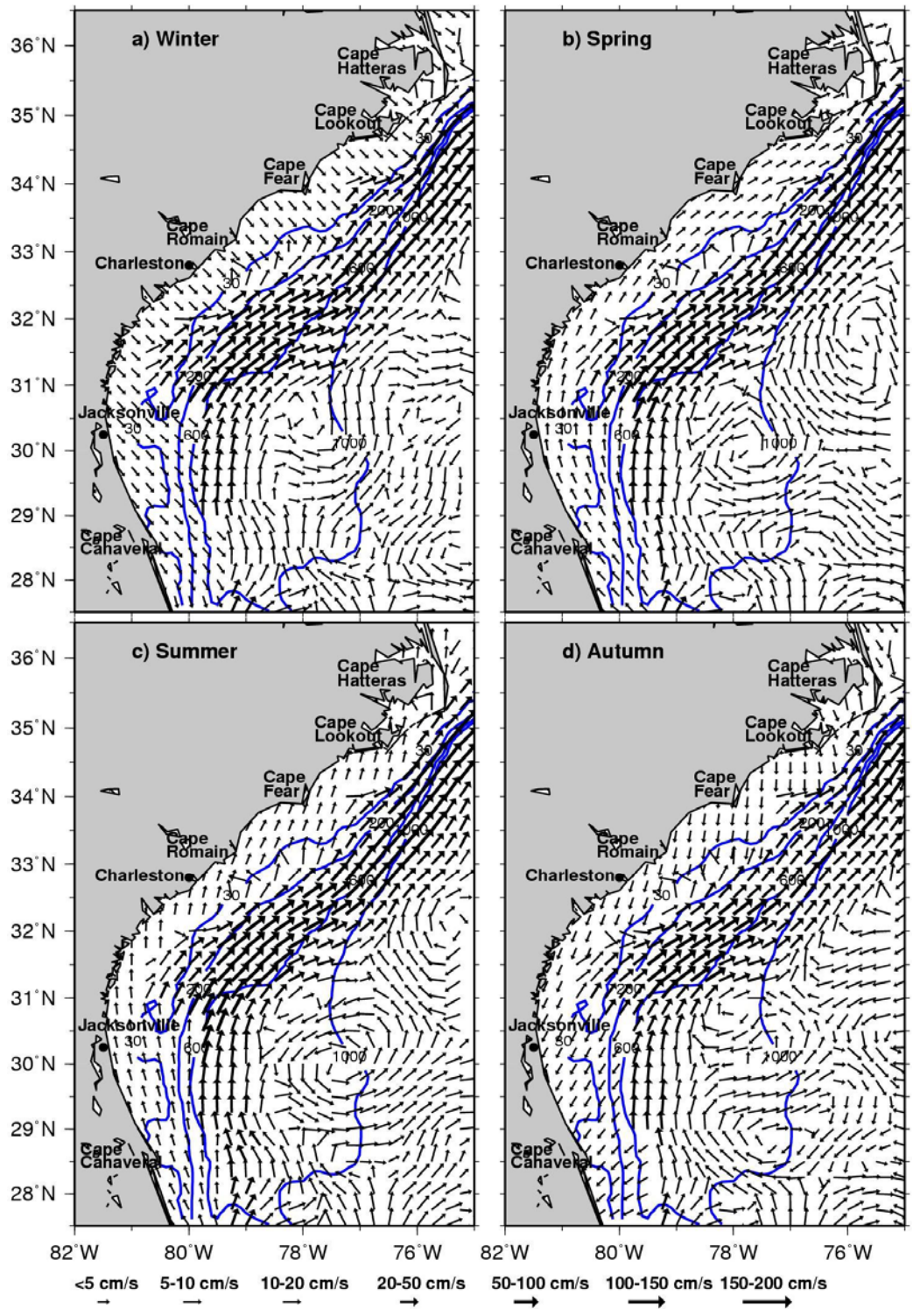

Figure 1. South Atlantic Bight seasonal surface currents derived from the sum of Aviso geostrophic components and Ekman drift.

SAB of nearly 50%, although no validation data was presented to support this result. *Yoder et al.* [2001] reported no significant trends in the CZCS time series

of SAB pigment concentrations. Finally, *Yoder et al.* [1987] and *Martins and Pelegrí* [2006] used the CZCS data to examine spatial scales of pigment variability for various regimes across and along the shelf using the variogram analysis method, while *Yoder et al.* [2001] used the same technique to determine temporal time scales.

For the purposes of study and definition, the continental shelf of the SAB has been regionally divided by the bathymetry as inner shelf (0–20m), middle shelf (20–40m), and outer shelf (40–60m) [*Menzel*, 1993]. The inner shelf is influenced by a multi-inlet coastline connecting low-lying coastal marshes to the ocean. The circulation is influenced by river discharge [*Blanton and Atkinson*, 1983; *Kourafalou et al.*, 1996], tides [*Pietrafesa et al.*, 1985], and winds [*Blanton et al.*, 1989]. Tidal transport and mixing provide two-way exchange of materials between estuaries and the ocean. The chlorophyll *a* (Chl-a) concentrations range from 1 to 25 mg m^{-3} [*Hanson et al.*, 1990; *Jacobsen et al.*, 1983; *Yoder et al.*, 1981b; *Yoder et al.*, 1987] and reflect a decreasing abundance of phytoplankton in the seaward direction. Production is driven primarily by the rates at which nutrients are recycled and/or re-suspended from the sediments. The circulation on the middle and outer shelf regions is highly variable due to the combined influence of tides , winds [*Blanton et al.*, 1985], and Gulf Stream intrusions [*Atkinson*, 1977; *Atkinson et al.*, 1978; *Blanton et al.*, 1981]. Subsurface intrusions of North Atlantic Central Water (NACW) occur mostly from May to August [*Yoder et al.*, 1985]. In addition, there is more event-scale variability in plankton abundance and production than in the inner shelf. Plankton densities may change 10-fold or more within days [*Yoder et al.*, 1985]. Excursions of the Gulf Stream on and off the outer shelf and slope are largely driven by the seasonal variability of the North Atlantic Subtropical Gyre (NASG), which expands in the summer and contracts in the winter (see Figure 6).

Plankton productivity is highly affected by upwelling and onshore movement of nutrients driven by excursions of the Gulf Stream front [*Lee and Atkinson*, 1983; *Lee et al.*, 1981; *Martins and Pelegri*, 2006; *McClain et al.*, 1990]. These upwelling events, also called Gulf Stream intrusions, occur mostly during the summer and are the major processes affecting rates and dynamics of outer shelf and slope (40 to 200m isobaths) primary production [*Atkinson et al.*, 1978; *Bishop et al.*, 1980; *Dunstan and Atkinson*, 1976; *Pomeroy et al.*, 1983; *Yoder*, 1985; *Yoder et al.*, 1983; *Yoder et al.*, 1981a]. Cyclonic, cold core eddies, which are embedded in the Gulf Stream front, also provide a mechanism for the SAB shelf nutrient renewal [*McClain et al.*, 1990; *McClain et al.*, 1984; *Yoder et al.*, 1981b], but mostly affect the shelf break having a lesser impact than the subsurface Gulf Stream summer intrusions. Although Gulf Stream intrusions may not occur every summer, when they occur they are by far the most important processes controlling summer phytoplankton dynamics of the middle and outer shelf and of the inner shelf in the southern half of the study area [*Yoder*, 1985]. However, the intense episodic phytoplankton blooms driven by the nutrient-rich waters of the Gulf Stream summer sub-surface intrusions are not captured by the satellite Chl-a images as they lie mostly below the penetration depth (Z_{90}) of

ocean color sensors. Therefore, only the somewhat weaker manifestation of these sub-surface intrusions within the Z_{90} is captured by our analyses.

This study focuses on the relative influence of local versus remote forcing on the seasonal and interannual variability of Chl-a in the SAB based on satellite-derived products and a limited amount of in situ data. The major source of data for this study is the 9-year ocean color time series originating from the **Sea**-viewing **Wi**de **F**ield-of-view **S**ensor (SeaWiFS). It will be shown that local forcing is determined by river discharge, heat flux and winds, while remote forcing is primarily governed by the size and strength of the North Atlantic Subtropical Gyre (NASG) via Gulf Stream excursions on the shelf break.

2. Data and Methods

2.1 Satellite Data

Satellite-derived data were highly useful in our investigations of the relative importance of local versus remote physical forcing responsible for the observed Chl-a variability on the SAB shelf and slope regions. Data analyzed included a time series of sea surface height anomaly (SSHA) from Topex/Poseidon, sea surface temperature (SST) from AVHRR, and chlorophyll-a (Chl-a) derived from SeaWiFS.

Our analyses were based on SeaWiFS-derived SMI 9-km and MLAC 1-km Chl-a, one-degree Pathfinder SSHA and 4-km AVHRR SST, NOAA CoastWatch 1-km AVHRR SST, and Aviso absolute dynamic topography (ADT). The ADT 1/3^o grids were produced by Ssalto/Duacs and distributed by Aviso with support from CNES.

MODIS/Aqua SST LAC (4 μ-nighttime) and SeaWiFS MLAC Chl-a 1-km resolution cutouts for the SAB were used in conjunction with satellite-derived currents to produce composites of SST and Chl-a with surface currents superimposed. SeaWiFS MLAC data were also used to derive Chl-a and absorption coefficient by colored detrital material (CDOM plus non-living particulate organic matter) at 443nm ($a_{CDM}(443)$) using the Garver-Siegel-Maritorena 2001 [*Garver and Siegel*, 1997; *Maritorena et al.*, 2002] semi-analytical algorithm (GSM01).

2.2 Surface Currents

The surface currents were produced using Aviso geostrophic currents combined with wind driven flow obtained with a simple finite depth analytical Ekman model using QuikScat winds. Our wind and current direction convention is the direction the wind/current is blowing/flowing to. Thus, the east (u) and north (v) components of the surface currents can be written as

$$\begin{aligned} u &= u_g + u_E \\ v &= v_g + v_E \end{aligned} \qquad (1)$$

where u_g and v_g are the Aviso geostrophic components and u_E and v_E are the wind-driven (Ekman) components of the surface current.

The Aviso geostrophic currents are based on the balance between the dynamic height gradient and the Coriolis force and are given by

$$u_g = -\frac{g}{f}\frac{\partial \mathrm{DHT}}{\partial y}$$
$$v_g = +\frac{g}{f}\frac{\partial \mathrm{DHT}}{\partial x} \qquad (2)$$

where g is the acceleration due to gravity, DHT is the dynamic height (cm), and f (s^{-1}) is the Coriolis parameter. The 7-day variability of DHT is obtained by combining the 7-day/1/3° sea level anomaly (SLA), obtained from the blending of TOPEX/POSEIDON, ERS-1, ERS-2, and Jason-1 altimeter data, and a mean dynamic topography (MDT). The MDT is obtained through a multi step process [*Rio and Hernandez*, 2004; *Rio et al.*, 2005] that merges the averaged altimetric heights over 1993-1999 (mean sea surface, MSS) with Levitus climatology data [*Levitus and Boyer*, 1994; *Levitus et al.*, 1994]. The Levitus climatology provides realistic ocean circulation patterns where data are available (at low and mid latitudes), but rather poor quality at high latitudes. First, the MDT is computed using Levitus climatology dynamic heights to 1500 dbar, and extended toward the coast. Then the merging is performed by weighting the two surfaces (MSS and Levitus MDT): full contribution of the Levitus climatology at low and mid latitudes, then increasing the MSS contribution toward the poles.

The wind-driven, or Ekman, components of the surface currents are obtained using the Ekman solution for a finite depth (H) ocean [*Neumann and Pierson*, 1966] as follows:

$$u_E = S_{ox}\cos\alpha - S_{oy}\sin\alpha$$
$$v_E = S_{ox}\sin\alpha + S_{oy}\cos\alpha \qquad (3)$$

The surface speed (S_o) components and the turning angle (α) are obtained from

$$S_{o,x,y} = \frac{\tau_{x,y}}{\left(\rho_w \left| f \right| A_z\right)} \qquad (4)$$

$$\alpha = arc\tan\left[\frac{\sinh a - \sin a}{\sinh a + \sin a}\right] \qquad (5)$$

where $\tau_{x,y}$ are the east and north components of the wind stress (dynes cm^{-2}), ρ_w is the water density (g cm^{-3}), A_z is the vertical eddy coefficient of viscosity (g cm^{-1} s^{-1}), and $a=2\pi h/D$ with D being the critical depth and $h=\min(H,D)$. The critical Ekman depth is given by

$$D = \pi\left(\frac{2A_z}{\rho_w f}\right) \tag{6}$$

The vertical eddy coefficient of viscosity is assumed to be a function of wind speed [*McLellan*, 1968] such that

$$\begin{aligned} A_z &= 1.02W^3 \text{ for } W \le 6\ m/s \\ A_z &= 4.3W^2 \text{ for } W > 6\ m/s \end{aligned} \tag{7}$$

2.3 Ancillary Data Sets

The river discharge data originated from the United States Geological Survey (USGS). The daily Florida Current transport originated from NOAA-AOML (http://www.aoml.noaa.gov/phod/floridacurrent/background.php). The data were obtained using voltage data of the submarine cable from South Florida to Grand Bahama Island.

Hydrographic and biogeochemical data from a Georgia Bight transect occupied during four cruises in 1973-1974 were digitized from data reports [*Atkinson*, 1975; *Atkinson*, 1976] and analyzed in this TM. We also used monthly mixed layer climatologic data (NODC_WOA94) provided by the NOAA/OAR/ESRL PSD, Boulder, Colorado, USA, from their web site at http://www.cdc.noaa.gov/.

The surface heat flux originated from the **O**bjectively **A**nalyzed Air-Sea **Flux**es (OAFlux) data set from the Global Oceans site via ftp from http://oaflux.whoi.edu/, which is located at the Woods Hole Oceanographic Institution (WHOI).

2.4 Cross-Wavelet Analysis

Cross-correlation analyses in time and frequency were performed using cross wavelet transform (XWT) and wavelet coherence (WTC) methods [*Grinsted et al.*, 2004]. This method is superior to the traditional Fourier analysis because it expands time series into time frequency space and can therefore find localized intermittent periodicities. There are two classes of wavelet transforms; the Continuous Wavelet Transform (CWT) and the Discrete Wavelet Transform (DWT). The DWT is a compact representation of the data and it is particularly useful for noise reduction and data compression, whereas the CWT is better suited for feature extraction processes. Here we used the CWT as we are interested in extracting low signal/noise ratio signals in time series. A MatLab software package by *Grinsted et al.* [2004] was obtained from

http://www.pol.ac.uk/home/research/waveletcoherence/ to perform the XWT analyses.

3. Discussion

3.1 Seasonal Variability of Chl-a and SST

The seasonal (quarterly) variability of Chl-a (September 1997−September 2004) and SST (September 1997−December 2004) derived from SeaWiFS and NOAA CoastWatch AVHRR 1-km resolution data are shown in Figures 2 and 3, respectively. Chl-a concentrations decrease offshore from nearly 10 mg m^{-3} in the nearshore areas to less than 0.1 mg m^{-3} in water deeper than 500m. The inner shelf Chl-a is highest on the inner shelf during winter-spring when nutrient concentration increases as a result of elevated river discharge. Chl-a concentrations were derived using the empirical band-ratio OC4v4 algorithm [*Signorini and McClain*, 2005]. Based on the application of a semi-analytical algorithm, it will be shown later in this paper that the nearshore Chl-a concentration derived with the OC4v4 algorithm may have been biased high due to the presence of dissolved organic matter of fluvial origin.

Relatively high concentrations of Chl-a are observed on the inner and middle shelves throughout the year. North of 33°N the highest nearshore Chl-a concentrations are near the capes (Romain, Fear, and Lookout), in great part due to topographically enhanced wind-driven upwelling [*Blanton et al.*, 1981], but also due to point source coastal discharge such as the Cape Fear River mouth. South of that latitude the estuaries are marsh-dominated and the river discharges, including those from the Savannah River and Altamaha River, have a more diffuse effect on the nutrient loading and resulting Chl-a concentrations. There is also Chl-a enhancement on the middle and outer shelves as a result of nutrient 'pumping' from Gulf Stream meanders, cold-core eddies, intrusions, and filaments, but these occur in scales much shorter than seasonal. However, Gulf Stream sub-surface intrusions occur more often in summer [*Yoder et al.*, 1985].

The SST seasonal cooling/warming of the SAB shelf waters is clearly seen in Figure 3. The shallowest waters of the inner shelf cool faster in winter than the adjacent, deeper offshore waters giving rise to cross-shelf temperature contrasts [*Oey*, 1986; *Oey et al.*, 1987]. This rapid winter cooling is performed via convective overturning, and tidal and wind mixing. These waters exhibit the coolest SSTs (~10°C) towards the north in response to a decrease in solar radiation. The influence of the warmer Gulf Stream waters is clearly seen, especially during autumn through spring when the SST contrast is highest. The warmest SST (>28°C) is observed in summer offshore of the 60m isobath due to Gulf Stream northward transport of heat and local increase in solar radiation. The shallower mixed layer depths associated with these warmer temperatures result in higher vertical stratification and a corresponding decrease in surface Chl-a as shown in Figure 2.

Figures 4 and 5 show the Chl-a and SST seasonal anomalies, respectively. These were obtained by removing the yearly mean from the seasonal composites of Figures 2 and 3 and are expressed as relative percent

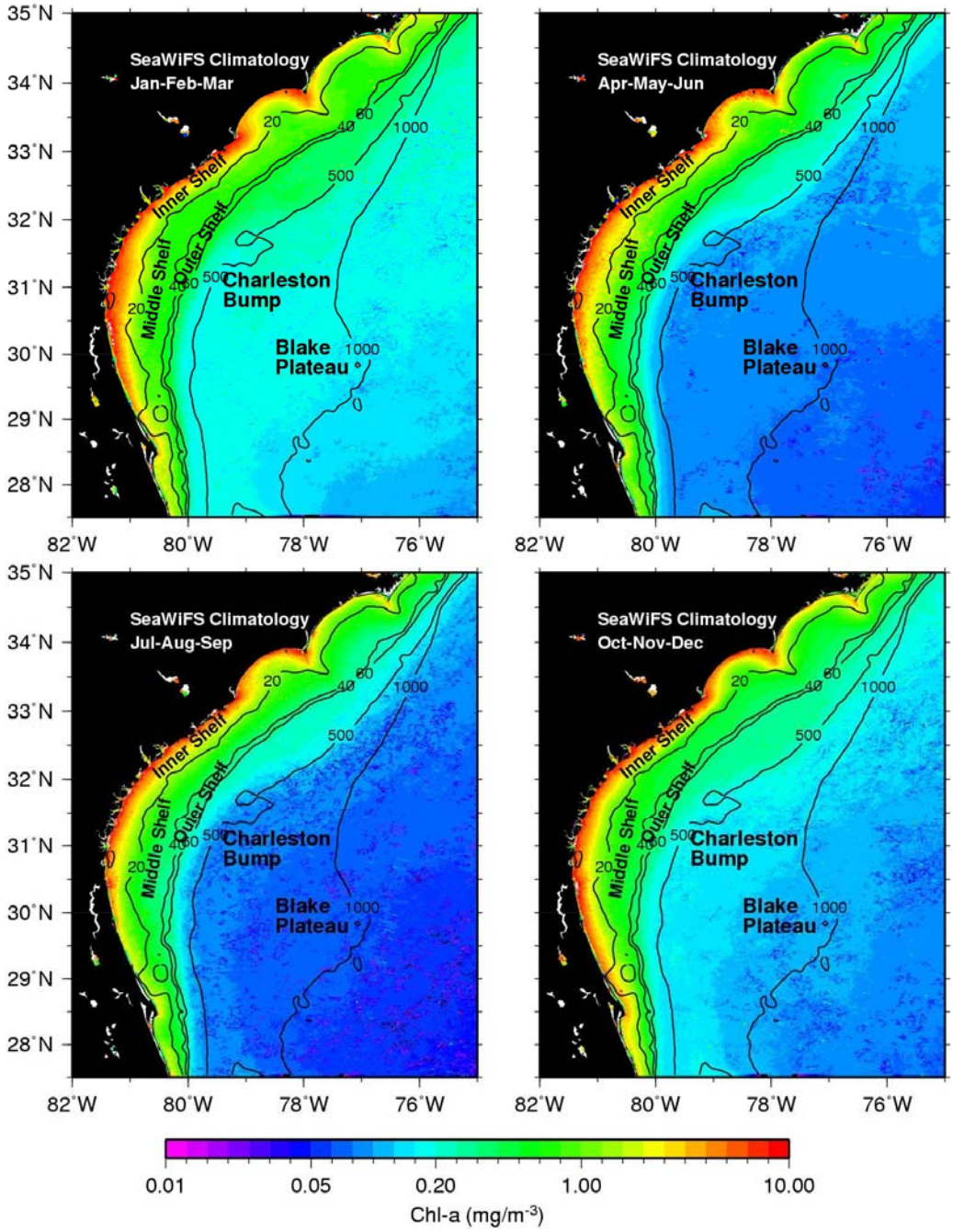

Figure 2. Seasonal maps of SeaWiFS-derived Chl-a for the South Atlantic Bight. The shelf region is divided according to the bathymetry into inner (0-20m), middle (20-40m), and outer (40-60m) shelves.

differences (RPD=100(season-year)/year). The RPD form of the images shown in Figures 4 and 5 emphasizes the seasonal cycle and regional differences within a given season. An interesting regional pattern emerges from the seasonal

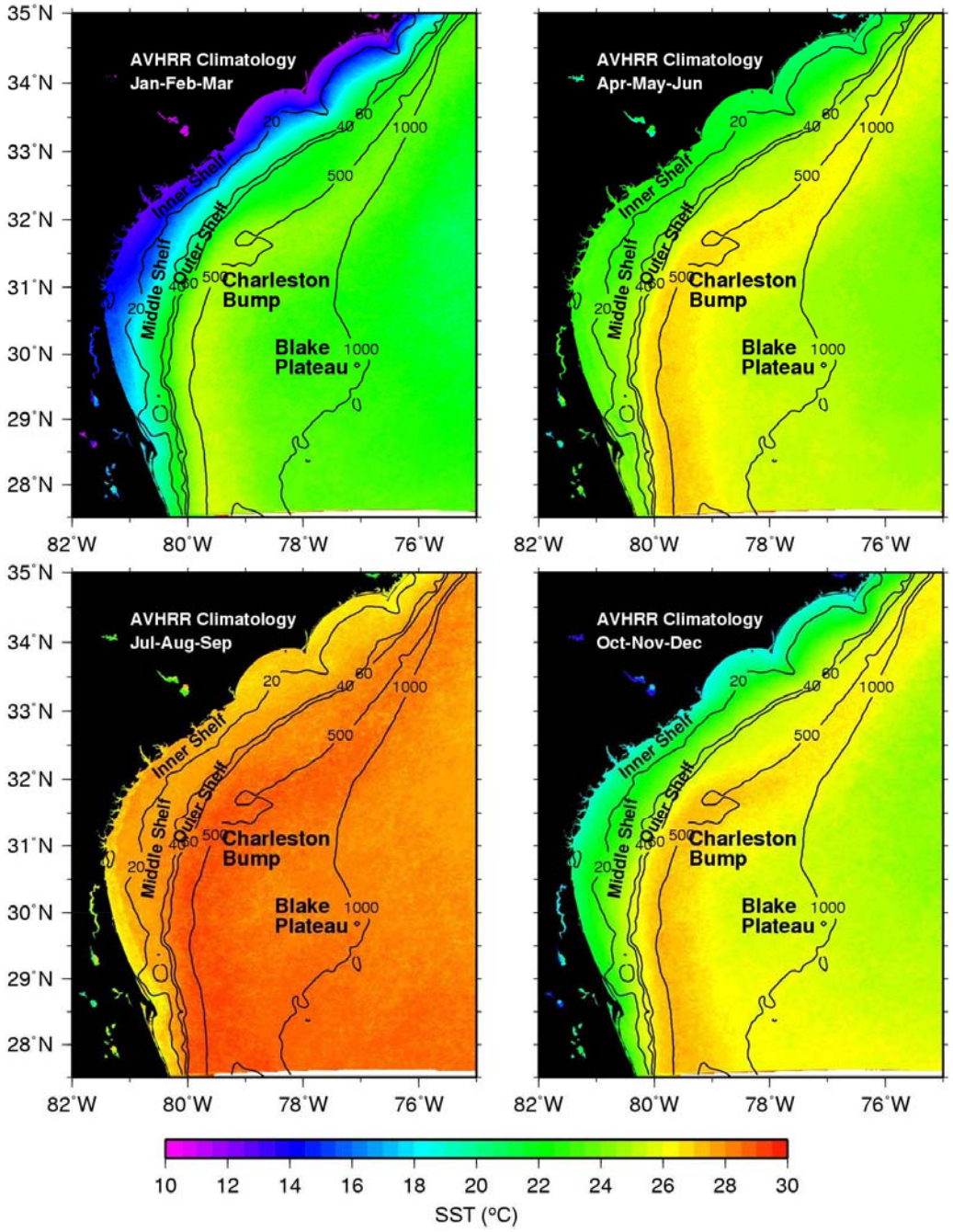

Figure 3. Seasonal maps of AVHRR-derived SST for the South Atlantic Bight. The shelf region is divided according to the bathymetry into inner (0-20m), middle (20-40m), and outer (40-60m) shelves.

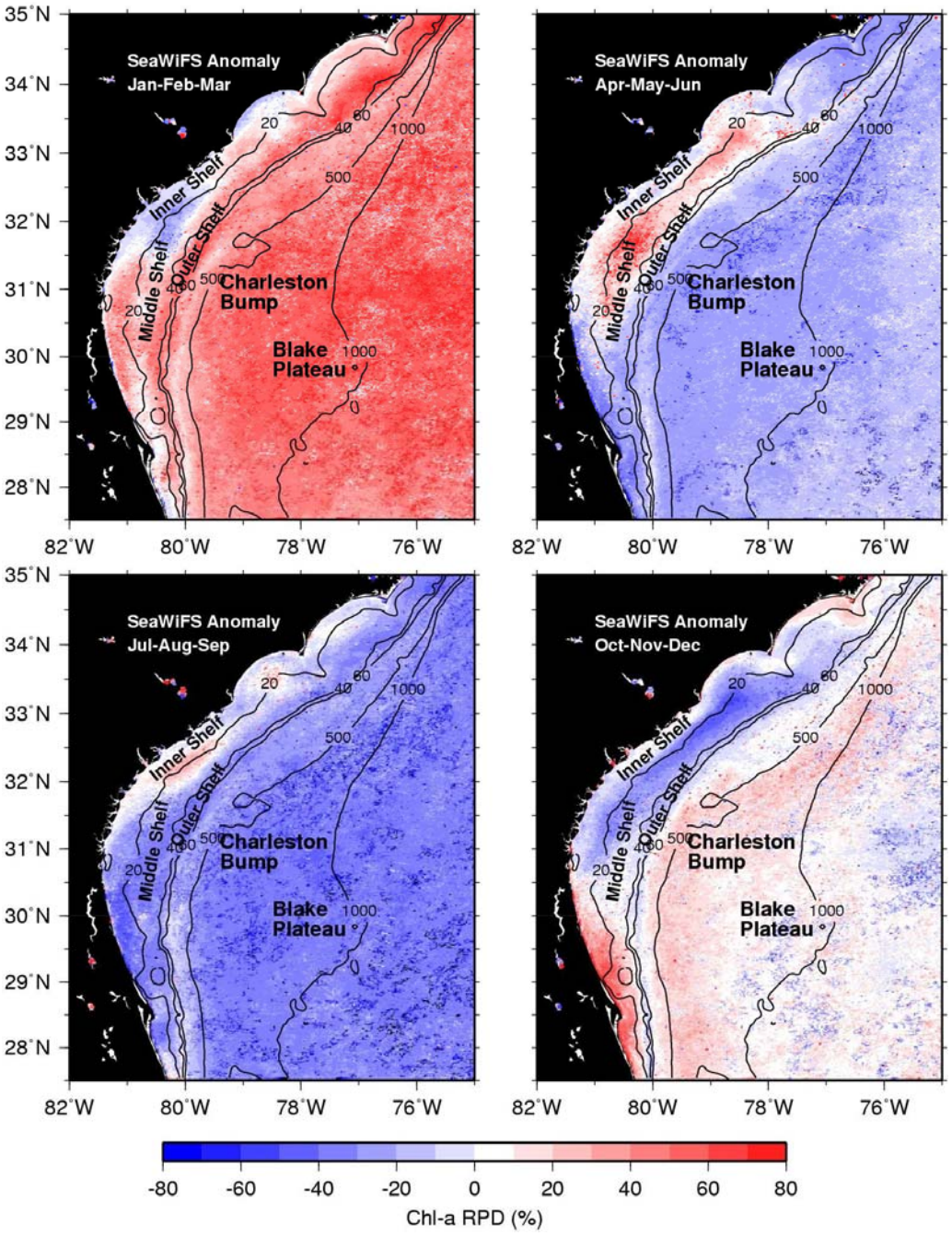

Figure 4. Seasonal maps of SeaWiFS-derived Chl-a anomaly (in relative percent difference, RPD) for the South Atlantic Bight. The shelf region is divided according to the bathymetry into inner (0-20m), middle (20-40m), and outer (40-60m) shelves.

images of Chl-a in Figure 4. First, the peak-to-peak seasonal cycle is clearly shown within ±60% of the variability between winter (high) and summer (low) and with large spatial coherence, most probably related to vertical mixing seasonal

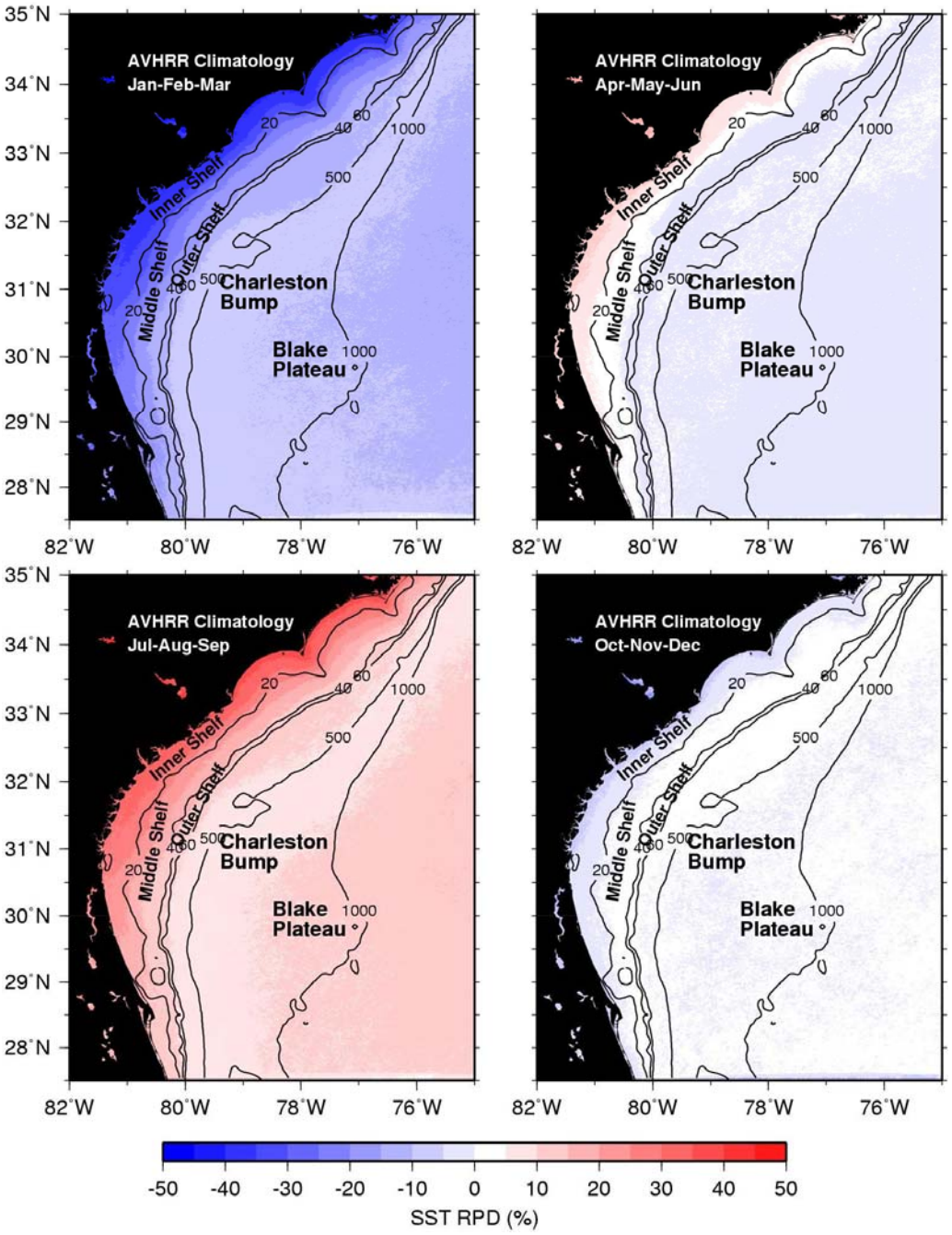

Figure 5. Seasonal maps of AVHRR-derived SST anomaly (in relative percent difference, RPD) for the South Atlantic Bight. The shelf region is divided according to the bathymetry into inner (0-20m), middle (20-40m), and outer (40-60m) shelves.

changes. The anomaly distributions during spring and autumn are much less spatially coherent over the shelf region. There is a distinct reversal in the sign of the anomaly near 30.5°N. North of 30.5°N there is a positive Chl-a anomaly in spring which is mostly confined to the middle shelf, while south of 30.5°N the anomaly is reversed and mostly confined to the inner shelf. During autumn the pattern is reversed.

The bimodal pattern in the Chl-a seasonal anomaly distribution in spring and autumn does not have a counterpart in the SST seasonal anomaly shown in Figure 5. Also note the change in the RPD scale for SST, ±20% as opposed to ±60% for Chl-a, meaning that seasonal changes in Chl-a are about 3 times larger than SST. The largest SST seasonal changes occur on the inner and middle shelves. SST warming in spring, and SST cooling in autumn, starts first in the shallower regions of the inner shelf.

It will be shown later that the bimodal pattern in the Chl-a seasonal anomaly distribution is also observed in the correlation between dynamic height and Chl-a, an indication that the Gulf Stream forcing has opposite effects on the Chl-a concentration north and south of 30.5^{o}N in the SAB.

3.2 Large Scale Forcing

Here we emphasize the large scale effect of the seasonal variability of the North Atlantic Subtropical Gyre (NASG) on the shelf and slope regions of the SAB. The connection between the NASG variability and the SAB shelf response is the Gulf Stream forcing, which is the western branch of the NASG. Therefore, the size and strength of the NASG, which is governed by the large-scale wind circulation and seasonal solar radiation, has an impact on the oceanographic processes of the SAB.

The size of the NASG was calculated from the ratio between the total number of Chl-a pixels with concentration less than 0.07 mg/m^3 to the total number of pixels inside a polygon delimiting the gyre domain (Figure 6a). This ratio is an indicator for the expansion and contraction of the oligotrophic region of the gyre and thus its size and strength [*McClain et al.*, 2004]. Figure 6a shows that the NASG is largest in the summer and smallest in winter, as indicated by the size of the oligotrophic region within the gyre. The variability is in phase with the seasonal variability of the MLD, as shown by its seasonal mean values in Figure 6a. The mean MLD values were calculated for the domain inside the polygon. They are 109, 37, 20, and 53 meters for winter, spring, summer, and autumn, respectively. The shape and size of the polygon was chosen in such a way to minimize coastal influence and contain the expansion of the chosen contour. The 0.07 mg/m^3 value was chosen to provide a closed contour throughout the seasons.

The seasonal composites of Aviso dynamic height (DHT) for the same North Atlantic region are shown in Figure 6b. The seasonality of the DHT within the gyre indicates a contraction in winter and an expansion in summer, in phase with the size variability of the oligotrophic region inside the gyre. The common forcing factor in the Chl-a, DHT, and MLD variability within the gyre is the seasonal change in surface thermal forcing. The warming of surface waters promotes shallower mixed layers, higher DHT resulting from elevated sea level height (SLH), and lower Chl-a due to reduced vertical mixing. The opposite happens during the winter cooling period. The seasonal variability of the size of the oligotrophic region (size of the NASG), the climatologic seasonal MLD, SST,

and DHT are plotted for the period of 1998-2005 in Figure 7a. Note that DHT, SST, and the size of the NASG are all in phase (within ~1 month of each other),

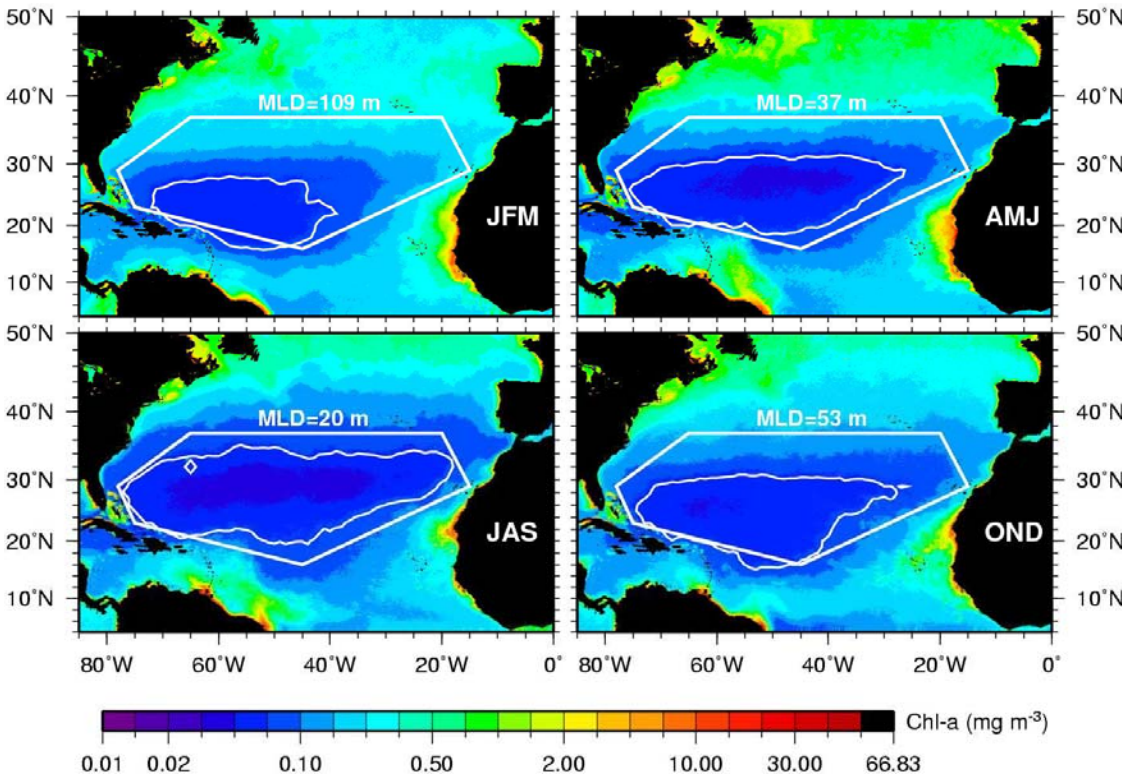

Figure 6a. Seasonal composites of SeaWiFS-derived Chl-a. The white polygon delimits the control area of the NASG. The white contours are 0.07 mg m^{-3} Chl-a contours and the mean MLD inside the polygon is shown for each season.

while the MLD is ~180^{o} out of phase. The effect of surface thermal forcing on DHT is clearly shown in the DHT vs. SST regression (r^2=0.94) in Figure 7b. The SST time series was shifted forward by one month before the regression was made as the peak SST leads the peak DHT by ~1 month, presumably the time scale required for the NASG to respond to the thermal forcing. The regression in Figure 7b indicates that an increase of ~1^{o}C is required to raise the DHT by 2 cm.

Figure 8 shows time series of Topex/Poseidon sea-surface height anomaly (SSHA) extracted from three locations along the SAB shelf slope between 100 and 500m depth. The size of the NASG is superimposed on the three SSHA time series. There is a remarkable correlation between the SSHA and the size of the NASG, which indicates the strong influence of the gyre dynamics on the shelf slope SSHA variability via the Gulf Stream front displacement in response to the expansion and contraction of the NASG. This result is consistent with *Olson et al.* [1983] that showed a distinct seasonal cycle of the Gulf Stream front displacement, offshore in spring and onshore in fall.

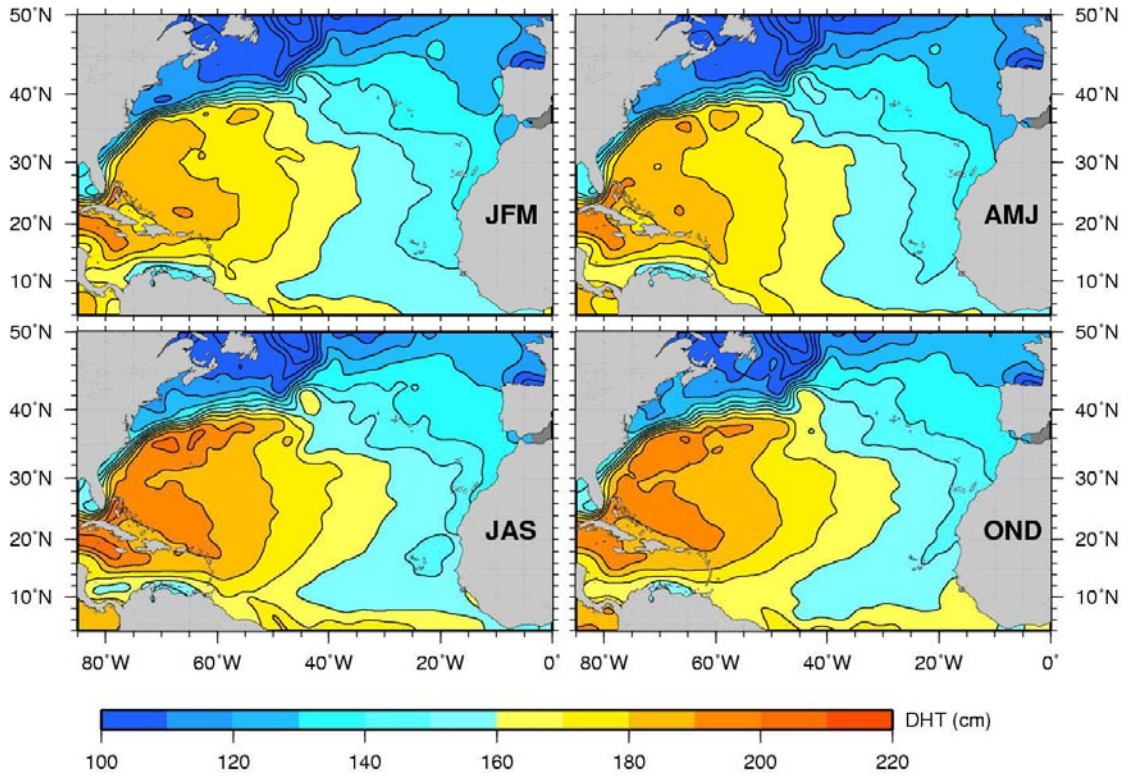

Figure 6b. Seasonal composites of dynamic height from Aviso data. Note the increase of dynamic height of ~20 cm from winter-spring to summer-autumn.

More evidence of the SAB response to the NASG variability is given by DHT versus Chl-a (Figure 9a) and SST versus Chl-a (Figure 9b) linear correlation maps. The spatial distribution of the DHT vs. Chl-a correlation shows a band just offshore of the 500m isobath northward of Cape Canaveral where the two parameters are anti-correlated. This means that when the Gulf Stream approaches the slope region the DHT is elevated and the surface Chl-a decreases and vice versa. This is because the surface tropical waters of the Gulf Stream are poor in nutrients and, consequently, phytoplankton concentrations are very low. When the Gulf Stream moves offshore, the tropical waters are replaced by shelf break waters that contain more nutrients and phytoplankton. The region of the inner and middle shelves in the vicinity of Cape Canaveral behaves quite differently. There the DHT is in phase with the Chl-a variability. Theoretical studies have shown that in this strongly cyclonically sheared frontal region, topographically induced upwelling (downwelling) occurs in the region where the isobaths diverge (converge) in the downstream direction [*Janowitz and Pietrafesa*, 1982]. Very likely, the in-phase correlation between DHT and Chl-a indicates an increase in the topographically induced upwelling when the Gulf Stream gets closer to Cape Canaveral, manifesting itself as higher DHT and Chl-a. The spatial distribution of the SST vs. Chl-a shown in Figure 9b indicates a strong anti-correlation between the two parameters, which increases offshore towards the NASG. This means that lower SST corresponds to higher Chl-a and vice-versa. One possible driving mechanism, more likely for the offshore areas, is

the deepening of the mixed layer in winter allowing for stronger vertical mixing of nutrients and, consequently, increased phytoplankton production.

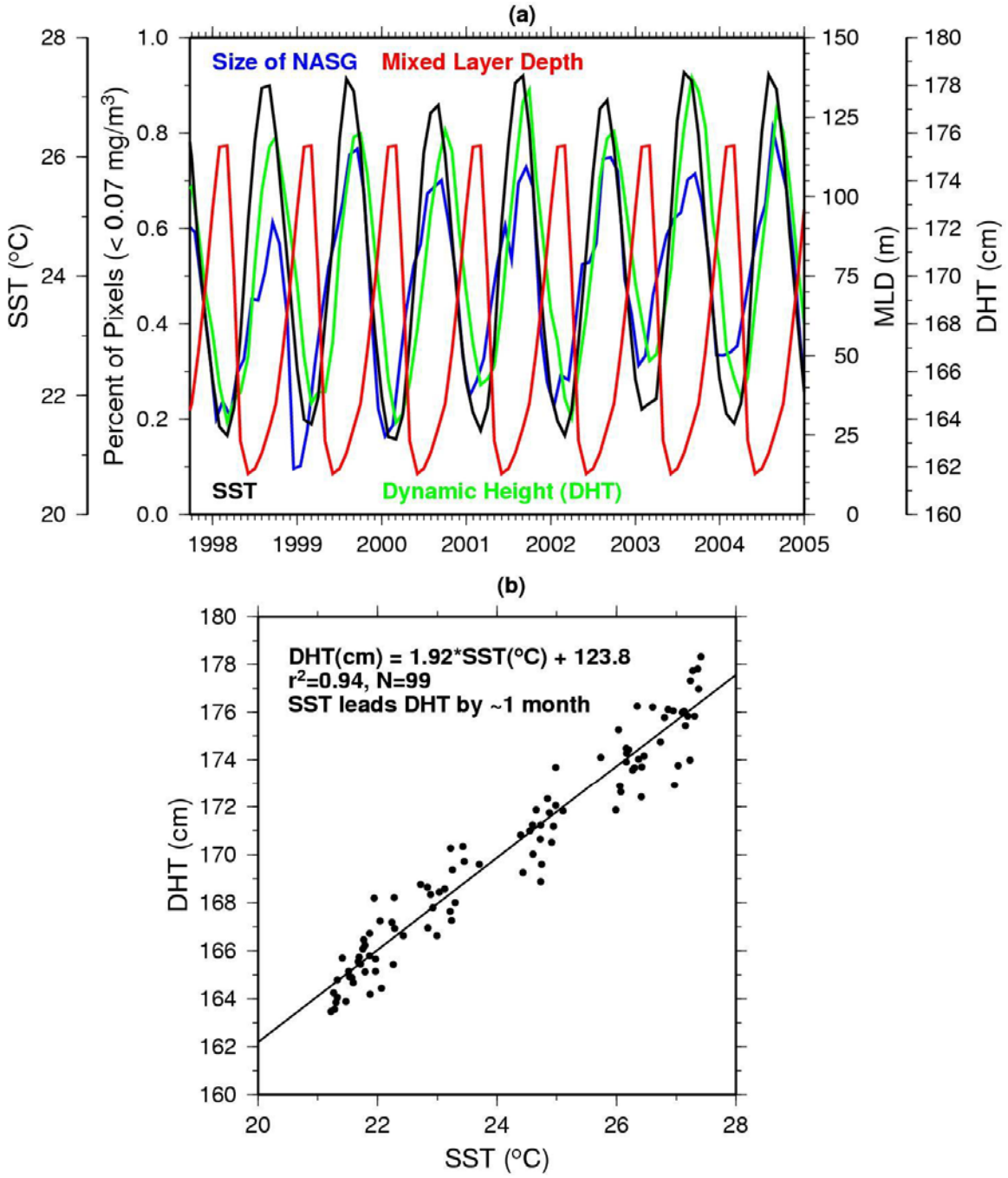

Figure 7. a) Time series of NASG size, MLD, SST, and DHT for 1998-2005. b) Scatter plot of DHT versus SST with corresponding regression equation.

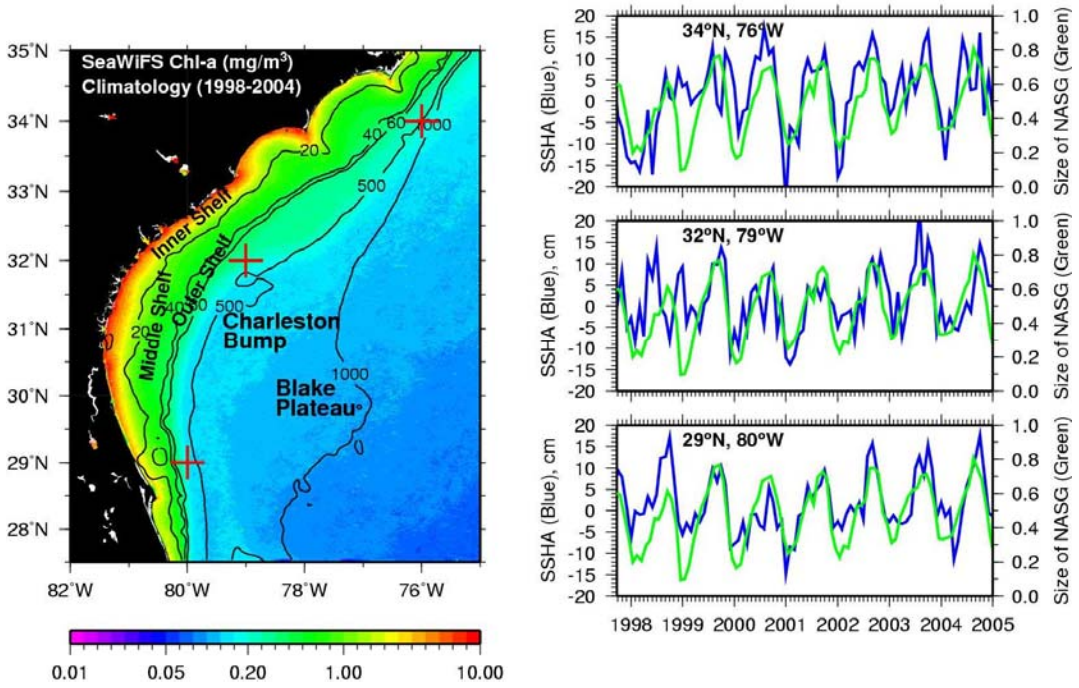

Figure 8. Time series of SSHA at three sites along the SAB shelf break. The left panel shows SeaWiFS Chl-a climatology and the locations from which the three SSHA time series were extracted (red crosses). The right panel shows the time series of SSHA at the three locations (blue lines) with the size of the NASG superimposed (green lines).

This mechanism is also observed in the Sargasso Sea near Bermuda where the annual cycle of biogeochemistry is intricately linked to the physical forcing, since vertical mixing brings nutrients into the euphotic zone during winter [*Steinberg et al.*, 2001]. On the shelf area, the anti-correlation peaks near the Florida-Georgia boundary line, with a minimum correlation near the Georgia-South Carolina border, and increasing again north of the Charleston Bump. Downstream from the Florida Strait, the shelf begins to widen and Gulf Stream meanders and frontal eddies become more energetic. Cyclonic, cold core eddies are embedded in the Gulf Stream front in the region of the Florida, Georgia, and North Carolina shelves (40m to the shelf edge) and serve as a "nutrient pump" for the shelf new carbon production [*Lee et al.*, 1991; *McClain et al.*, 1990; *McClain et al.*, 1984; *Yoder et al.*, 1981b]. The pattern of SST vs. Chl-a shown in Figure 9b agrees with the frontal eddy forcing scenario described above.

3.3 Impact of Gulf Stream Variability

The location of the Gulf Stream cyclonic front at the shelf break is the most important physical oceanographic characteristic of the SAB. The excursions

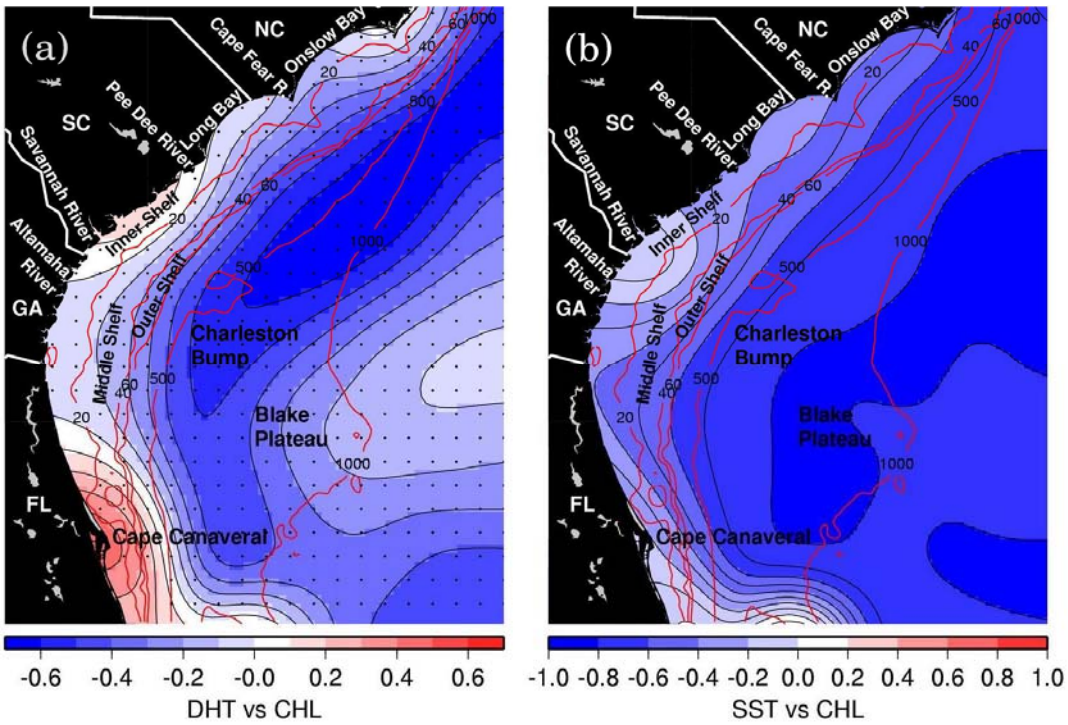

Figure 9. Correlation maps between (a) Aviso dynamic height (DHT) and SeaWiFS Chl-a, and (b) between AVHRR Pathfinder SST and SeaWiFS Chl-a.

of the Gulf Stream front are the main mechanism of nutrient supply to the outer shelf. Very energetic growth of frontal perturbations takes place immediately downstream (north) of the Straits of Florida and the Charleston Bump [*Chao and Janowitz*, 1979; *Lee et al.*, 1991; *McClain and Atkinson*, 1985; *Singer et al.*, 1983], near Cape Fear, N.C. The growth of finite amplitude disturbances depends primarily on the cross-stream distance from the slope to the axis of the Gulf Stream [*Oey*, 1988]. This distance increases north of the Straits of Florida and downstream of the Charleston Bump, which is the preferred area of eddy growth. Eddy growth decreases sharply in the greater depths off Cape Lookout, N.C., and Cape Hatteras, N.C., and as the stream lines converge downstream of the Charleston Bump, which are the areas of preferred eddy decay [*Lee et al.*, 1991].

These previous findings can be confirmed by examining Figure 10, which shows the seasonal position of the Gulf Stream shelf slope front (GSF) using DHT and Chl-a as indicators. Figure 10a shows the seasonal GSF based on the 144 cm DHT contour, while Figure 10b shows the seasonal GSF based on the 0.25 mg/m^{-3} Chl-a contour. The contour values appear to be good proxies for the GSF and were chosen within the region of sharpest gradients and based on the known position of the Gulf Stream axis with respect to bathymetry [*Bane*, 1983]. South of 32^{o}N, the western edge of the Gulf Stream generally lies within ±15 km of the shelf break [*Bane and Brooks*, 1979], which seems consistent with Figure 10. In contrast, SST contours do not provide a good proxy for the GSF,

especially in summer when there is no sufficient surface temperature gradient to identify fronts. The Chl-a contours seem to provide a more accurate

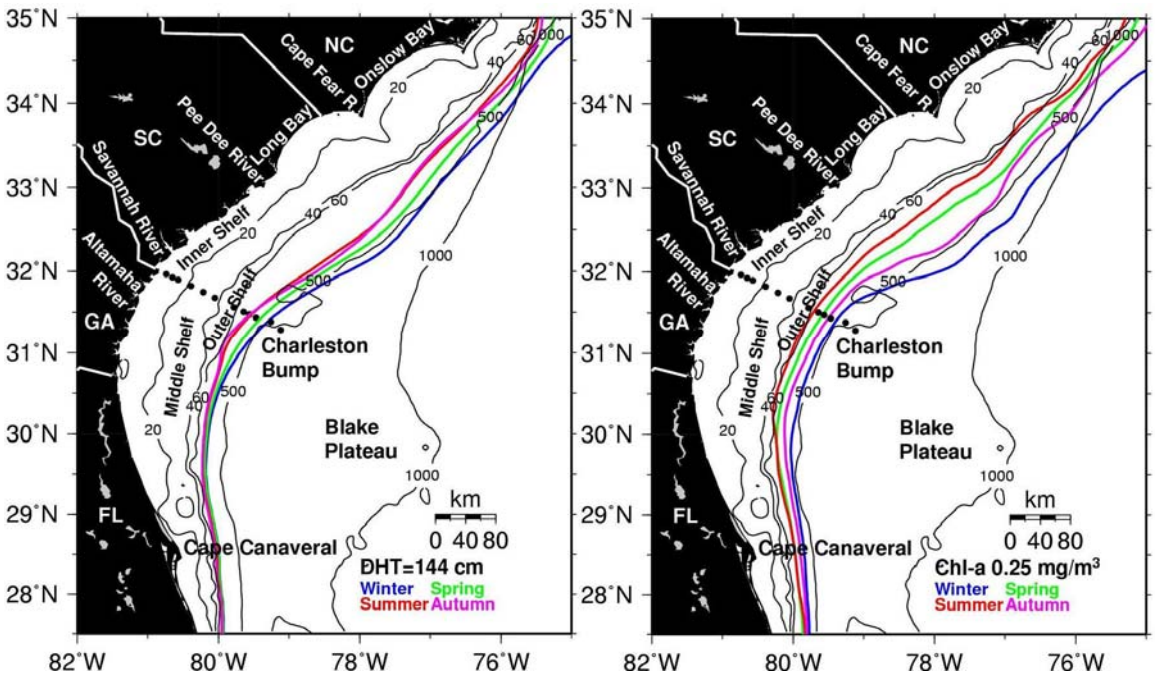

Figure 10. Seasonal position of the Gulf Stream (GS) front derived from (a) Aviso DHT and (b) from SeaWiFS Chl-a. The 144 cm DHT contour and the 0.25 mg m^{-3} Chl-a contour are used to derive the GS front. The black dots represent the station locations for the offshore transect conducted during 1973-1974 in the Georgia Bight.

representation of the seasonal GSF than DHT because they are based on higher resolution MLAC data, e.g., 1 km versus 1/3^{o} (~37 km) for the Aviso DHT data, which tend to be much smoother, especially north of the Charleston Bump. However, both representations of the GSF show that the front is closer to the shelf break in summer and moves offshore towards the winter. This seasonal behavior is consistent with our previous discussions regarding the expansion-contraction of the NASG. Also, the contours are farther apart immediately north of the Charleston Bump, a region of active eddy generation.

Miller [1994] identified an annual cycle in the fluctuations of the Gulf Stream frontal position between Cape Hatteras and the Straits of Florida using AVHRR SST data. He identified an annual mode for the Gulf Stream frontal position that accounted for 43% of the total variance, which was in phase along the entire SAB and exhibited a local increase of amplitude at and just north of the Charleston Bump. This finding is in agreement with our analysis. In addition, he found a second less energetic mode that accounted for 16% of the variance, also with maximum amplitude near the bump, which was out of phase north and south of the bump. This second mode had little annual variability but did exhibit an energetic peak at 50 days. He also alluded to the existence of an annual wave generated at and propagating away from the bump but the wavelengths and

phase speeds indicated by his analyses do not match any known theoretical modes.

The black dots in Figure 10 represent the station locations of a cross-shelf transect conducted in the Georgia Bight during September 1973, December 1973, April1974, and July 1974. The hydrographic and biogeochemical data from this transect for the four cruises were digitized from data reports [*Atkinson*, 1975; *Atkinson*, 1976] and reproduced in Figure 11. The transect starting ~20km offshore of the Savannah River mouth was chosen among the six transects available because the nearshore stations were within the discharge plume of one of the major SAB rivers. Density (σ_t) and nitrate cross-sections, as well as surface Chl-a and DHT were plotted in Figure 11 for the four cruises. Low density water is present in all cruises nearshore due to the low salinity from the river plume discharge. The shelf is highly stratified during September and well mixed in other months, with highest vertical mixing in December as a result of winter convective overturning.

The surface nitrate in the shelf waters is below detection limit during all cruises but the surface Chl-a concentration is between 0.1 and 1 mg m^{-3}, an indication that phytoplankton growth was primarily sustained by regenerated nutrients. The nitrate concentration near the bottom reaches 2 μM in September as a result of a Gulf Stream intrusion. It is very likely that relatively high rates of production were taking place in the shelf subsurface waters as light reaches the ocean bottom in most areas of the SAB shelf [*Jahnke et al.*, 2005; *Nelson et al.*, 1999; *Signorini and McClain*, 2005], but contemporaneous subsurface Chl-a data are not available to verify this assertion.

There is evidence of Gulf Stream driven subsurface nitrate pumping during the April and July 1974 cruises, which is clearly shown by the uplifting of the pycnocline and nutricline near the shelf break. A surface manifestation of these events is noticeable by the surface Chl-a peaks at the same locations. The surface Chl-a decreases offshore towards the shelf break and more rapidly at the shelf break as the DHT rises with a steeper slope offshore within the oligotrophic waters of the Gulf Stream proper. The inverse relationship between DHT and Chl-a near the shelf break shown in Figure 9 is quite clear from the transects of Figure 11. More specifically, Chl-a is high and DHT is low west of the Gulf Stream front and vice-versa east of the Gulf Stream.

In the Straits of Florida, perturbations of velocity and density fields can be generated by flow over topography and by local along-channel wind forcing [*Johns and Schott*, 1987; *Lee and Williams*, 1988]. Model results show that the growth of perturbations of the Florida Current is primarily the result of baroclinic instability and results in meanders with wave properties that match observations [*Boudra et al.*, 1988]. Fluctuations of volume transport of ±3 to ±5 Sverdrups (Sv, or 10^6 m^3/s), which change the slope of isopycnal surfaces, accompany these disturbances on time scales of about 1 week. The perturbed velocity and density fields are advected northward from the Straits of Florida by the mean flow of the Gulf Stream [*Lee and Williams*, 1988; *Zantopp et al.*, 1987].

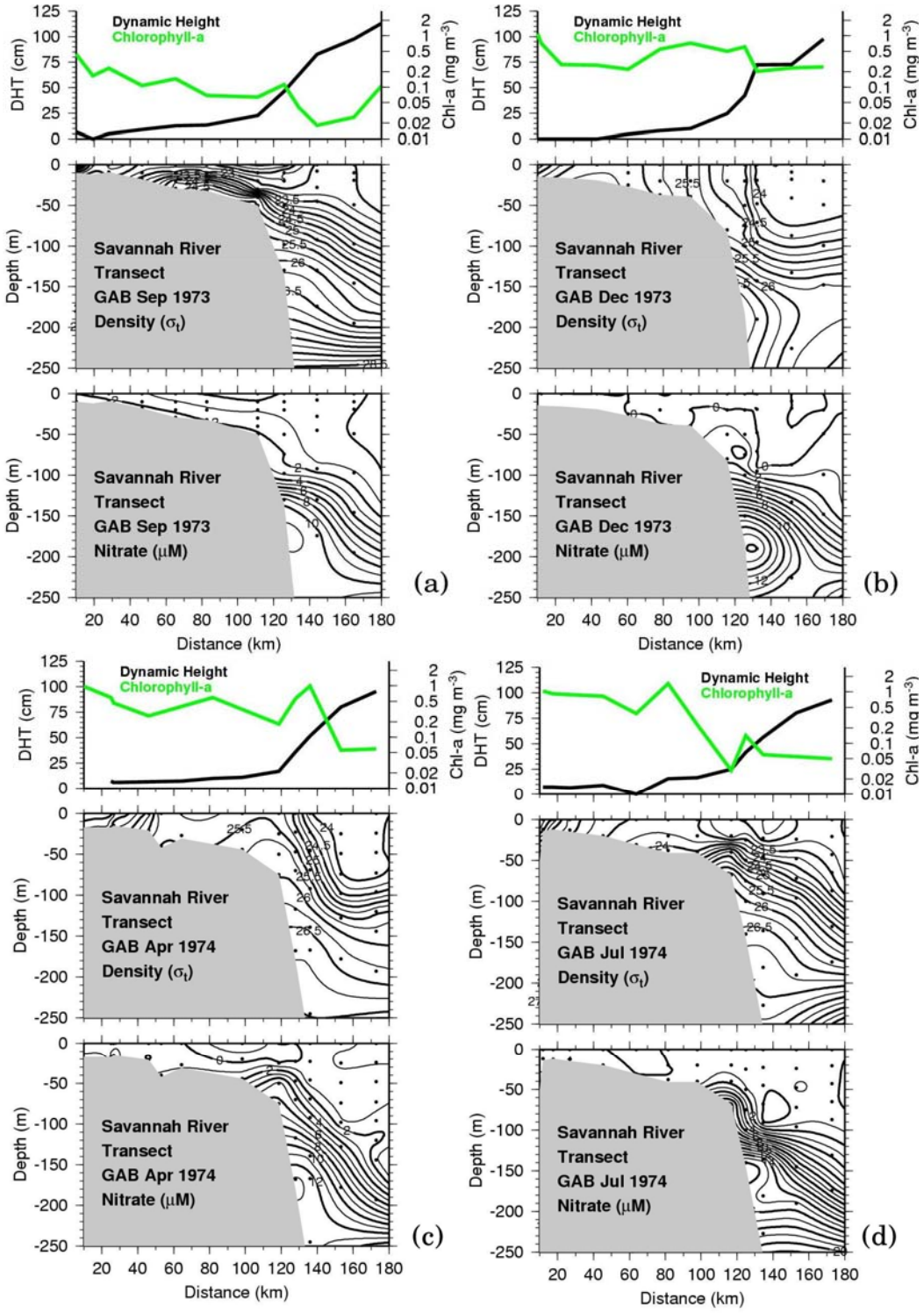

Figure 11. Transects of dynamic height, surface Chl-a, density, and nitrate for (a) September 1973, (b) December 1973, (c) April 1974, and (d) July 1974 from field data digitized from cruise reports on oceanographic observations in the Georgia Bight.

We analyzed the Gulf Stream transport variability along three transects, one in the northern Straits of Florida, one in the Georgia Bight (GB), and one off

Cape Hatteras (CH). Figure 12 shows the seasonal composites of DHT and the location of the transects. The transect across the Straits of Florida coincides with the location of the submarine cable between Jupiter, Florida, and Settlement Point, Grand Bahamas Island. At this location, the cross-stream voltage generated by the flow of the Florida Current (FC) through the earth's magnetic field has been used for several decades to derive volume transport at that location [*Larsen and Sanford*, 1985]. We compared two methods of obtaining the FC transport, the cable voltage method and the transport derived from DHT differences across the transect. Figure 13 shows the time series of FC transport derived from the two methods (top tier), and the GB and CH transports derived from the DHT method (middle and bottom tiers, respectively). The time series of FC daily cable transport (circles in top tier) and the 7-day FC Aviso DHT difference (red line in top tier) are in good agreement. The overall mean FC transport derived from the cable voltage method for the period of September 1997 − January 2006 is 33.3 Sv and ranged from 20 to 49 Sv. The overall mean DHT differences for the FC, GB, and CH transects are 34.5, 57.5, and 69.8 cm, respectively. If we use the conversion factor of 0.9652, derived from the ratio between the cable and DHT FC transports, we obtain 55.5 and 67.4 Sv for the GB and CH mean transports, respectively. Figure 13 shows that the transport across all three transects vary with time scales of one week to several months but without a distinct strong seasonal cycle.

Figure 14 shows time series of SeaWiFS-derived Chl-a for the FC, GB, and CH transects. The data were obtained from pixel averages of 8-day, 9 km standard mapped images within the limits of the transect lines. Note that all three time series, unlike the transport time series, exhibit very strong seasonal signature with less energetic higher frequency oscillations superimposed. Also note that the maximum Chl-a concentration occurs during summer in the FC transect, while the Chl-a in the GB and CH transects peaks in winter. The Chl-a maxima across the FC transect is a result of upwelling favorable southerly (northward) winds in summer, while the winter Chl-a maxima across the other two transects is in synch with the NASG seasonal forcing discussed in Section 3.2. Local surface heat loss to the atmosphere and wind mixing in the shelf regions also play a role in promoting higher Chl-a concentrations in winter. Cross-wavelet transforms between transport and Chl-a time series are shown in Figure 15. In all cross-wavelet transform figures hereafter, the thick black contour lines designate the 5% significance level against red noise and the cone of influence (COI) where edge effects might distort the pictures is shown as a lighter shade. The relative phase relationship is shown as arrows, with in-phase pointing right and anti-phase pointing left. In this case, Chl-a leading transport by 90 degrees pointing straight down. Both time series are normalized by the standard deviation. The color scale is the dimensionless cross-wavelet power.

There are periods of significant correlation (thick black contours) within the 1-year band that occurs at different times on each transect. Some examples are 2002-2006 for the FC transect with in-phase correlation (arrows pointing right) between transport and Chl-a, and 1999-2003 for the GB transect with a somewhat unstable phase relationship.

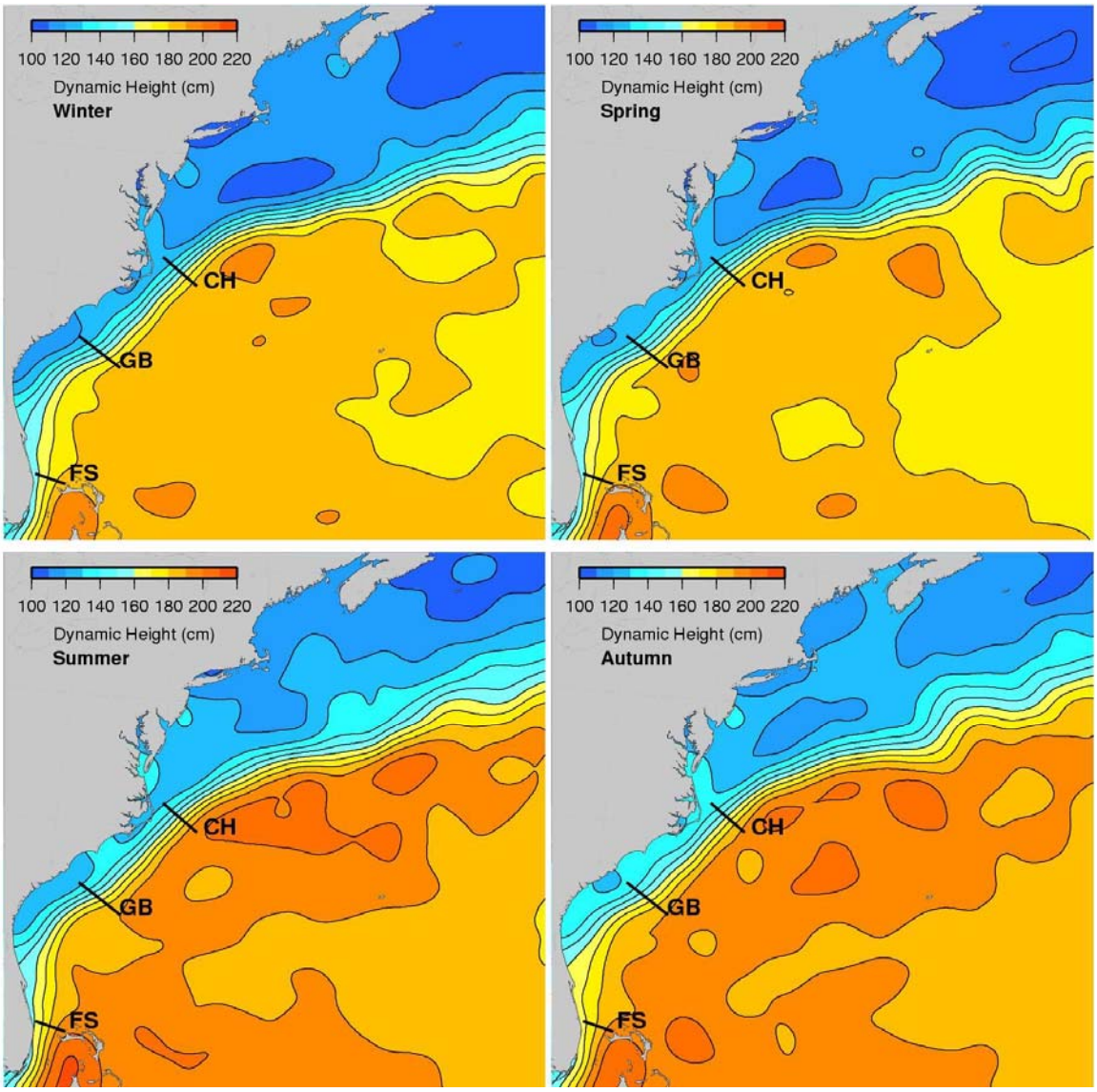

Figure 12. Seasonal maps of Aviso dynamic height (DHT). The three thick black lines across the Gulf Stream axis (region of stronger DHT gradient) represent the Gulf Stream transects across the Florida Strait (FS), Georgia Bight (GB), and Cape Hatteras (CH) from which time series of DHT gradient were obtained for analysis.

There is a much stronger correlation between the Chl-a and the north component of the wind along the FC transect. This is shown by the individual wavelet transforms and cross-wavelet transform in Figure 16. The correlation is strong and steady within the 1-year band for the entire period (1998-2006). The phase relationship is ~15^{o} (~2 weeks at the yearly cycle), with the wind leading the Chl-a. As previously mentioned, this is a result of stronger and steadier summer northward winds promoting stronger upwelling and consequently higher chlorophyll concentrations near the surface.

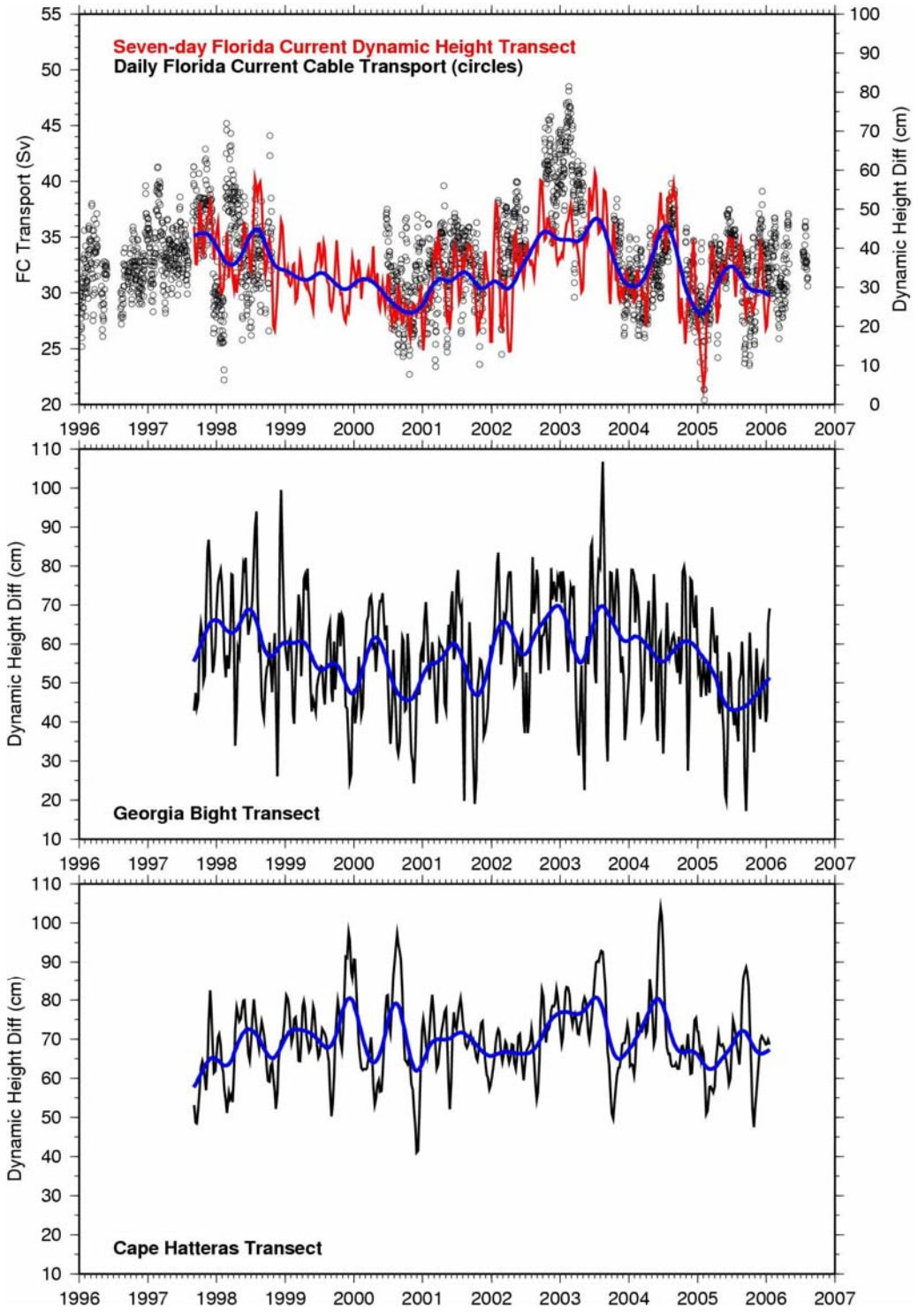

Figure 13. From top to bottom: (1) time series of daily Florida Current cable-derived (circles) transport with across-transect DHT difference (in red) superimposed, (2) DHT difference across the Georgia Bight transect, and (3) DHT difference across the Cape Hatteras transect. Low-pass filtered lines are superimposed on each tier. The blue lines are the low-passed seasonal components.

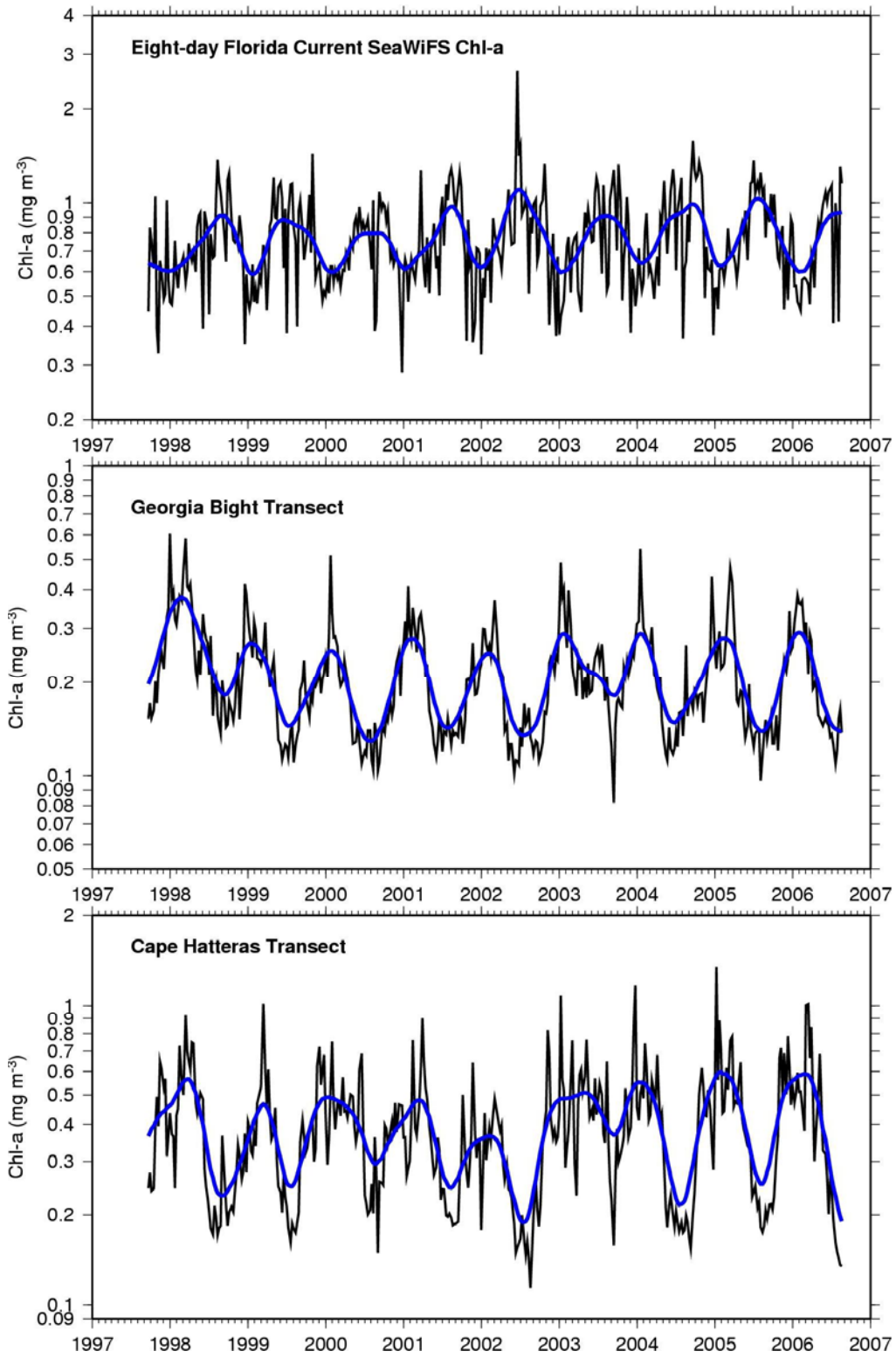

Figure 14. Time series of SeaWiFS-derived Chl-a averaged over the Florida Current, Georgia Bight, and Cape Hatteras transect lines. Note that the scales are different for each location. Low-passed filtered lines are superimposed on each tier. The blue lines are the low-passed seasonal components.

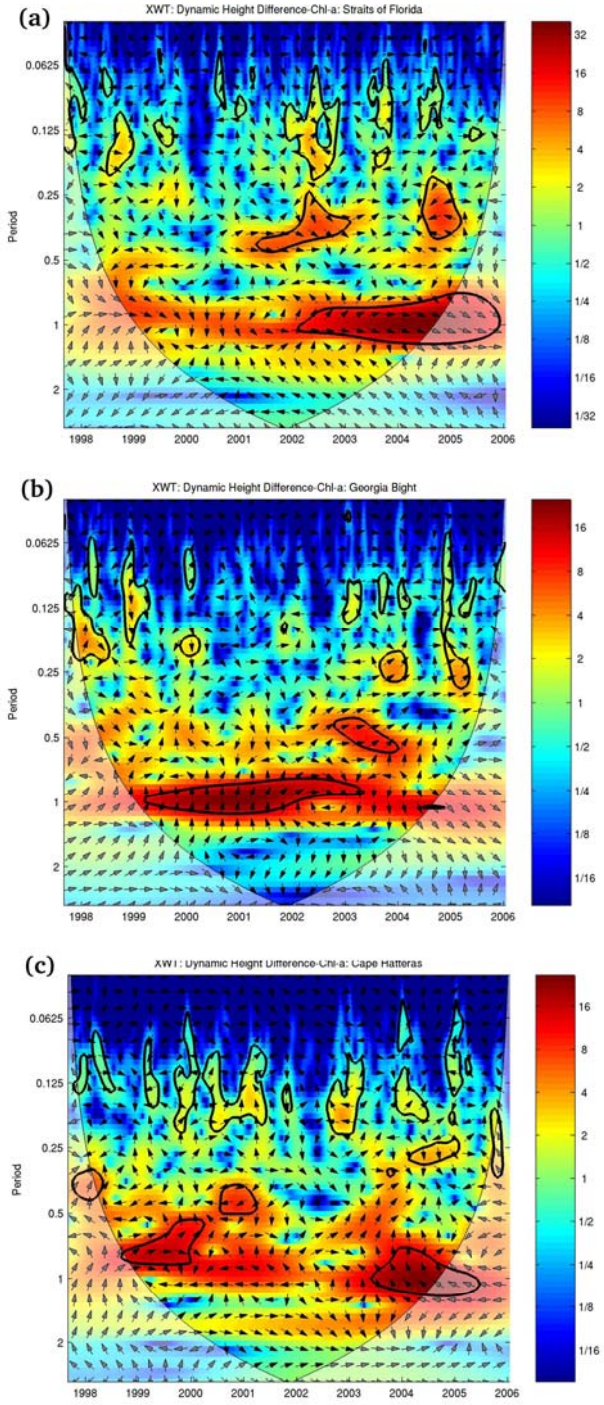

Figure 15. Cross-wavelet transforms between Gulf Stream transport derived from Aviso DHT differences and SeaWiFS Chl-a along FC, GB, and CH transects. The thick black contour lines designate the 5% significance level against red noise and the cone of influence (COI) where edge effects might distort the picture is shown as a lighter shade. The relative phase relationship is shown as arrows, with in-phasing pointing right and anti-phase pointing left, and Chl-a leading transport by 90 degrees pointing straight down.

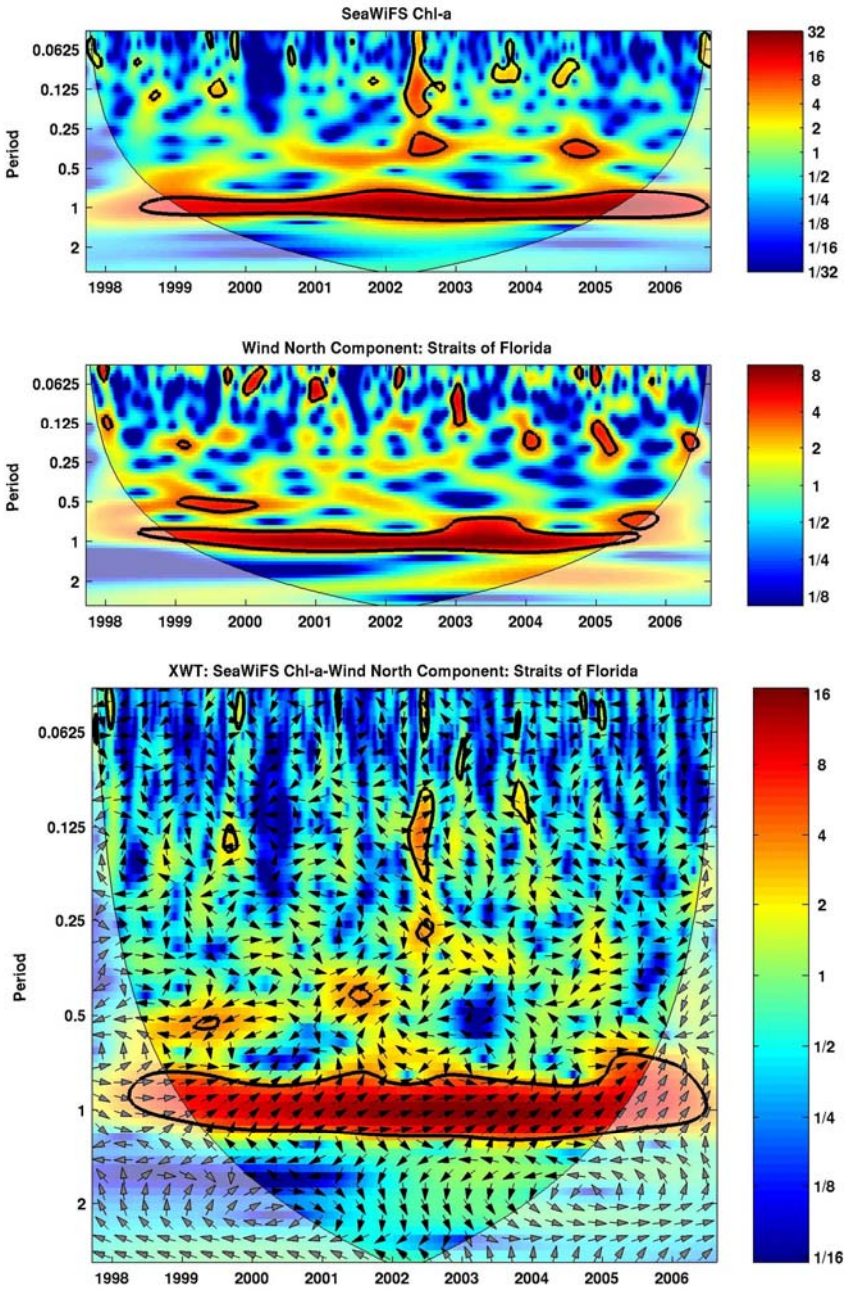

Figure 16. Wavelet and cross-wavelet transforms between SeaWiFS Chl-a and NCEP north component of the wind (upwelling-favorable) in the region of the Florida Current. Graph notations are as in Figure 15.

3.4 Local versus Large-scale Forcing

Three major forcing mechanisms responsible for the seasonal and inter-annual variability of Chl-a were identified: river discharge, local winds, and the displacement and strength of the Gulf Stream front. The river discharge is a local

component of the forcing mostly confined to the inner (0-20m) and middle (20-40m) shelf regions, while the Gulf Stream displacement is a remote forcing component linked to seasonal and inter-annual variability in the strength and size of the North Atlantic Subtropical Gyre (NASG). South of Cape Canaveral there is much less influence of the NASG seasonal forcing and more seasonal variability imparted by upwelling-favorable summer winds.

Dynamic height is directly correlated with Chl-a near Cape Canaveral but the size of the NASG is not. This means that the GS axis position at that location is much less affected by the seasonal variability of the NASG size and more by the actual strength of the flow, which in turn is conducive to stronger topographically induced upwelling [*Janowitz and Pietrafesa*, 1982].

The nearshore SAB shelf can be divided into three distinctive oceanographic domains alongshore according to wind forcing (upwelling), Gulf Stream influence, and river discharge. Between Charleston and Cape Hatteras there are point sources of freshwater from the Santee, Pee Dee and Cape Fear rivers and Pamlico Sound outflow. Also, upwelling along the coast may be enhanced by the divergence of the isobaths north of capes [*Blanton et al.*, 1981]. Between Jacksonville and Charleston the coastline is marsh-dominated and the freshwater discharge from the major rivers is much more diffuse. The impact of the freshwater discharge and upwelling near the capes via nutrient enrichment is quite clear in the Chl-a images in Figure 2. South of Jacksonville wind driven upwelling, Gulf Stream frontal eddies, and the onshore position of the Gulf Stream all contribute to the advection of nutrient-rich Atlantic Central Water from the Gulf Stream to stimulate strong episodic responses by phytoplankton and zooplankton [*Paffenhofer et al.*, 1987]. Two such events were documented and analyzed during the summer of 1981 in the vicinity of Cape Canaveral using a combination of field data and numerical model [*Lee and Pietrafesa*, 1987; *Lorenzzetti et al.*, 1987].

We divided the SAB into regional domains according to the oceanographic properties described above. Figure 17 shows the chosen SAB regional domains for time series analyses. The domain divisions follow bathymetric, e.g., inner shelf (0-20m), middle shelf (20-40m), outer shelf (40-60m), and slope water (60-500m), and two cross-shelf boundaries, one starting at the Florida-Georgia boundary, and another starting at Cape Romain. The regions are further divided into 9 domains separated by the cross-shelf boundaries and the 20, 60, and 500 m isobaths. The middle and outer shelf regions were lumped together for simplicity as they share similar properties.

First, we analyze the forcing and response of Chl-a within the entire SAB shelf. Figure 18 shows time series of the size of the NASG, climatologic seasonal MLD, the Cape Fear River discharge, and the mean Chl-a within the four shelf domains, e. g., inner, middle, outer shelves, and slope region. The NASG is smallest in winter and largest in summer (see top tier time series in Figure 18).

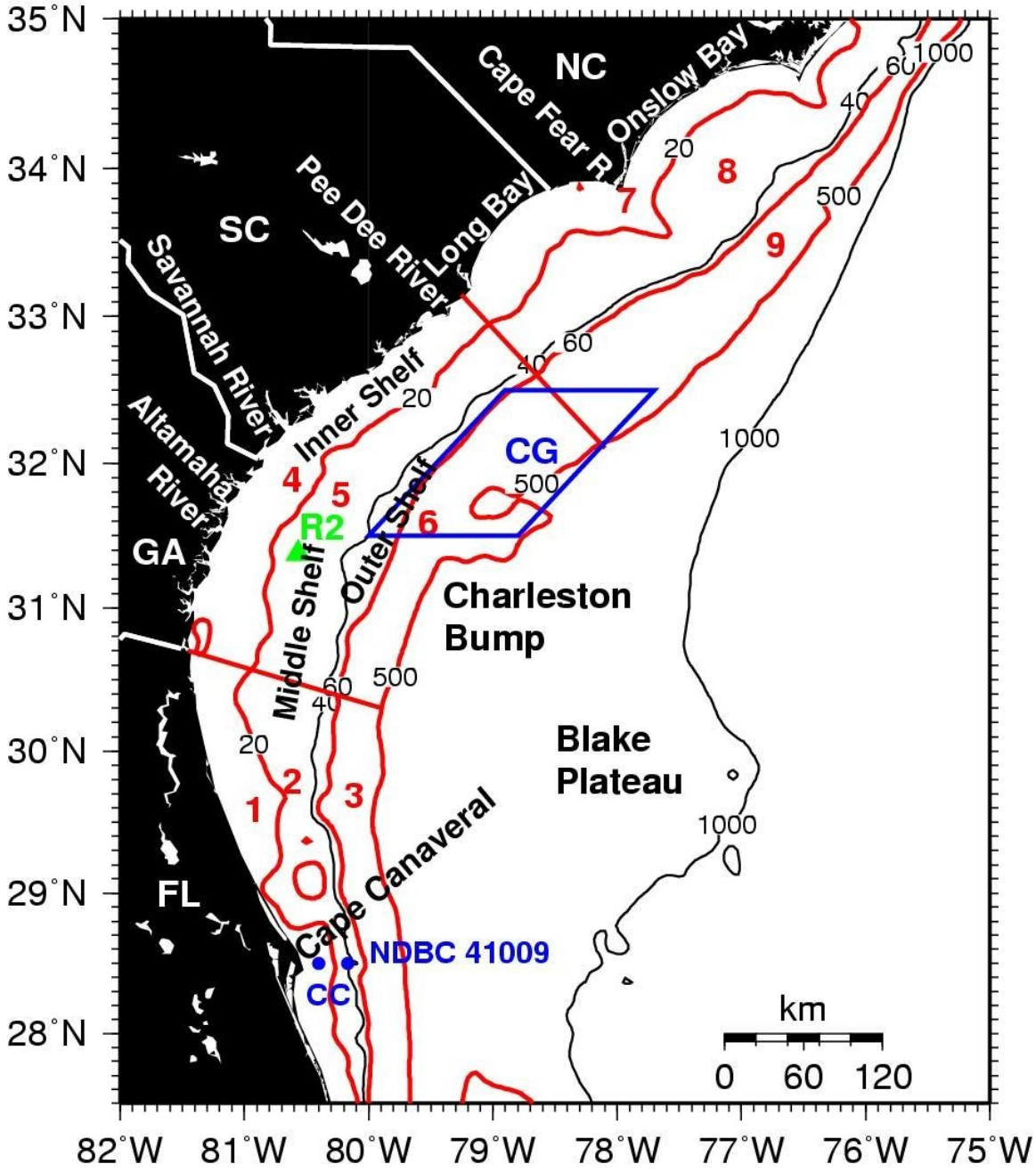

Figure 17. Map showing nine regional domains of the SAB shelf region. The blue polygon delimits the region of the Charleston Gyre. The NDBC, SABSOON R2 Tower, and nearshore Cape Canaveral (CC) locations are marked on the map as well.

There is an inverse relationship between the NASG size derived from the Chl-a variability inside the gyre (oligotrophic domain expansion/contraction) and the MLD seasonal variability, consistent with the surface thermal forcing discussion in subsection 3.2.

As shown in Table 1, the correlation coefficient between river discharge and mean Chl-a decreases from 0.84 in the inner shelf to 0.53 in the slope water region (Figure 18), a clear indication of decreasing river discharge influence on

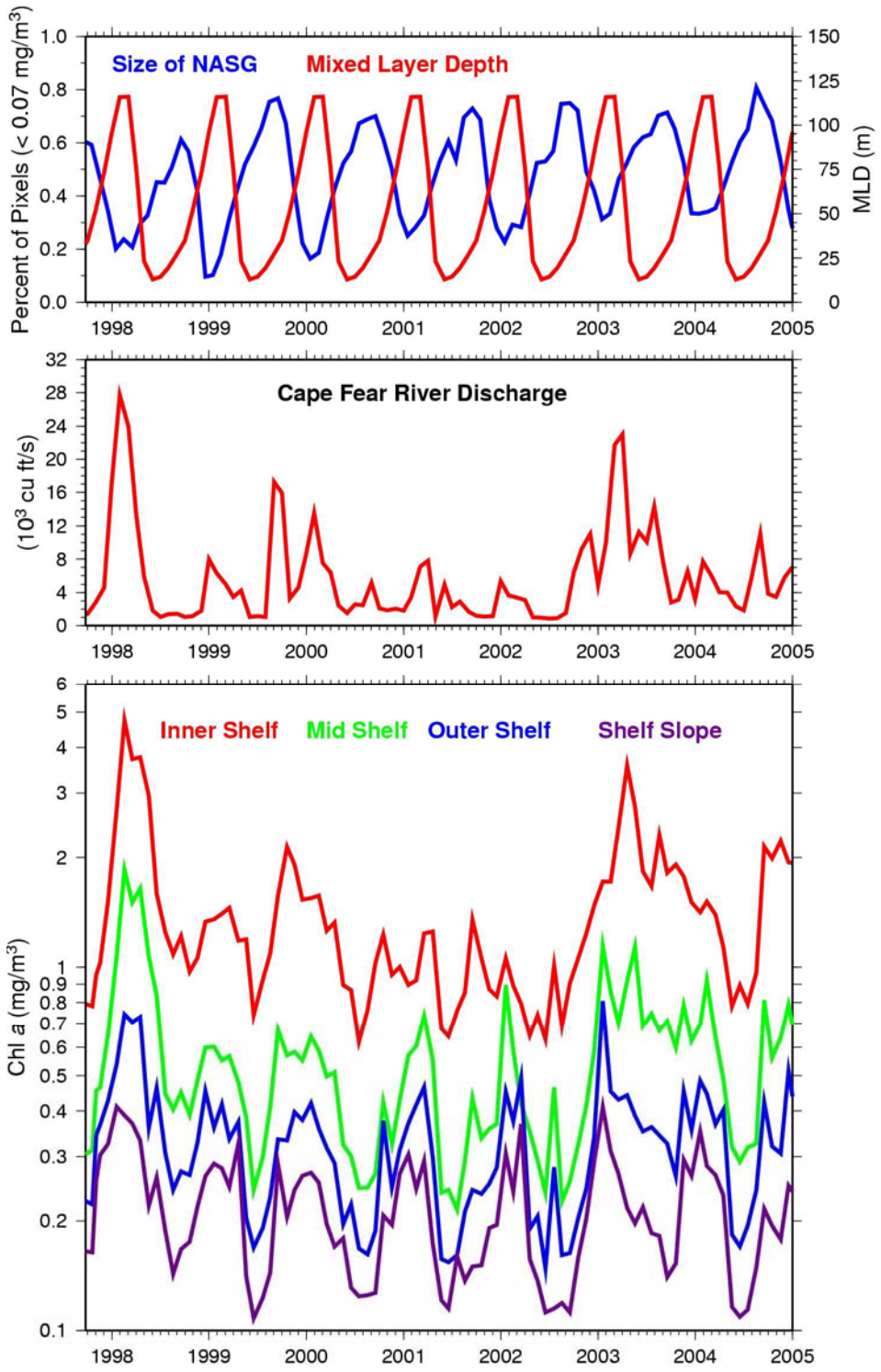

Figure 18. Time series of size of the NASG, Cape Fear River discharge, and mean Chl-a for the SAB inner, middle, and outer shelves and slope water region (left panel). The correlation coefficients between river discharge and mean Chl-a, and size of the NASG versus mean Chl-a are shown in Table1.

Chl-a in the offshore direction. Conversely, the correlation coefficient between the NASG size and the mean Chl-a (Table 1) increases offshore, ranging from 0.28 in the inner shelf to 0.71 in the slope water region, consistent with the stronger influence of the Gulf Stream front displacement in the latter region. Note that the correlation coefficients between the NASG size and mean Chl-a are negative, indicating that the lowest Chl-a occurs when the gyre size is maximum in summer-fall, and the maximum Chl-a occurs when the NASG size reaches a minimum in winter-spring.

Table 1. Linear correlation between river flow and size of the NASG forcing versus Chl-a response in the SAB.

Region	River Flow vs. Chl-a	Size of NASG vs. Chl-a
Inner Shelf	0.84	-0.28
Mid Shelf	0.73	-0.47
Outer Shelf	0.60	-0.62
Shelf Slope	0.53	-0.71

Table 2 shows a correlation matrix among the NASG size, the Altamaha River and Cape Fear River discharges, and the Chl-a concentration within each of the 9 shelf regions. The time series for each of the above parameters are shown in Figure 19. Unlike the linear coefficients shown in Table 1, in this more refined regional division the square of the linear correlation (r^2) coefficients are tabulated but the sign of the coefficients are preserved to indicate the phase relationship between the various components. In Table 2, correlations greater than 0.3 are marked in red, i.e., correlations explaining 30% or more of the total sample variance. Using this criterion, the size of the NASG is significantly anti-correlated only with Chl-a in regions C6 and C9 (-0.49 and -0.45, respectively), which are the two slope regions north of Jacksonville, Florida. The Altamaha River and Cape Fear River discharges are significantly correlated with all regions, except C3 and C6, which are slope regions south of the Cape Romain cross-shelf boundary. The river discharge from both rivers is still significantly correlated (0.31 to 0.38) with the Chl-a of the slope region north of Cape Romain (C9). This result indicates that the offshore deflection of the Gulf Stream by the Charleston Bump allows freshwater to invade waters of the outer shelf and slope, unlike regions to the south where the Gulf Stream is much closer to the outer shelf. The correlations among Chl-a concentrations show an offshore decrease in significance, with the exception of region C2 (middle shelf south of Jacksonville), which shows r^2 values greater than 0.3 with all the other regions, which is an unexpected and elusive result.

The contrast between the influence of river discharge and the size of the NASG on the SAB Chl-a variability is better illustrated in Figure 20. Figure 20a shows the r^2 spatial distribution for the correlation between river discharge and

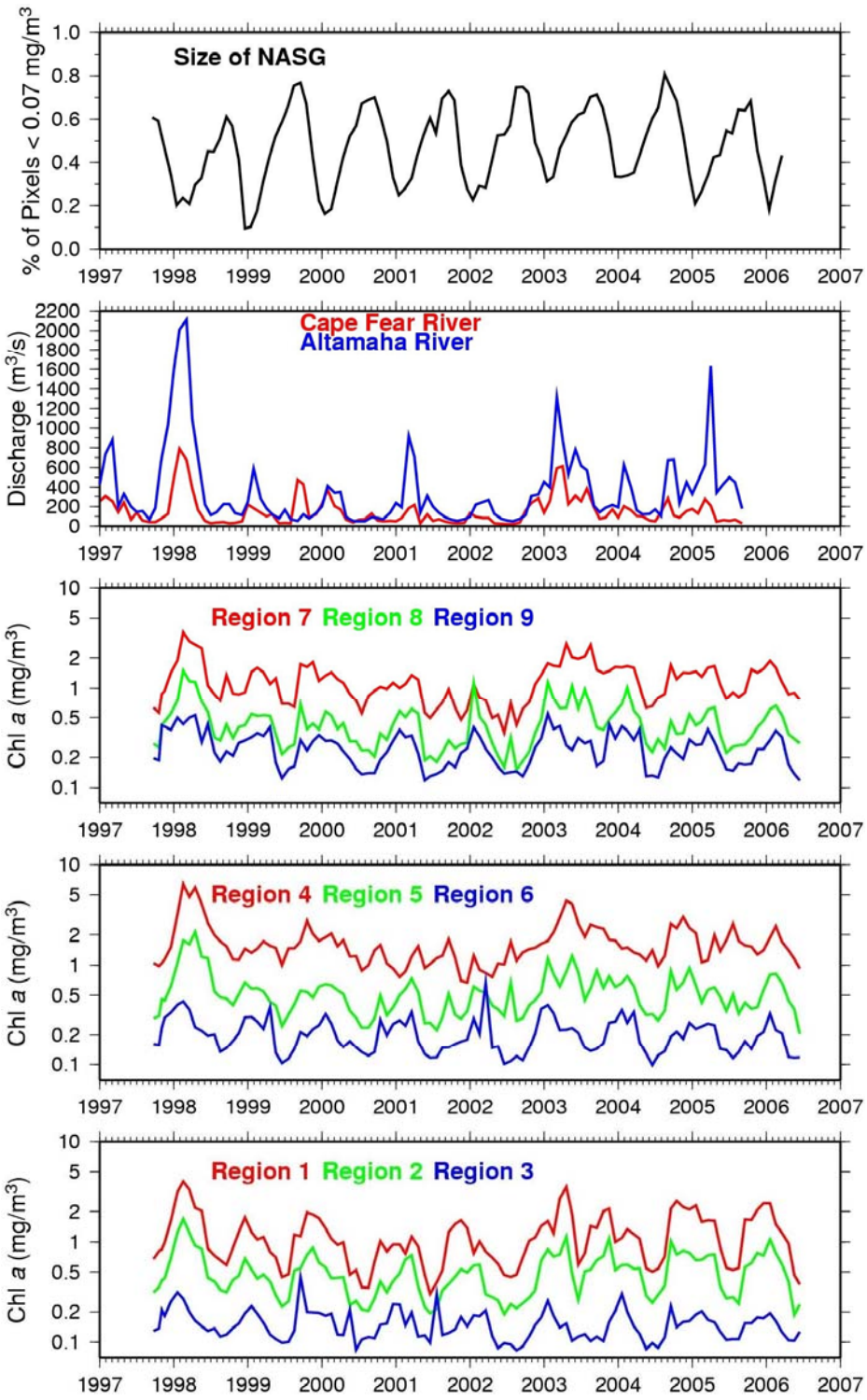

Figure 19. From top to bottom: (1) time series of the size of the NASG, (2) Altamaha and Cape Fear Rivers discharge, (3) SeaWiFS-derived Chl-a for regions 7, 8, and 9, (4) SeaWiFS-derived Chl-a for regions 4, 5, and 6, and, (5) SeaWiFS-derived Chl-a for regions 1, 2, and 3.

Chl-a. The monthly discharge from four major rivers, Altamaha, Savannah, Pee Dee, and Cape Fear, were combined and correlated on a pixel-by-pixel basis

with monthly time series of Chl-a SeaWiFS images. Chl-a is highly correlated with freshwater discharge in the inner shelf near the river mouths, and spread across the middle and outer shelves north of 30°N. The climatologic surface currents (1998-2006) for winter-spring, the time period of peak runoff, are superimposed on Figure 20a. The currents are obtained by adding the wind-driven component to the geostrophic flow. The surface circulation patterns are consistent with the observed spreading of the zones that have high correlation between river discharge and Chl-a. This Chl-a pattern has been previously observed using pigment concentrations derived from the Coastal Zone Color

Table 2. Correlation (r^2) matrix between the North Atlantic Subtropical Gyre size (NASG), Cape Fear (CPFR) and Altamaha (ALTR) rivers discharge, and mean chlorophyll concentrations within the 9 regions define in Figure 16 (C1, C2, C3, C4, C5, C6, C7, C8, and C9, respectively). A sign is attributed to each r^2 (negative means anti-correlation and positive a direct correlation). Correlations above 0.3, e.g., correlations explaining 30% or more of the total sample variance, are marked in red. The sample size is 99.

	NASG	CPFR	ALTR	C1	C2	C3	C4	C5	C6	C7	C8	C9
NASG	1.0	-0.10	-0.10	-0.12	-0.19	-0.22	-0.02	-0.16	-0.49	-0.10	-0.25	-0.45
CPFR	–	1.0	0.59	0.45	0.46	0.24	0.37	0.30	0.22	0.51	0.43	0.31
ALTR	–	–	1.0	0.41	0.50	0.17	0.37	0.40	0.28	0.46	0.45	0.38
C1	–	–	–	1.0	0.86	0.20	0.51	0.45	0.24	0.57	0.34	0.30
C2	–	–	–	–	1.0	0.30	0.47	0.55	0.37	0.64	0.51	0.47
C3	–	–	–	–	–	1.0	0.03	0.11	0.43	0.16	0.22	0.36
C4	–	–	–	–	–	–	1.0	0.75	0.07	0.67	0.43	0.20
C5	–	–	–	–	–	–	–	1.0	0.28	0.66	0.70	0.50
C6	–	–	–	–	–	–	–	–	1.0	0.25	0.44	0.60
C7	–	–	–	–	–	–	–	–	–	1.0	0.71	0.45
C8	–	–	–	–	–	–	–	–	–	–	1.0	0.70
C9	–	–	–	–	–	–	–	–	–	–	–	1.0

Scanner (CZCS) satellite sensor [*McClain et al.*, 1988]. The Cape Fear plume, and a portion of the Pee Dee River plume, are entrained and flow northeastward with the prevailing currents. The Savannah and Altamaha river plumes flow southward in the inner shelf and then are entrained by the mid-shelf northward flow.

However, it is not possible to accurately identify the proportion of Chl-a and dissolved and particulate organic material contained in these waters of fluvial origin without in situ measurements. Previous field work studies have determined that freshwater discharge provides a major source of CDOM to the central SAB [*Nelson and Guarda*, 1995]. *Alberts et al.* [1990] reported concentrations of dissolved organic carbon (DOC) of 4.0−10.7 g C m^{-3} in the Pee Dee, Savannah, and Altamaha Rivers, and higher concentrations in several smaller rivers. DOC/POC ratios determined in that study indicated that about 95% of the total organic carbon supplied by the rivers was in the dissolved pool. As pointed out by *Nelson and Guarda* [1995], seasonal difference in absorption properties has implications for mapping near-surface Chl-a on the SAB shelf by remote sensing technique. Application of a Chl-a algorithm with no correction for the absorption of CDOM and detritus might show the high CDOM water parcel as a band of

elevated near surface Chl-a. We will further analyze this potential Chl-a algorithm bias in a later section by comparing the OC4v4 Chl-a retrievals

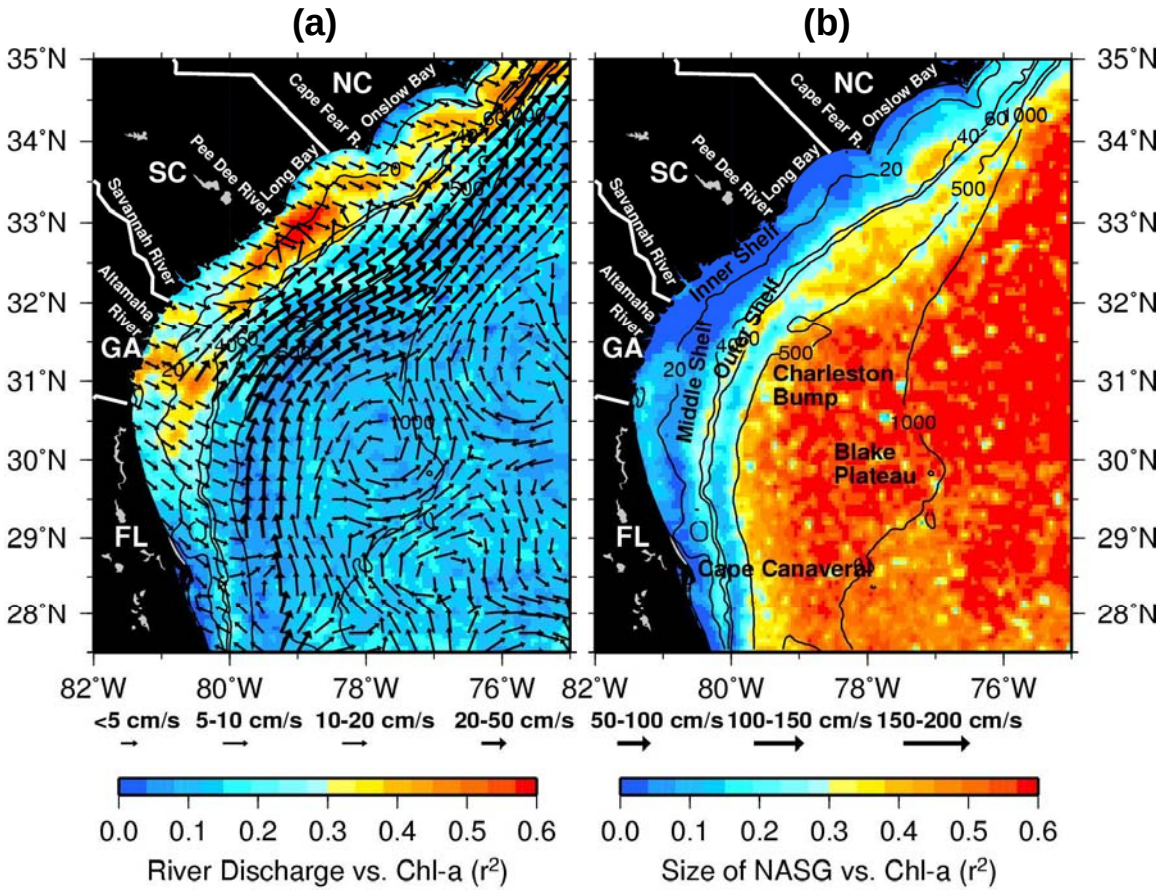

Figure 20. Correlation maps between (a) river discharge and SeaWiFS Chl-a, and, (b) between the size of the NASG and SeaWiFS Chl-a. The climatologic surface currents for winter-spring, the period of peak river discharge, are superimposed on (a).

from a semi-analytic algorithm that includes CDOM absorption coefficient retrievals as well.

The spatial distribution of the linear correlation between the size of the NASG and Chl-a is shown in Figure 20b. In contrast with Figure 20a, the highest correlation lies within the gyre itself and in the slope region north of the Charleston Bump where excursions of the Gulf Stream and frontal eddies are more frequent and energetic, acting as a nutrient pump to the outer shelf waters. There is also a narrow band of elevated correlation along the outer shelf south of the Charleston Bump to 28°S. This seems to be a result of Gulf Stream frontal excursions as well, but within a more confined range of distance.

More localized effects of freshwater discharge and wind forcing are shown in the time series of Figures 21 and 22. Figure 21 shows time series of offshore and alongshore components of the wind (vectors and components) at the location of NDBC buoy 41009 off Cape Canaveral near the 40m isobath (see Figure 17), SeaWiFS Chl-a at the buoy location and another location closer to

shore on the inner shelf (see Figure 17), AVHRR SST at the same locations, and the SST difference (nearshore minus offshore) between the same two locations. There are nine high Chl-a events throughout the period (September 1997 −

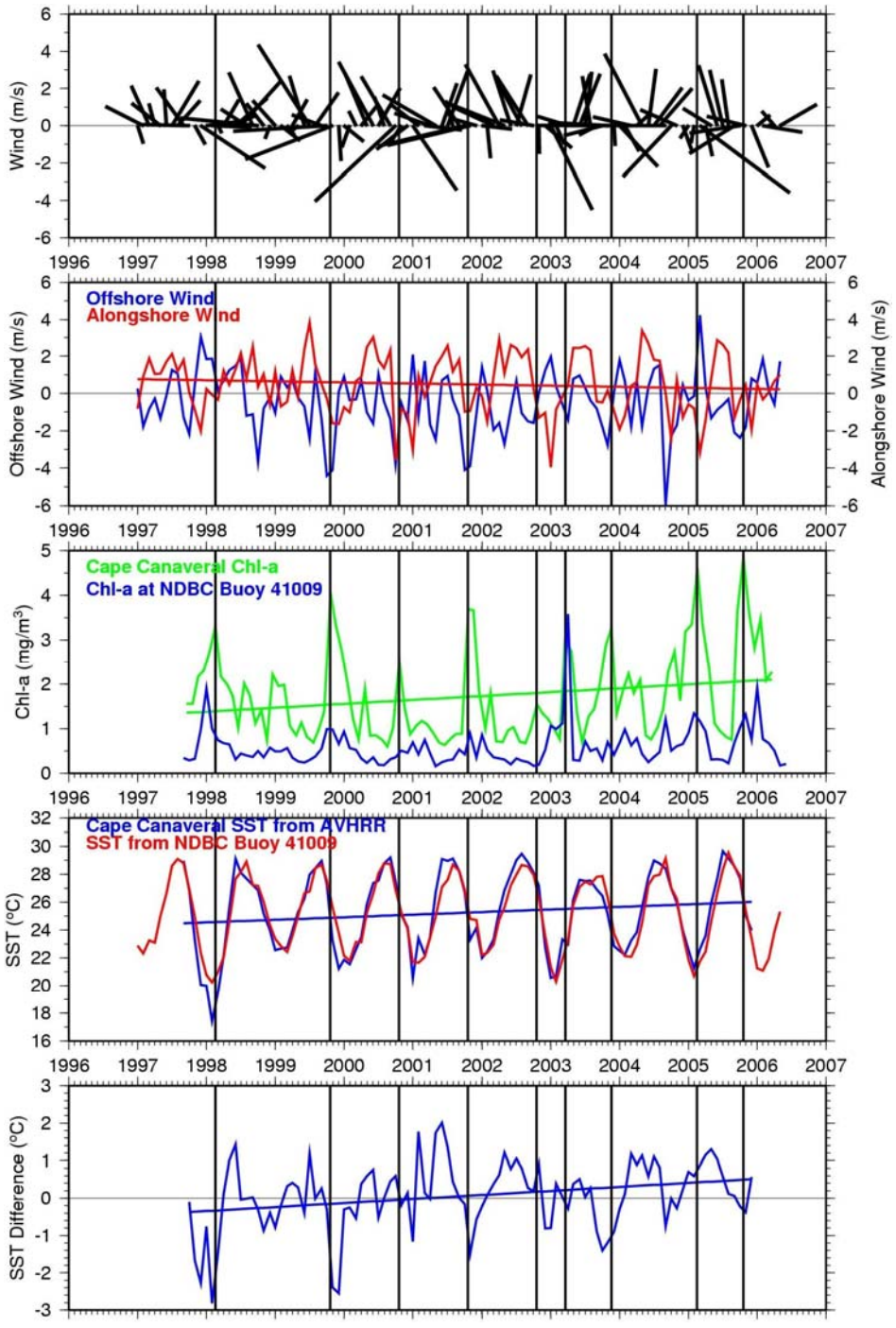

Figure 21. From top to bottom: time series of (1) vector winds from NDBC 41009, (2) offshore and alongshore components of the wind from NDBC 41009, (3) SeaWiFS Chl-a from the CC site (green) and from the NDBC 41009 site (blue), (4) AVHRR SST at CC and SST from NDBC 41009, and, (5) SST difference between NDBC and CC sites. Trend lines are superimposed on (2) through ((5).

March 2006), five of them occur in October, two in February, one in March, and one in November. Vertical lines have been placed on all the time series to mark the events. The Chl-a concentration has large nearshore peaks on February 1998,

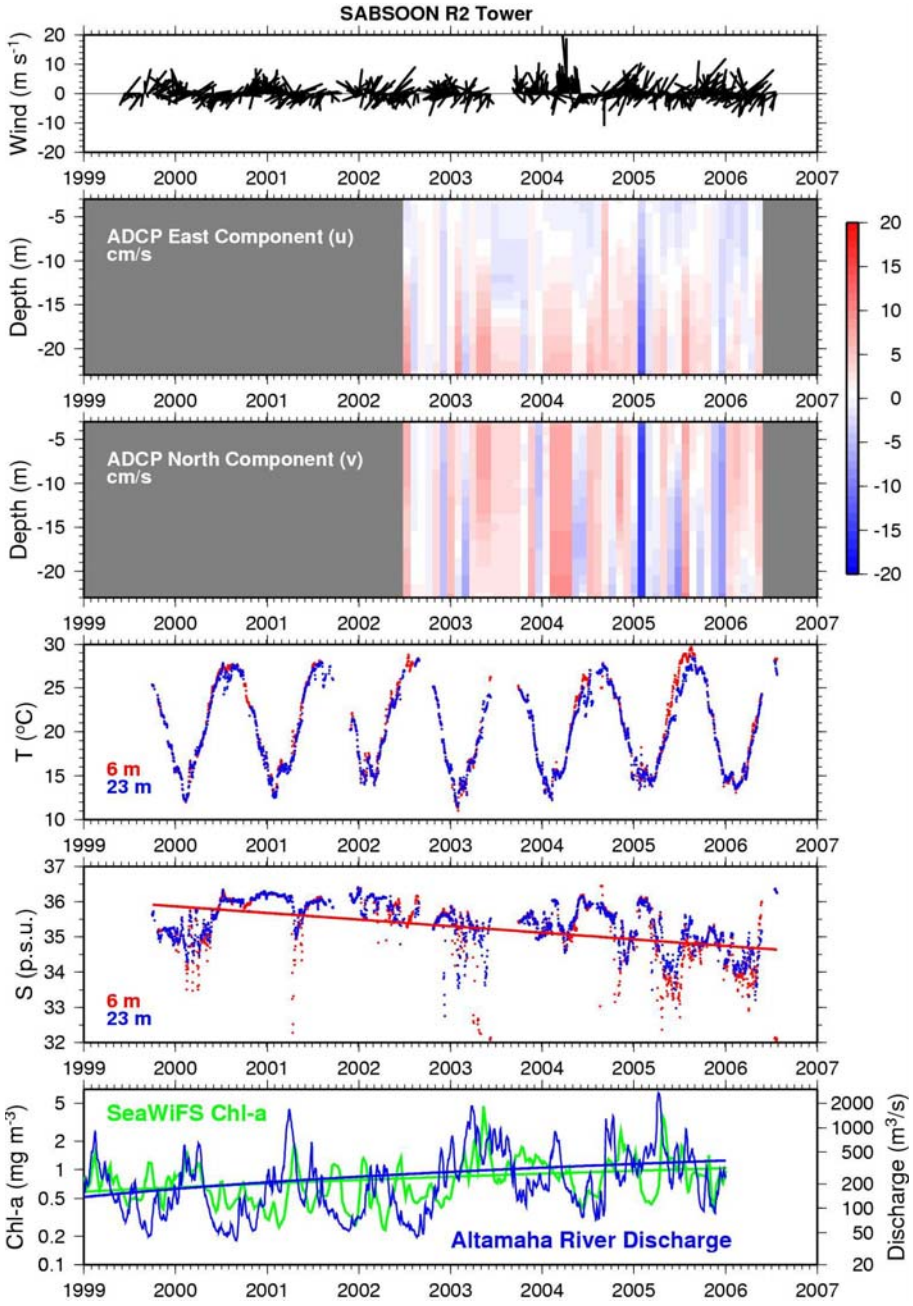

Figure 22. From top to bottom: time series at the SABSOON R2 Tower of (1) wind vectors, (2) ADCP east component current profiles, (3) ADCP north component current profiles, (4) *in situ* temperature at 6 and 23m, (5) *in situ* salinity at 6 and 23m, and (6) SeaWiFS Chl-a at the R2 Tower location and Altamaha River discharge. Trend lines are superimposed on (5) and (6).

March 2003, and February 2005, coinciding with peak discharges of the Altamaha River (see Figure 19) and after wind events with a strong southward component. Very likely, these high Chl-a events, which have a duration of several months, are related to the Altamaha River plume reaching the location via the southward geostrophic flow parallel to the salinity front, which is accelerated by the southward winds. The main wind direction is toward the north, mainly in summer when Chl-a reaches a minimum, probably because the northward winds prevent the Altamaha River plume to reach the region and summer warming reduces the mixed layer depth. The majority of the peak Chl-a events that occur in October and November coincide with negative SST differences (-1 to -2^{o}C) and southward winds. Since the southward winds are downwelling favorable, the SST reduction cannot be attributed to wind-driven upwelling. Two possible mechanisms for the SST drop and Chl-a increase are: (1) the southward winds promote advection of colder water with higher Chl-a from the north, and (2) the southward wind-driven flow interacts with the bathymetry to generate topographically-induced upwelling [*Blanton et al.*, 1981; *Janowitz and Pietrafesa*, 1982].

Figure 21 also shows some interesting trends in the nearshore location off Cape Canaveral. There is an upward trend in the Chl-a time series (~1 mg m^{-3} in 9 years) concurrent with a downtrend in the alongshore wind component (~1 m/s in 10 years), and an upward trend in SST (~2^{o}C in 9 years). The SST upward trend may be a result of a reduction of the upwelling-favorable (positive alongshore component) of the wind, and the increase in Chl-a (and CDOM) as a result of an increase in river discharge.

The influence of freshwater discharge on Chl-a is more pronounced further north in the Georgia Bight (GAB). Figure 22 shows time series of wind, ADCP current profiles, temperature (T) and salinity (S) at 6 and 23 meters (near surface and near bottom), and SeaWiFS Chl-a, with the Altamaha River discharge superimposed, at the location of the SABSOON R2 Tower 40 miles offshore of St. Catherines Island in the Georgia coast (see Figure 17). The tower is located in the middle shelf at a depth of ~25m and within 60 miles of the mouths of the Savannah and Altamaha Rivers. The wind and ADCP data are 3-day averages of hourly records, the Chl-a is from monthly SeaWiFS composites, and the Altamaha River discharge and T and S time series are daily averages. Both wind and currents are highly variable at the site. The currents are mainly wind-driven with numerous reversals from northeastward to southwestward throughout the period of available records (July 2002 to June 2006), which is shorter than the available period for the other parameters (1999-2006). Both T and S are uniform with depth, except during times of high river discharge, indicating a well-mixed water column throughout the year. This is because strong winds and tidal currents provide vigorous mixing for the relatively shallow middle shelf in the GAB. Low salinity events (less than 34 p.s.u.) occur during peak river runoff, which are accompanied by Chl-a peaks in excess of 2 mg m^{-3}, as shown in the bottom two tiers in Figure 22. A downward trend in salinity is quite clear due to an upward trend in river discharge and, consequently, an equivalent upward trend in Chl-a.

3.5 Charleston Gyre

The eastward deflection of the Gulf Stream off the Georgia-South Carolina coast has been discussed in various past studies [*Bane*, 1983; *Chao and Janowitz*, 1979; *Legeckis*, 1979; *Olson et al.*, 1983; *Singer et al.*, 1983]. It has been determined that the cause for this deflection is a topographic feature called the Charleston Bump. One result of the seaward deflection of the Gulf Stream, which may have important regional oceanographic consequences, is the existence of a volume of cool water just downstream of the deflection. The cool water is normally situated between the upper continental slope and the main body of the Gulf Stream in the area where it arcs from its deflection seaward cyclonically back toward the north, approximately offshore of Long Bay [*Bane*, 1983]. This is a sub-surface domelike structure also known as the 'cold dome'. Temperature, salinity, and nutrient properties indicate that upwelling is probably important in the maintenance of the dome [*Singer et al.*, 1983]. There is also evidence that doming occurs less frequently farther downstream from the deflection/cold dome region, but the doming there is probably due to the cold core cyclonic frontal eddies which travel downstream in the troughs of propagating Gulf Stream meanders [*Bane*, 1983; *Singer et al.*, 1983].

A semi-permanent cyclonic eddy, which was theoretically predicted [*Chao and Janowitz*, 1979], is situated in the trough of the deflection and it is called the Charleston Gyre. The upwelling associated with this cyclonic gyre produces an enhancement in the surface layer primary production that can be detected by ocean color satellites [*McClain and Atkinson*, 1985].

The Gulf Stream deflection by the Charleston Bump is modulated by the intensity and direction of the coastal winds. Figures 23 and 24, which consist of MODIS/Aqua SST and SeaWiFS Chl-a with surface currents superimposed, illustrate the variability of the Gulf Stream deflection for February, May, August, and November 2004. The eastward deflection is enhanced during February and November when the wind favors a southwestward flow on the SAB shelf. The deflection is much more attenuated in May when the wind reverses and favors a northeastward flow on the shelf.

The evolution of the Gulf Stream eastward deflection and the formation of cold core cyclonic frontal eddies are shown in the 7-day time series of images in Figures 25-26 (9, 16, 23, and 30 April 2003) derived from MODIS/Aqua SST, SeaWiFS Chl-a and superimposed surface currents. The SST (Figure 23) and Chl-a (Figure 26) were derived using 14-day running averages with a 7-day overlap to eliminate clouds, while the surface currents were derived from 7-day averages of QuikScat winds and Aviso geostrophic currents. Note that the trough of the Gulf Stream deflection has colder SSTs and higher Chl-a. Also, the meandering of the Gulf Stream caused by the deflection does not remain locked to the location of the Charleston Bump, at least its surface expression which is directly influenced by the locally wind-driven component of the flow and more weakly coupled to the bottom topography. The Charleston Gyre upwelling also affects other biological properties such as dissolved organic matter (DOM) and

particulate organic carbon (POC). Figure 27 shows images of SeaWiFS-derived OC4v4 and GSM01 (Garver-Siegel-Maritorena) Chl-a, GSM01 detritus+gelbstoff absorption coefficient at 443 nm, adg(443), which is an indicator for DOM, and POC for 13 April 2003. The spring of 2003 was very wet with large river discharges into the SAB shelf. The GSM01 algorithm shows that the nearshore

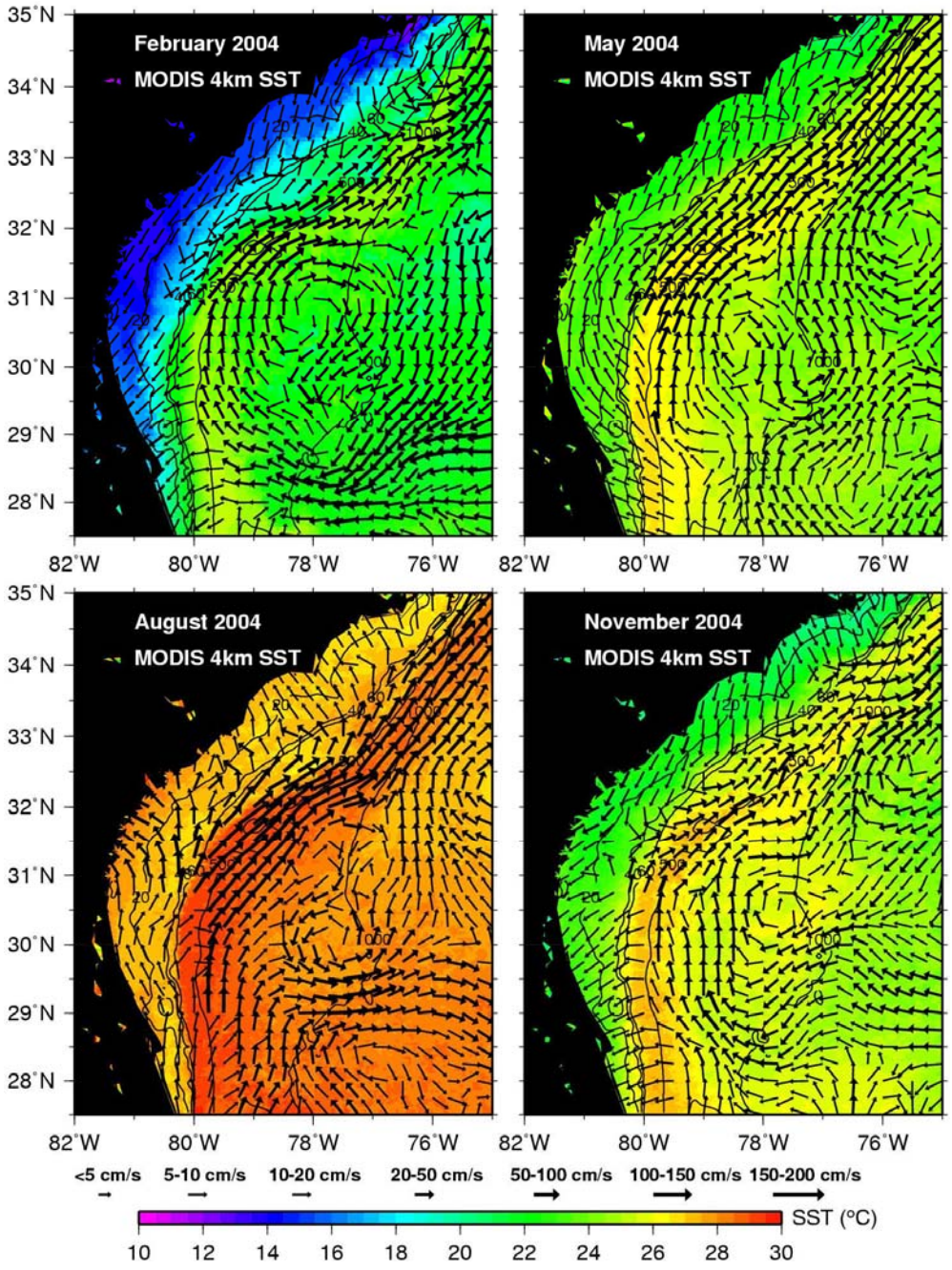

Figure 23. Monthly composites of MODIS-Aqua 4km SST and surface currents for February, May, August, and November 2004.

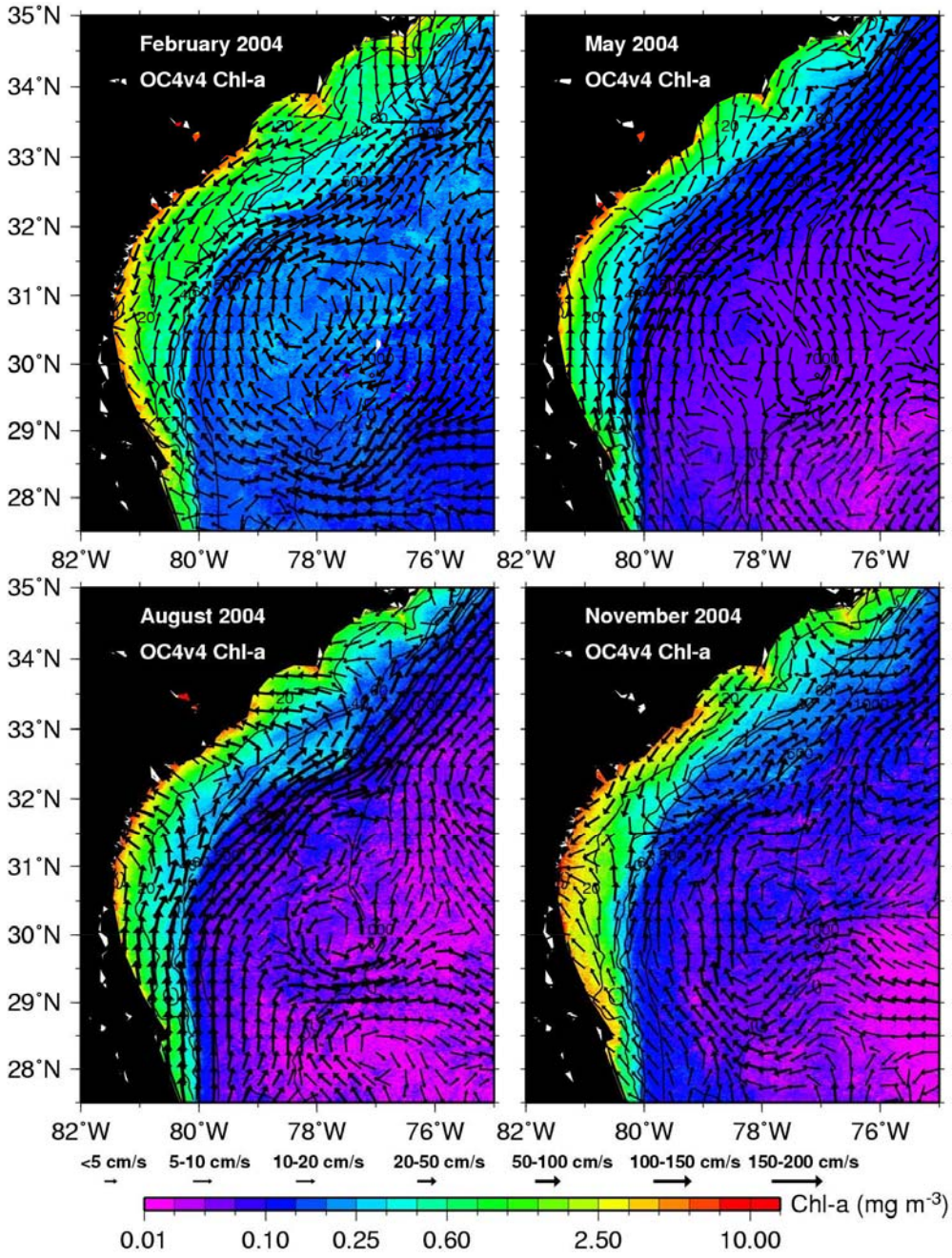

Figure 24. Monthly composites of SeaWiFS Chl-a and surface currents for February, May, August, and November 2004.

waters contain large concentrations of DOM and not as much Chl-a. The elevated inner shelf values shown by the OC4v4 algorithm may be an overestimate. All of these parameters are elevated in the cyclonic flow region known as the Charleston Gyre. The elevated concentrations may not be only a result of upwelling in the center of the gyre but also in part a consequence of

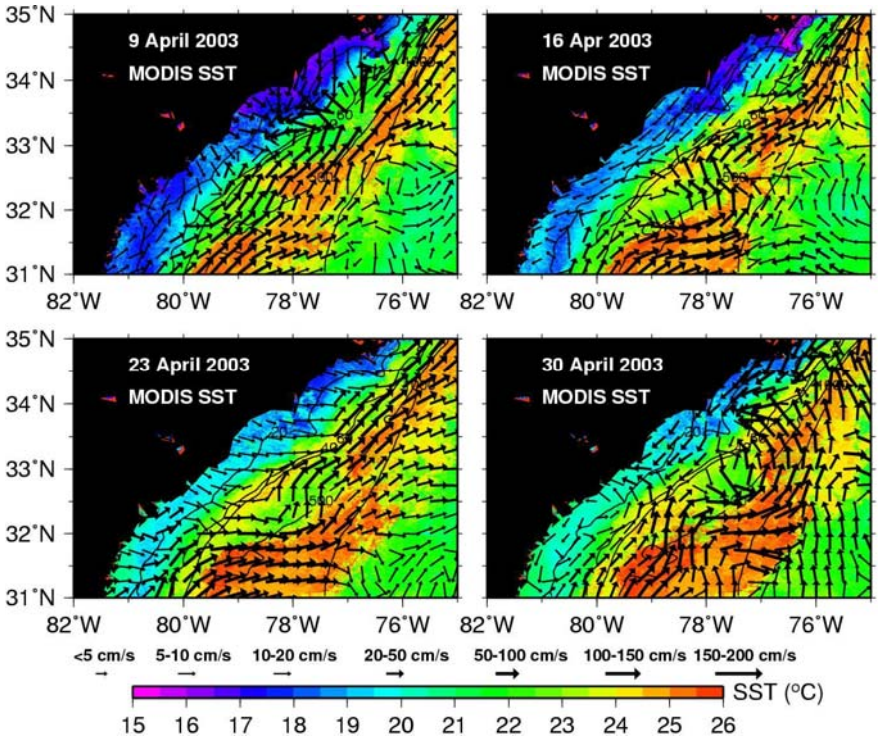

Figure 25. Sequence of MODIS-Aqua SST and surface currents in the Charleston Gyre region for 9, 16, 23, and 30 April 2003. Surface current vectors are superimposed on the images.

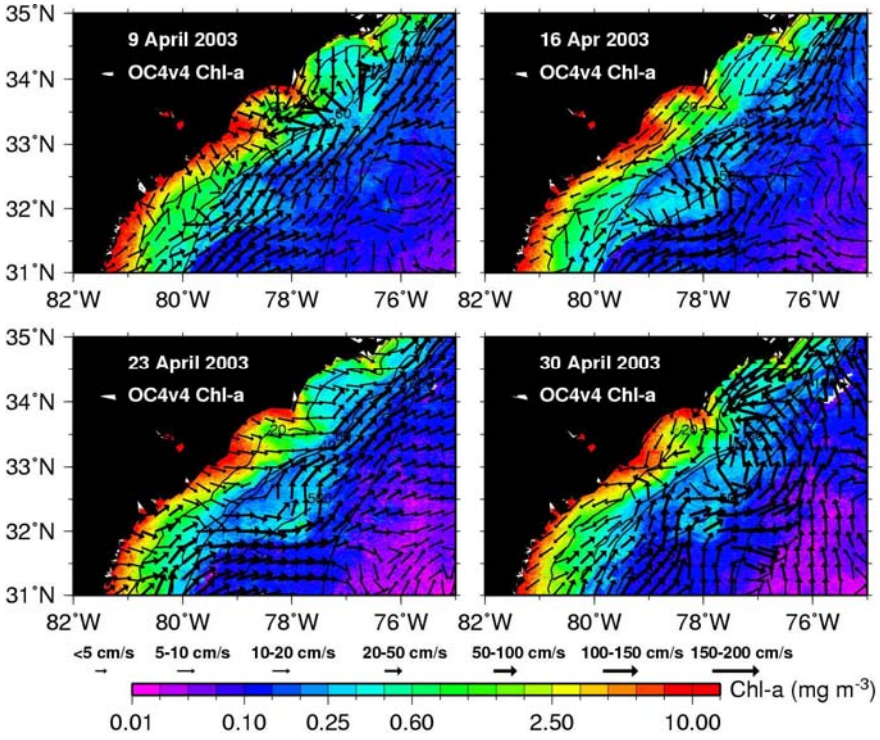

Figure 26. Sequence of SeaWiFS Chl-a and surface currents in the Charleston Gyre region for 9, 16, 23, and 30 April 2003. Surface current vectors are superimposed on the images.

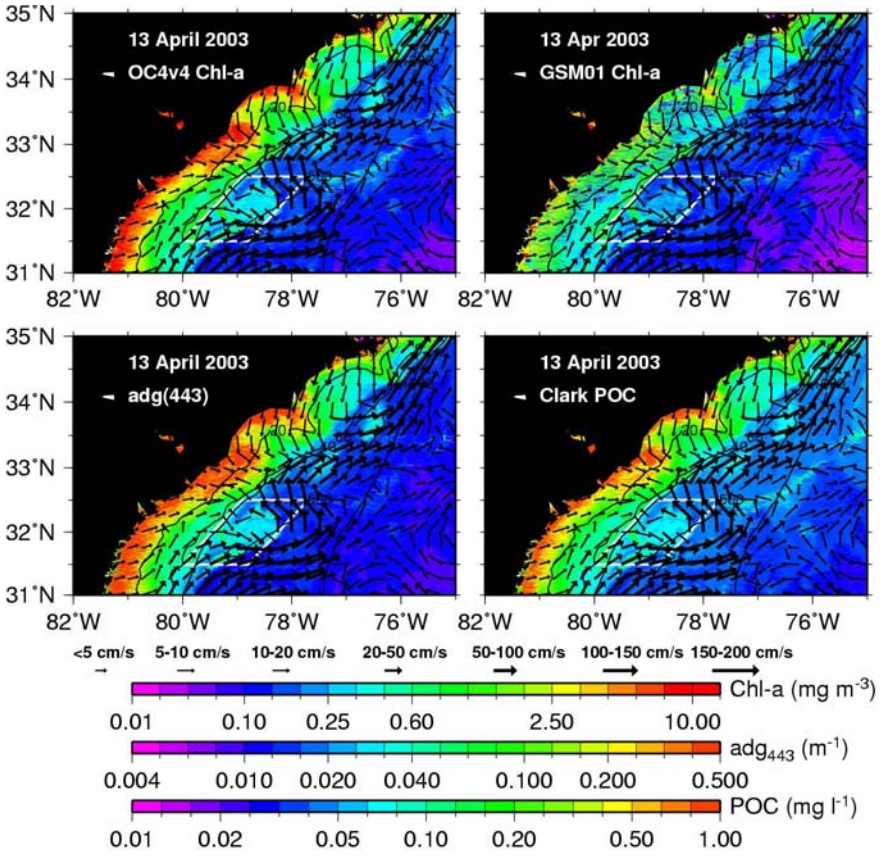

Figure 27. SeaWiFS-derived images of OC4v4 Chl-a, GSM01 Chl-a, GSM01 adg(443), or acdm(443), and POC from the Clark algorithm for the Charleston Gyre (CG) region. Surface current vectors are superimposed on the images. The white polygon delimits the CG region for analysis.

shelf DOM and POC being advected offshore by the surface currents. Also, the Charleston Gyre is not a permanent feature and thus difficult to isolate from cold core frontal eddies, which eventually propagate downstream and coalesce into the Gulf Stream.

A time series analysis of dynamic height and Chl-a was conducted to investigate the correlation between these two parameters and their primary modes of variability. Time series of averaged SeaWiFS-derived OC4v4 Chl-a and Aviso dynamic height within the limits of the white polygon bounding the likely position of the Charleston Gyre (see Figure 27) are shown in Figure 28. To better illustrate the correlation between the two parameters, the DHT was inverted, as the DHT in the interior of the gyre where upwelling takes place is anti-correlated with Chl-a. The wavelet and cross-wavelet transforms for DHT and Chl-a are shown in Figure 29. There is a highly coherent seasonal cycle in

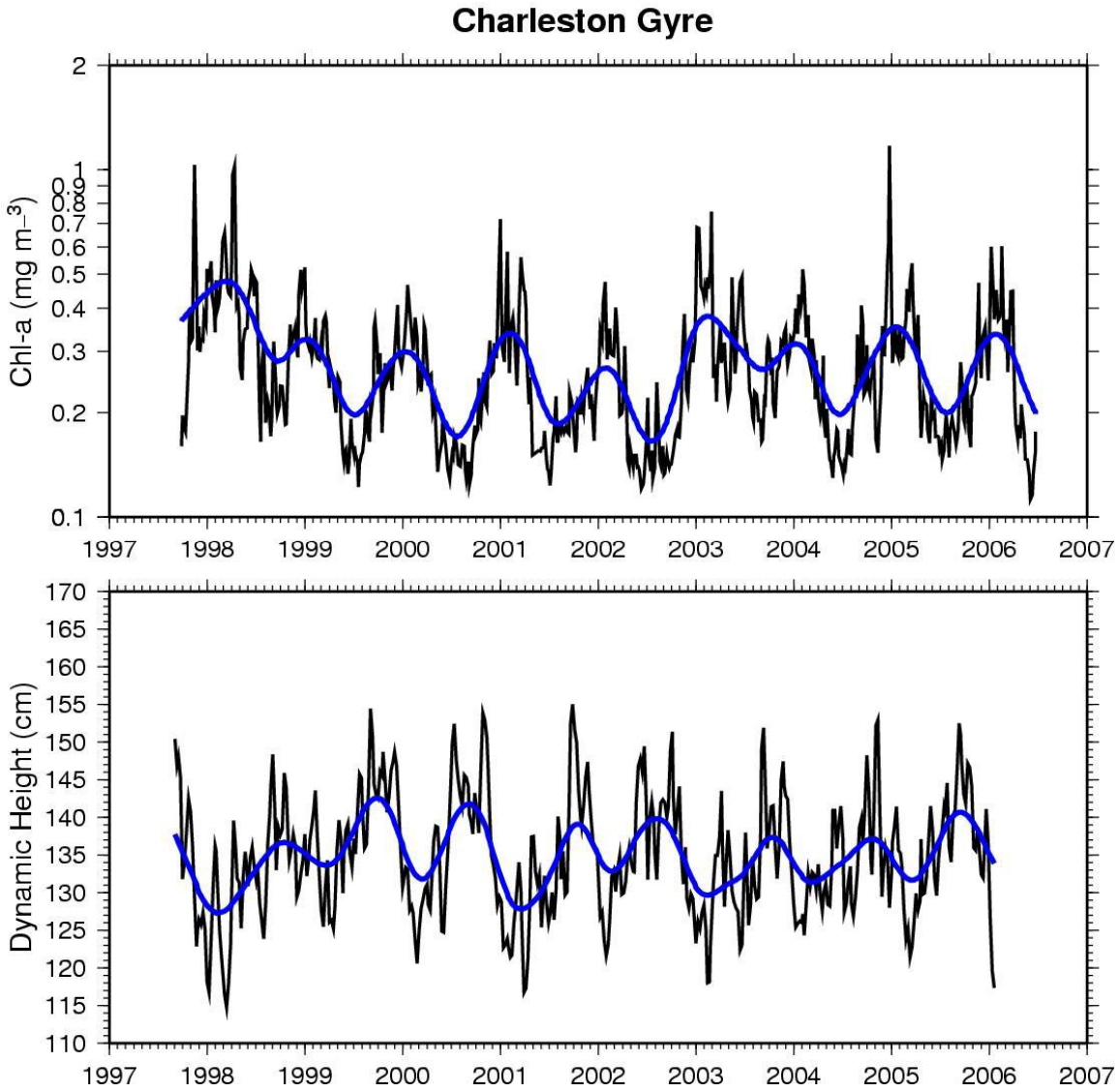

Figure 28. Time series of SeaWiFS Chl-a (top) and inverted Aviso dynamic height (bottom) averaged within the limits of the white polygon (see Figure 25) delimiting the Charleston Gyre region.

both DHT and Chl-a within the gyre location throughout the period of available concurrent data (1998-2006), with the Chl-a leading the DHT maximum by a few degrees. The strong seasonal cycle is likely a result of surface thermal forcing inducing changes in the MLD and thus Chl-a. Coherence is more episodic for periods less than 3 months (0.25 years), an indication of the ephemeral nature of the surface expression of the gyre upwelling identified by the relatively high Chl-a patches. We examined an animation of SeaWiFS Chl-a (J. O'Reilly's personal communication) obtained from the entire mission period (~9 years) and we were only able to identify 12 distinct apparent manifestations of the Charleston Gyre (non-propagating events).

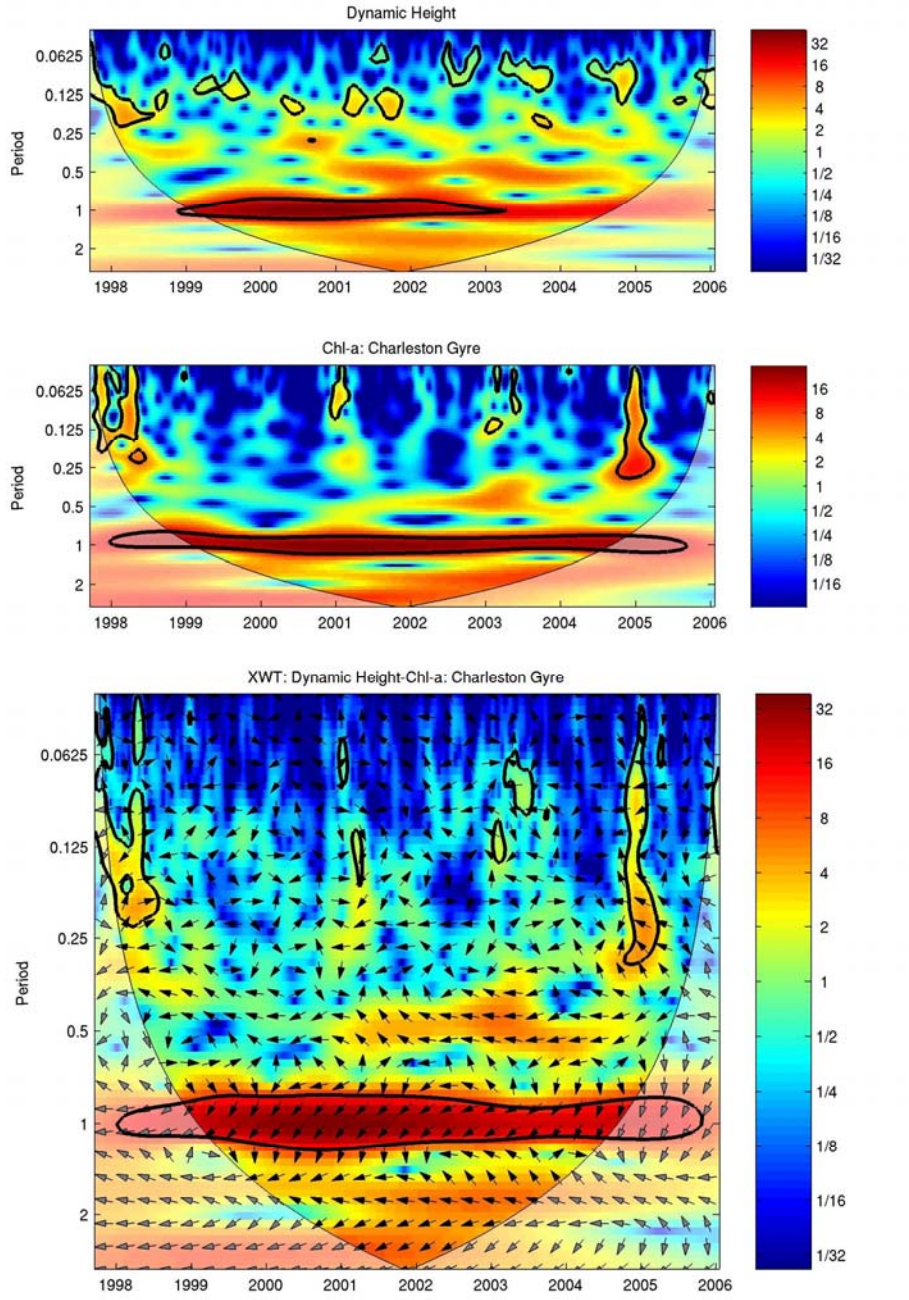

Figure 29. From top to bottom: (1) wavelet transforms for dynamic height and (2) Chl-a, and cross-wavelet transform between dynamic height and Chl-a for the Charleston Gyre time series of Figure 26.

3.6 Sea Surface Salinity Front

Based on hydrographic data from four oceanographic cruises in the GAB conducted on September and December 1973, and April and July 1974, *Atkinson* [1978] calculated the volume distribution of freshwater in the GAB shelf with the

key assumption that GAB waters would have a salinity of 36 p.s.u. if no runoff waters were present. The study revealed that salinities in the shelf waters decrease towards the coast and exhibit estuarine type structure with higher salinities near bottom. A salinity maximum usually occurs well east of the shelf break at depths of 100-200m. The offshore extent of river runoff extended 56 km offshore on average in the northern GAB (32.5^{o}N) but less than 3 km in the south (30^{o}N). The surface salinity data were obtained from cruise reports [*Atkinson*, 1975; *Atkinson*, 1976] and reproduced in Figure 30.

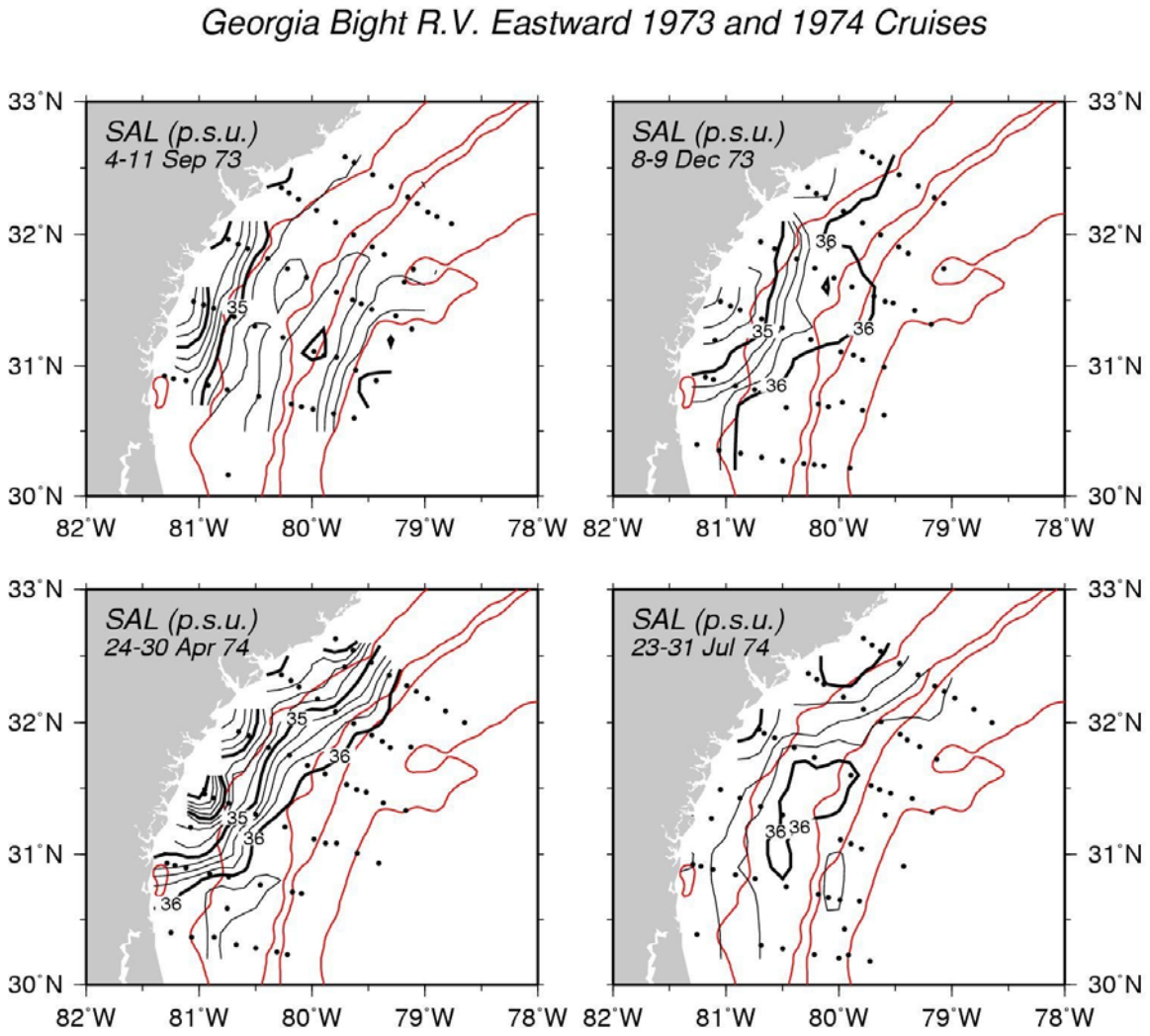

Figure 30. Surface salinity maps from data collected during four Georgia Bight cruises conducted in September 1973, December 1973, April 1974, and July 1974. The salinity contours are black and the 20, 40, 60, and 500m isobaths are shown in red.

The inner shelf of the SAB is mainly characterized by a coastal low salinity frontal zone resulting from the interaction between freshwater discharges, tidal mixing and wind forcing [*Oey*, 1986]. *Chen* [2000], using a 3D primitive turbulent closure equation model, analyzed the physical processes that control the episodic cross-frontal transport over the SAB inner shelf. Results from this study

reveal that significant cross-frontal water exchange occurred under upwelling-favorable wind conditions through the detachment of isolated low-salinity lenses at the outer edge of the front. Furthermore, the study showed that the formation of isolated lenses is a 3D feature associated with complex non-linear processes that depend on the amount of multiple river discharges, direction and magnitude of the wind, and tidal mixing. As previously discussed in Section 3.4, freshwater discharge provides a major source of DOM to the SAB shelf region. Therefore, cross-frontal transport of low-salinity waters may provide an important conduit of carbon between the inner and middle shelves. Surface DOC and POC maps reproduced with data obtained from the 1973-1974 GAB cruises [*Atkinson*, 1975; *Atkinson*, 1976] are shown in Figures 31 and 32, respectively. The surface DOC

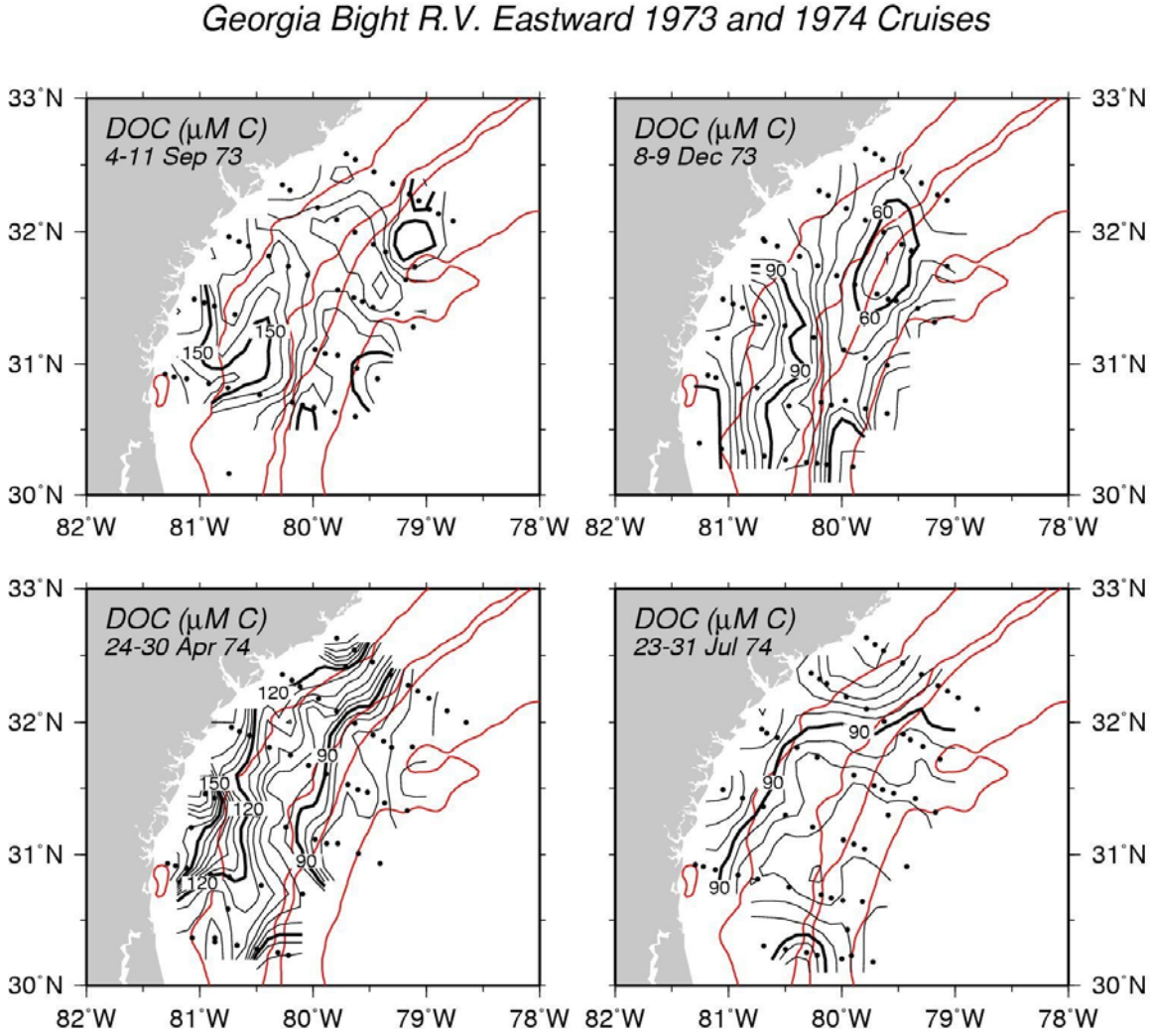

Figure 31. Surface DOC maps from data collected during four Georgia Bight cruises conducted in September 1973, December 1973, April 1974, and July 1974. The DOC contours are black and the 20, 40, 60, and 500m isobaths are shown in red.

distribution generally decreases offshore with highest values near the coast where the river sources are indicated by the low salinity tongues in Figure 30.

Note that DOC concentrations are highest in April following the peak runoff in February (no data available for this month). The surface POC concentration maps in Figure 32 are given in the same carbon units (μM C) used for DOC for comparison. In general, the DOC surface concentration is 3 to 5 times larger than the POC surface concentration.

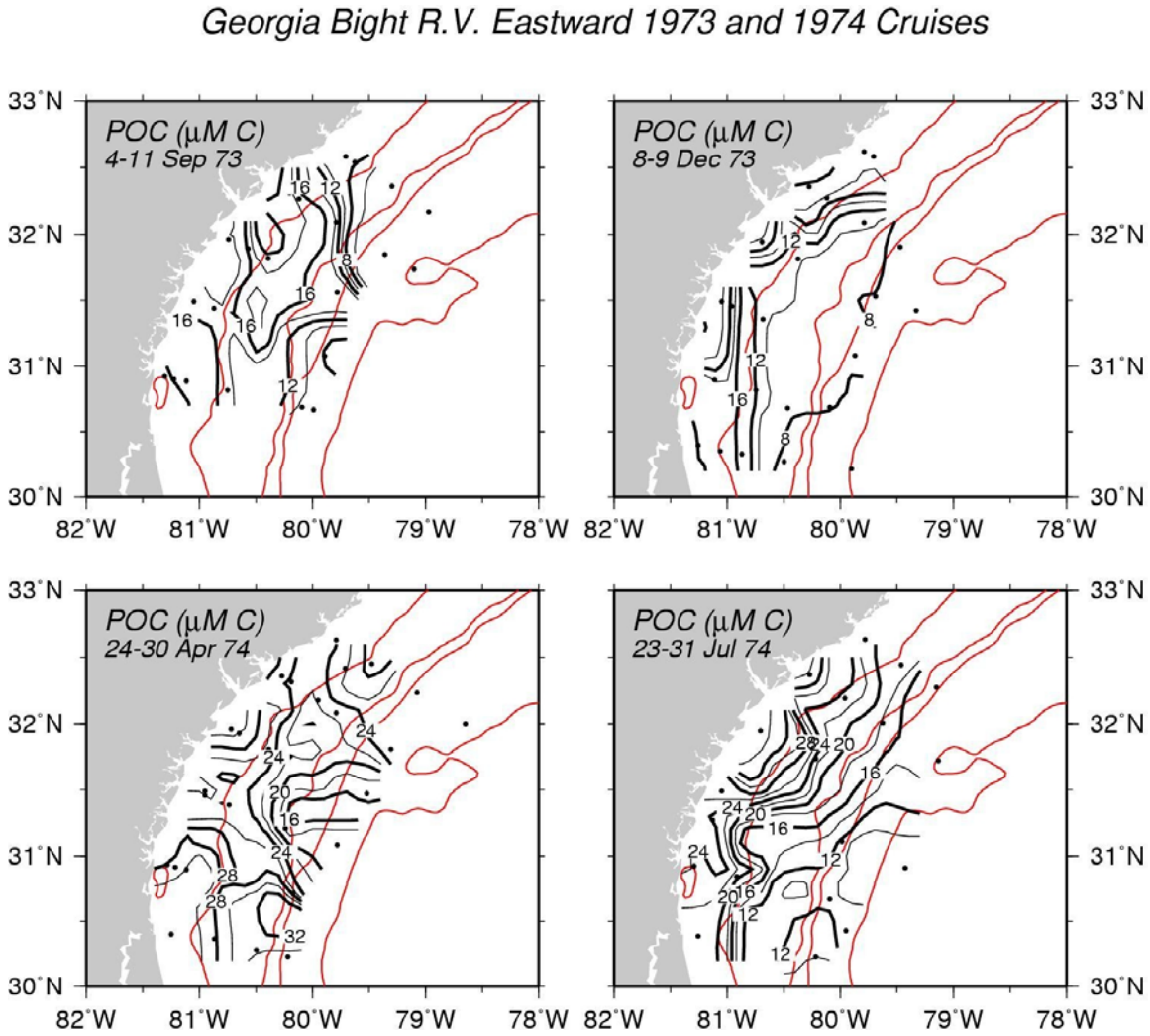

Figure 32. Surface POC maps from data collected during four Georgia Bight cruises conducted in September 1973, December 1973, April 1974, and July 1974. The POC contours are black and the 20, 40, 60, and 500m isobaths are shown in red.

The strong absorption by CDOM in the violet-to-blue region of the visible spectrum provides an optical signal that can be detected in ocean color satellite imagery. Figure 33 shows examples of SeaWiFS-derived absorption coefficient by colored detrital material (CDOM plus non-living particulate organic matter) at 443nm, $a_{CDM}(443)$, using the Garver-Siegel-Maritorena 2001 [*Garver and Siegel*, 1997; *Maritorena et al.*, 2002] semi-analytical algorithm (GSM01). Images are shown for 2 December 2002, and 23 April, 31 May, and 26 August 2003. Based on analyses of samples from a number of cruises seaward of the turbid coastal

zone [*Nelson and Guarda*, 1995], most of the a_{CDM} signal appears to be contributed by CDOM. While a_{CDM} cannot be considered a conservative tracer, the signal in the images of Figure 30 does indicate the distribution of lower salinity water masses on the shelf. The area of high a_{CDM} is mostly confined to the nearshore in winter but expanded during spring until it extended seaward to the shelf break. In late May 2003 the river discharge decreased significantly (see Figure 19) and thus a reduction of a_{CDM} as seen in Figure 33c. There was a subsequent increase of river discharge in summer that accounts for the increase of a_{CDM} in August 2003 (Figure 33d). Also, the amount of freshwater being discharged during 2003-2006 was substantially greater than during 1999-2002.

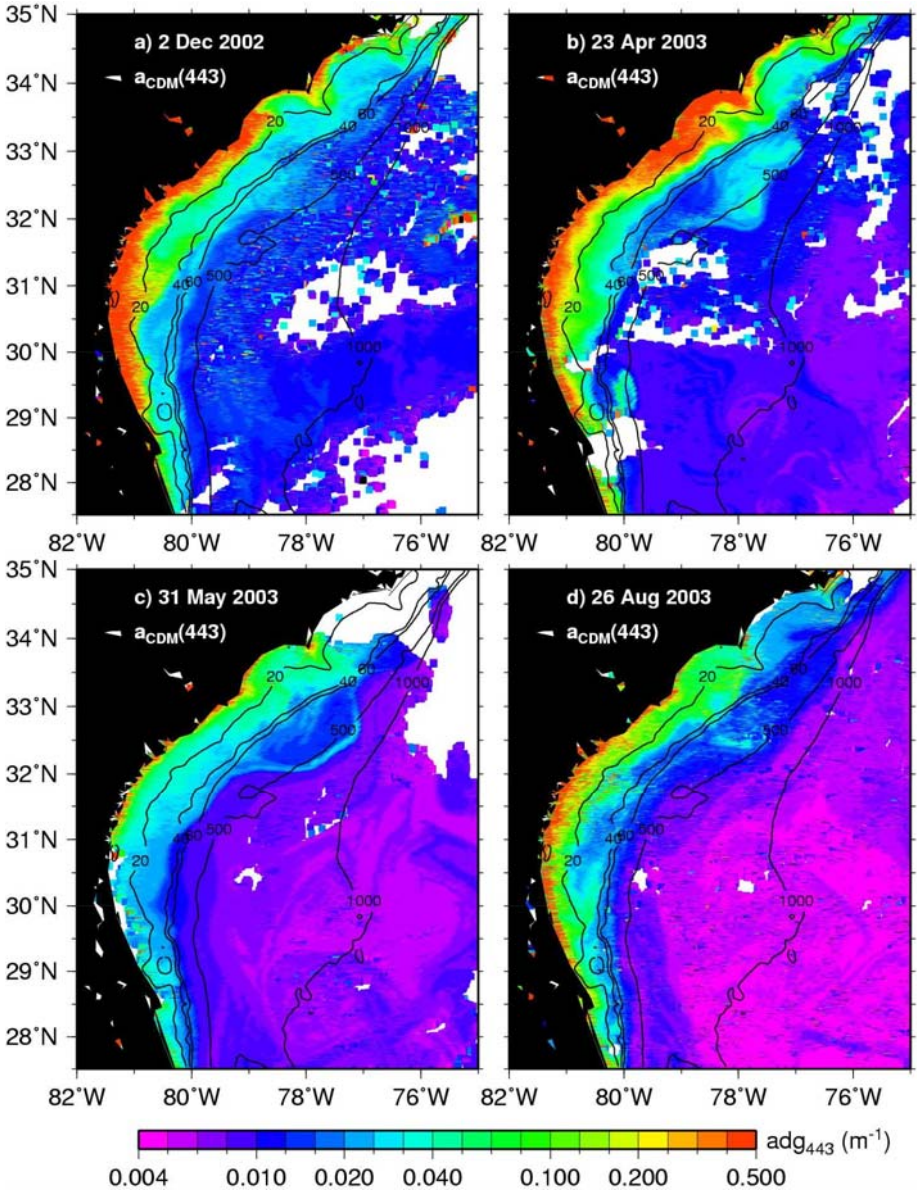

Figure 33. Sequence of SeaWiFS-derived GSM01 $a_{CDM}(443)$ images for (a) 2 December 2002, (b) 23 April 2003, (c) 31 may 2003, and (d) 26 August 2003.

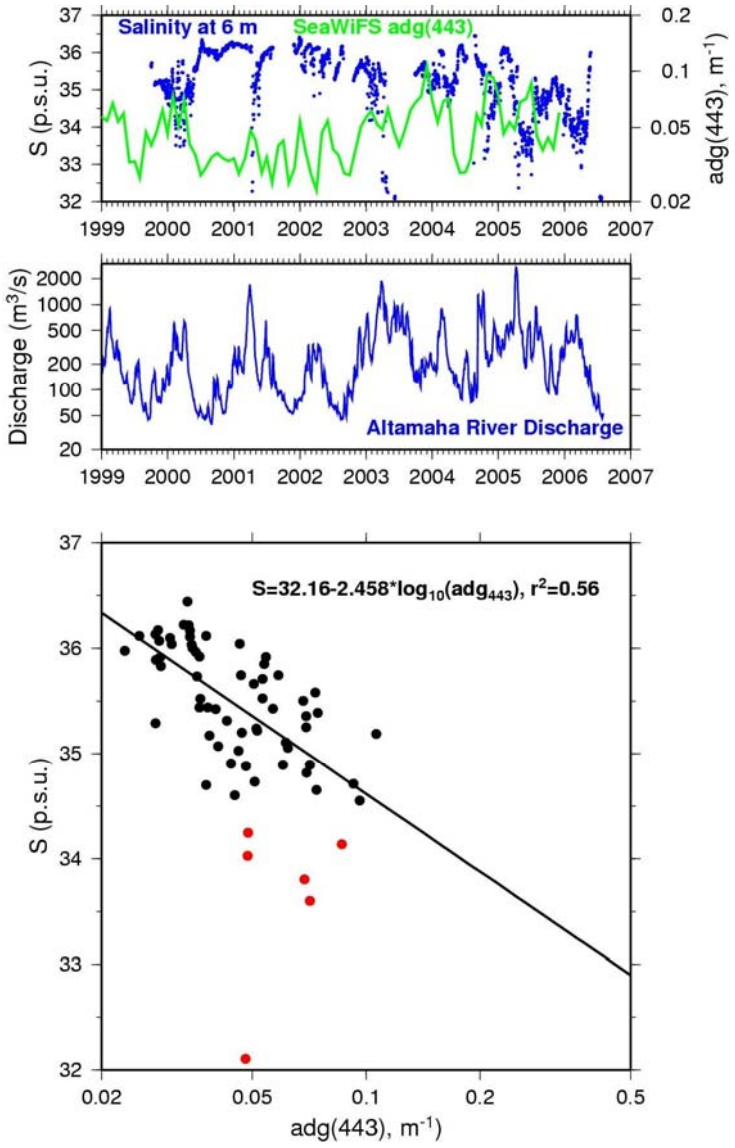

Figure 34. From top to bottom: (1) In situ salinity at 6m and SeaWiFS acdm(443) at SABSOON R2 Tower, (2) Altamaha River discharge, and (3) scatter plot of salinity at 6m and SeaWiFS acdm(443). The data displayed in the scatter plot was monthly averaged.

The overall negative relationship of CDOM absorption and salinity (*S*) is well known. For example, *Kowalczuk et al.* [2003] derived a regression between CDOM absorption at 350 nm and salinity based on *in situ* measurements around Cape Fear and Onslow Bay, N.C. The regression equation is as follows: $a_{CDOM}(350) = 26.281 - 0.717*S$; and the correlation coefficient for this relationship was r^2=-0.96, N=81. However, to obtain salinity from satellite ocean color data, an algorithm relating CDOM absorption to satellite reflectances would be also required. To our knowledge, no such algorithm has been published for SAB shelf waters. Therefore, as a first attempt to retrieve salinity from satellite ocean color data, we used a combination of SeaWiFS-derived GSM01 $a_{CDM}(443)$

and concurrent near surface in situ salinity data to obtain a regression equation relating salinity to $a_{CDM}(443)$.

Figure 34 shows time series of *in situ* salinity near the surface (at 6m) from SABSOON R2 tower (see Figure 17 for location), SeaWiFS-derived $a_{CDM}(443)$ at the same location, Altamaha River discharge, and a scatter plot of salinity versus $a_{CDM}(443)$ based on monthly averages of the two parameters. A linear regression of S versus $a_{CDM}(443)$ yields the relationship:

$$S = 32.16 - 2.458 \log_{10} a_{CDM}(443) \qquad (8)$$

The correlation coefficient (r^2) is 0.56, which means that nearly 60% of the salinity variance can be explained by the variability in $a_{CDM}(443)$. The time series of Figure 34 show that low salinity events are correlated with Altamaha River high discharge events and elevated $a_{CDM}(443)$. The dots on the *S* vs. $a_{CDM}(443)$ plot are considered outliers and received less weight by the 'robust' least squares fit method used in MatLab [*DuMouchel and O'Brien*, 1989].

Seasonal composites of SeaWiFS-derived $a_{CDM}(443)$ are shown in Figure 35. It is clear from these images that the seasonal cycle of $a_{CDM}(443)$ on the SAB shelf is influenced by the river discharge, with highest values during winter-spring and lowest values in summer. Using Equation (8) and monthly composites of $a_{CDM}(443)$ for the SeaWiFS mission period, seasonal composites of salinity were derived and presented in Figure 36. Although the salinity absolute values should be treated with caution, the salinity distribution and gradients seem to be consistent with low values in the inner shelf and gradual increase offshore towards the Gulf Stream western boundary. Using the criterion of *Atkinson* [1978], e.g., the ocean water undiluted by river discharge having a salinity of 36 p.s.u., we represent the offshore front that marks the transition between coastal and oceanic waters by the 36 p.s.u. contour line, as shown in Figure 36. In winter, the front is located along the 60m isobath, except north of the Charleston Bump where it extends further offshore due to the eastward deflection of the Gulf Stream. The front moves gradually westward towards summer, when it lies within the middle shelf immediately offshore of the 20m isobath, and then begins to move towards the shelf break in autumn. This coastal-oceanic salinity frontal motion is a combination of changes in freshwater volume on the shelf and seasonal excursions of the Gulf Stream western boundary via changes in the size of the NASG. There may also be changes in the salinity front due to local air-sea freshwater flux (evaporation-precipitation) which were not address in this study.

3.7 Heat Flux and Chlorophyll Variability

The net heat flux (Q_n) exchange between the ocean and atmosphere is given by

$$Q_n = Q_{Sol} + Q_L + Q_S \qquad (9)$$

Where Q_{Sol} is the solar radiation (longwave plus shortwave) reaching the ocean surface, Q_L is the latent heat exchange, and Q_S the sensible heat exchange.

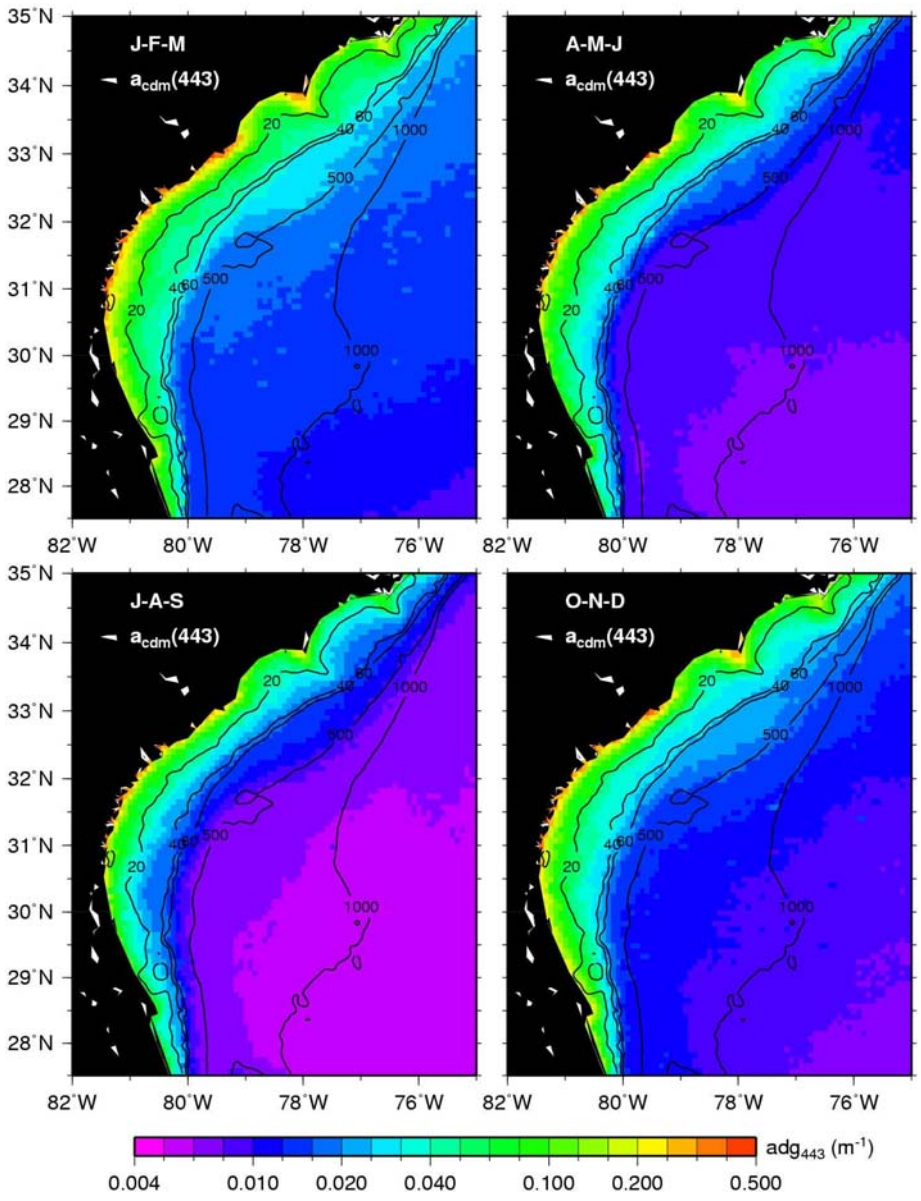

Figure 35. SeaWiFS derived seasonal climatology of $a_{CDM}(443)$. The 20, 40, 60,500, and 1000m bathymetry contours are superimposed on the images.

Changes in Q_n depend primarily on seasonal changes in solar radiation, wind speed, air-sea temperature difference, and sea state. These changes in net heat flux drive, among other effects, upper-ocean vertical mixing and, consequently, Chl-a variability. Comprehensive studies were conducted on the air-sea exchange processes and the resulting atmospheric boundary layer and oceanic responses during winter in the SAB under the Genesis of Atlantic Lows Experiment (GALE) and reported in a special issue of the *Journal of Geophysical Research* [*Bane*, 1989]. One area of concentration of these papers is the effect

of a large storm system that passed through the SAB region at the end of January 1986 when an intense cold-air outbreak covered the entire region.

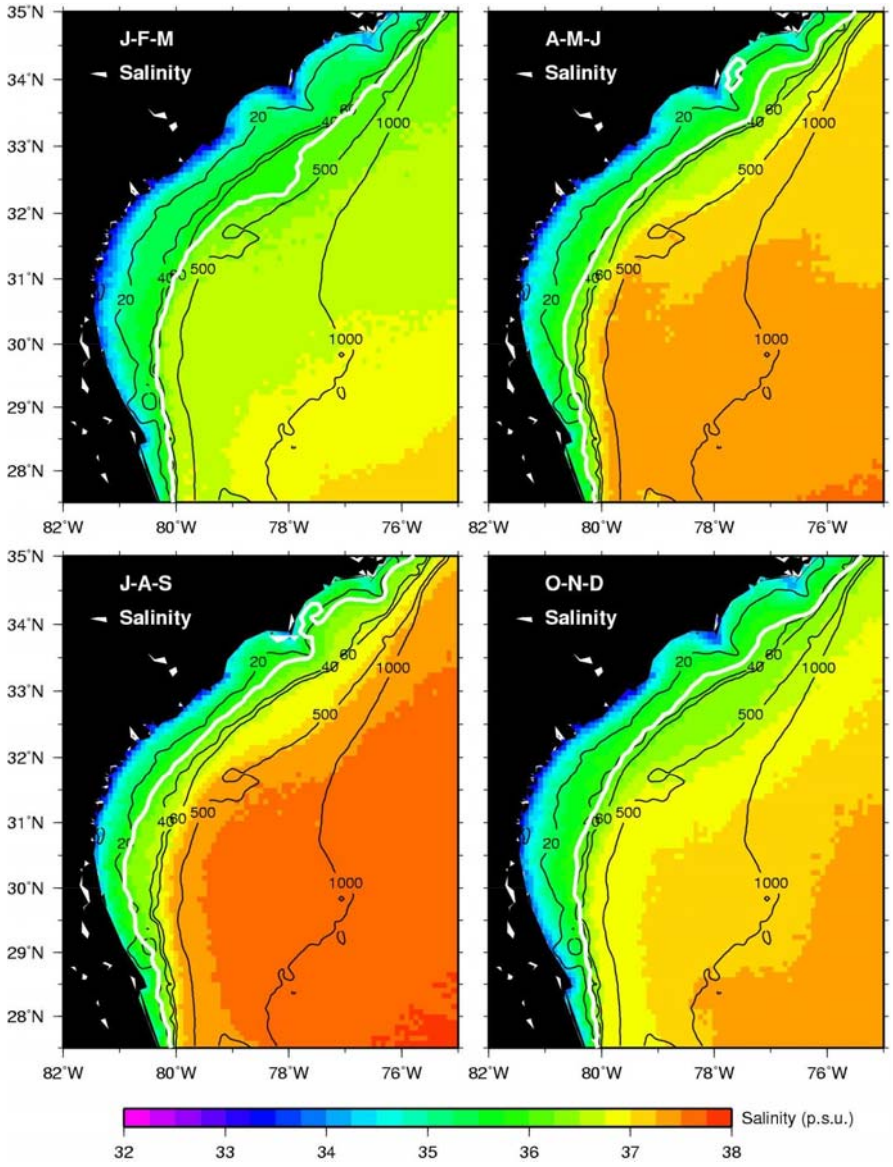

Figure 36. Seasonal surface salinity maps obtained from the regression in Figure 32 and using acdm(443) derived from the GSM01 algorithm and SeaWiFS reflectances. The black lines are bathymetry contours and the thick white line is the 36 p.s.u. salinity contour.

Extreme air-sea fluxes, and consequently vertical mixing and circulation variability, occurred during this event.

Five-day time series of SeaWiFS-derived (OC4v4) Chl-a and WHOI OAFlux net heat flux are shown in Figure 37 for a site in the middle shelf just south (30.5^{o}N and 80.5^{o}W) off the Georgia-Florida border. Low-pass filtered time series (thicker black lines) are superimposed on both series, which highlight the seasonal variability. The seasonal cycle between the two series is anti-

correlated, meaning that low heat flux corresponds to high Chl-a, and vice-versa. This behavior is consistent with the typical effect of vertical mixing on nutrient renewal in the euphotic zone via vertical mixing. In winter, the net heat flux is out

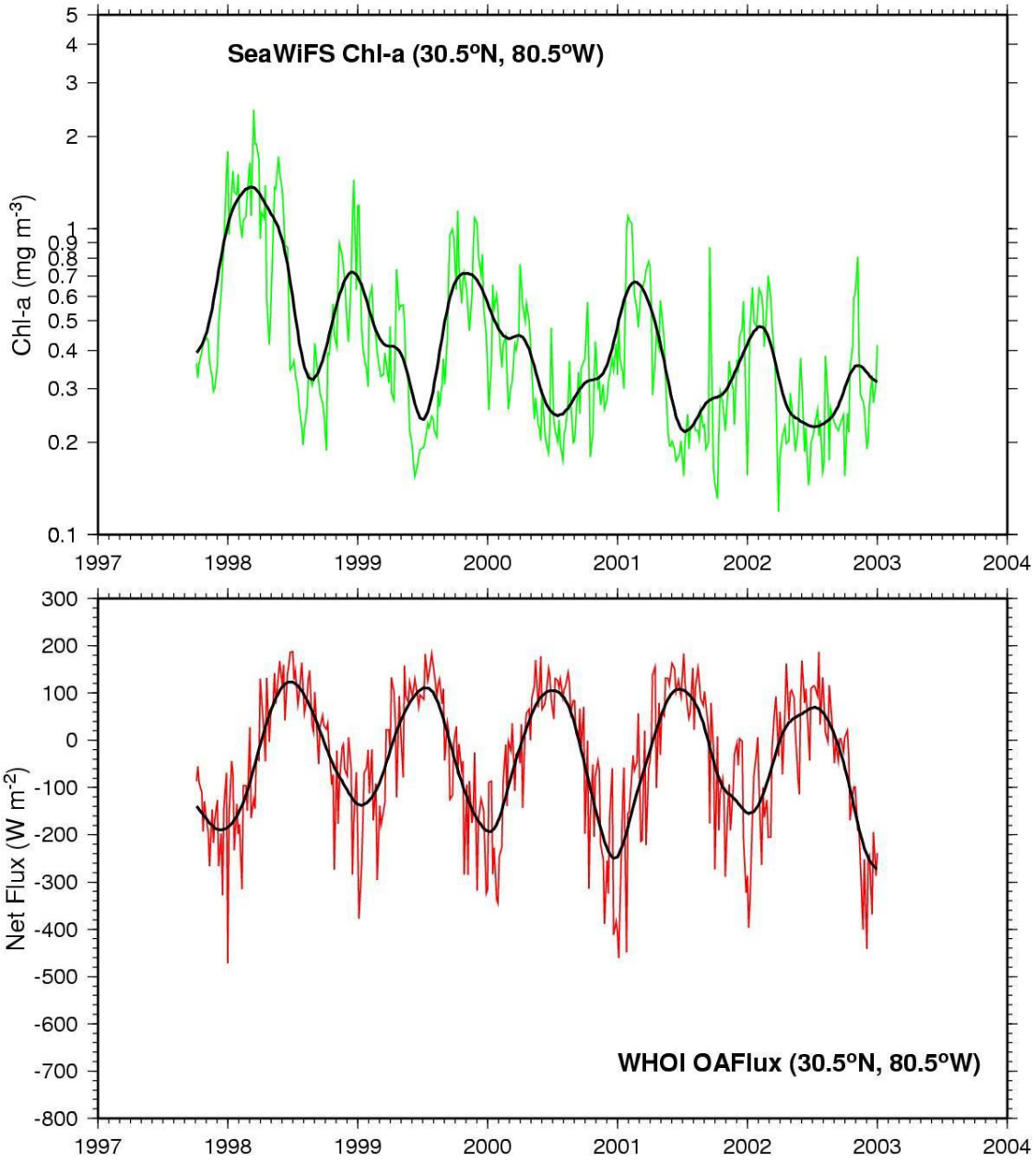

Figure 37. Time series of SeaWiFS Chl-a (top) and net air-sea heat flux (bottom) at a location near R2 Tower in the SAB middle shelf. The thick black lines are the low-pass filtered data showing a clear seasonal cycle.

of the ocean (negative) promoting more intense vertical mixing via convective overturning. The mixed layer gets deeper and nutrients can be brought to the euphotic zone to increase photosynthesis. In summer, the increase in solar radiation increases the heat flux (positive) into the ocean and warms up the

surface waters creating a shallower mixed layer within which nutrients are quickly consumed reducing photosynthesis and, consequently, Chl-a concentration.

The time scales involved in this process are clearly shown in the Q_n and Chl-a wavelet transforms, and corresponding wavelet cross transform shown in

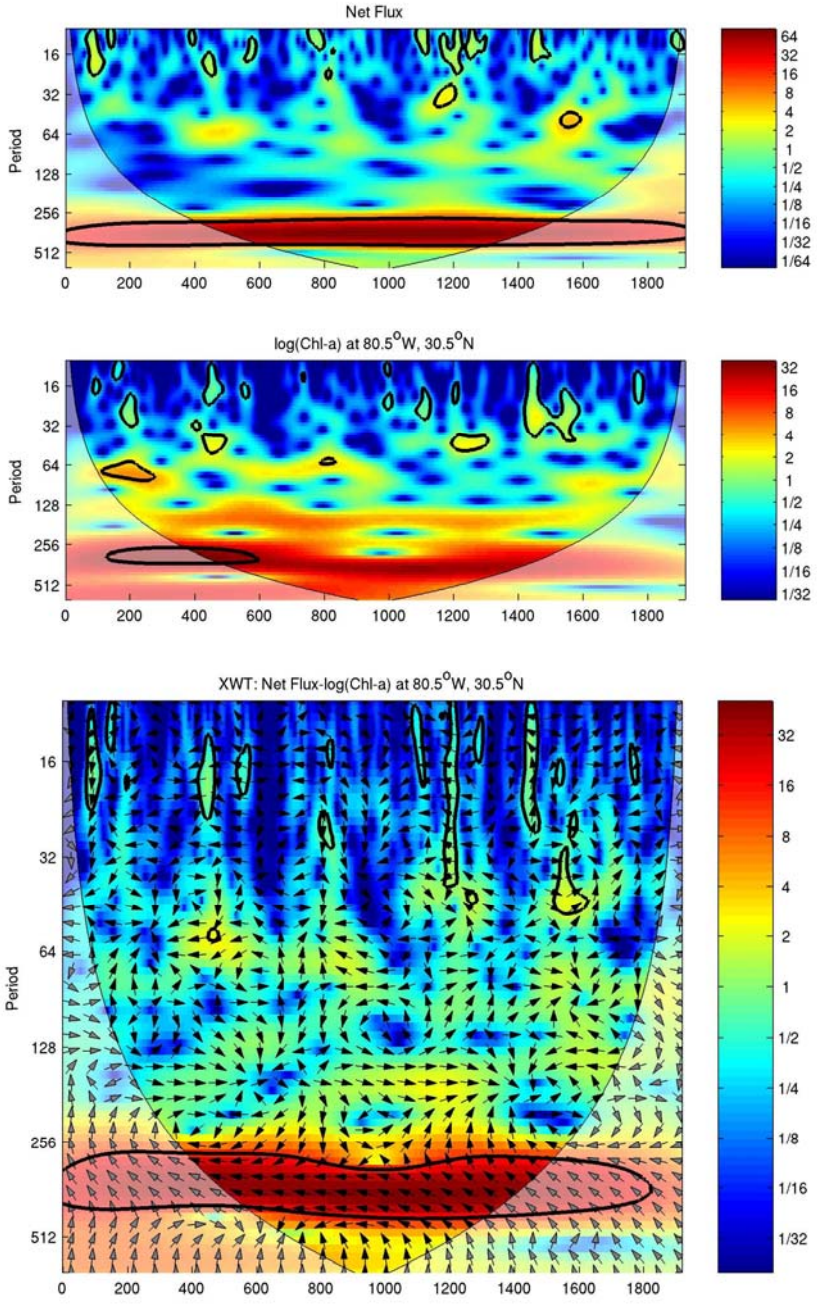

Figure 38. From top to bottom: (1) net heat flux wavelet transform, (2) SeaWiFS log(Chl-a) wavelet transform, and (3) cross-wavelet transform between net heat flux and log(Chl-a). The transforms are based on time series data displayed in Figure 37.

Figure 38. The common seasonal cycle is clearly shown by a band of high anti-correlation (red area inside thick contour with arrows pointing to the left) that extends throughout the series centered at 365 days. There are also episodic and short duration events of high correlation in the higher frequency band with periods ranging from 10 days (Nyquist period of the 5-day time series) to 64 days, most probably due to mixing events related to passing storms.

3.8 Summary and Conclusions

A study of the effects of local and remote forcing of the Chl-a variability was conducted for the SAB based on the analysis of satellite-derived products and a limited amount of in situ data.

Relatively high concentrations of Chl-a are observed on the inner and middle shelves throughout the year. North of 33^{o}N the highest nearshore Chl-a concentrations are near the capes (Romain, Fear, and Lookout), in part due to topographically enhanced wind-driven upwelling, but also due to point source coastal river discharge. South of that latitude the estuaries are marsh-dominated and the river discharges have a more diffuse effect on the nutrient loading and resulting Chl-a concentrations.

There is a connection between the NASG variability and the SAB shelf response via Gulf Stream forcing, which is the western branch of the NASG. The size and strength of the NASG, which is governed by the large-scale wind circulation and seasonal solar radiation, has an impact on the oceanographic processes of the SAB as a result of Gulf Stream onshore/offshore motion. The seasonal position of the Gulf Stream shelf slope front (GSF) was obtained using Aviso DHT and SeaWiFS Chl-a as indicators. South of 32^{o}N, the western edge of the Gulf Stream generally lies within ±15 km of the shelf break. The front is closer to the shelf break in summer and moves offshore towards the winter. Immediately north of the Charleston Bump, a region where the Gulf Stream is deflected eastward and eddy generation is very active, the seasonal location of the front is much more variable. These excursions of the Gulf Stream front have an impact on the observed surface Chl-a and the concentrations change according to which side of the front the observation is taken. East of the front the thermocline and nutricline are deeper, DHT is high and Chl-a is low. West of the front the relationship between DHT and Chl-a reverses.

Variations in the Gulf Stream transport do not affect the Chl-a variability as much as the variability of the Gulf Stream front position. Wind-driven upwelling has a strong seasonal impact in the Chl-a variability on the west side of the Florida Current, between Florida and the Bahamas, where the continental shelf is narrow with a steep slope region. There the strong and steady northward upwelling-favorable winds in summer enhance the local production and increase the Chl-a concentration by bringing new nutrients to the surface. Topographically-induced upwelling, which enhances surface Chl-a concentration, occurs in the vicinity of Cape Canaveral where the Gulf Stream flows over a bathymetry divergence region.

There is a clear cross-shelf zoning of the river discharge and the NASG size (Gulf Stream front displacement) influence on Chl-a variability. The correlation between river discharge and Chl-a is greater nearshore with decreasing influence beyond the middle shelf. The influence of the Gulf Stream forcing is greater at the shelf break with decreasing influence towards the inner shelf.

The Gulf Stream deflection by the Charleston Bump is modulated by the intensity and direction of the coastal winds. The eastward deflection is enhanced during February and November when the wind favors a southwestward flow on the SAB shelf. The deflection is much more attenuated in May when the wind reverses and favors a northeastward flow on the shelf. The evolution of the Gulf Stream eastward deflection and the formation of the Charleston Gyre were analyzed using SST, Chl-a, and surface currents. A time series analysis of dynamic height and Chl-a was conducted within the gyre domain. A highly coherent annual seasonal cycle in both DHT and Chl-a was identified throughout the period of available concurrent data (1998-2006), with the Chl-a maximum leading the DHT minimum by approximately 1 month. This seems to be a result of surface thermal forcing driving the MLD variability rather than upwelling within the gyre [*McClain and Firestone*, 1993]. Coherence was more episodic for periods less than 3 months (0.25 years), which indicate the ephemeral nature of the cold core eddy formation in the region.

SeaWiFS derived images of CDOM+detritus absorption coefficient were used to trace the riverine sources of DOM and the low salinity front on the inner and middle shelves, which are consistent with historical data. Long-term (9 years) upward trends in Chl-a were found in the middle shelf, consistent with downward trends in salinity and upward trends in river discharge.

Seasonal and episodic variations in heat flux have an impact on Chl-a variability because they drive changes in vertical mixing and consequently nutrient renewal. Time series analysis of Chl-a and surface heat flux show a strong seasonal anti-phase correlation in the SAB middle shelf.

References

Alberts, J.J., J.R. Ertel, and L. Case, Characterization of organic matter in rivers of the Southeastern United States, *Verh. Int. Ver. Theor. Angew. Limnol.*, *24*, 260-262, 1990.

Atkinson, L., The results of four oceanographic cruises in the Georgia Bight, pp. 71, Georgia Marine Science Center, Skidaway Island, 1978.

Atkinson, L., D.W. Menzel, and K.A. Bush, Oceanography of the Southeastern U. S. Continental Shelf, in *Coastal and Estuarine Sciences*, pp. 156, American Geophysical Union, Washington D. C., 1985.

Atkinson, L.P., Oceanographic Observations in the Georgia Bight: Data Report for R. V. Eastward Cruises E-13-73 (4-11 September) and E-19-73 (8-9 December 1973), pp. 156, Georgia Marine Science Center, University System of Georgia, Savannah, Georgia, 1975.

Atkinson, L.P., Oceanographic Observations in the Georgia Bight: Data Report for R. V. Eastward Cruises E-3-74 (24-30 April 1974) and E-12-74 (23-31 July 1974), pp. 124, Georgia Marine Science Center, University System of Georgia, Savannah, Georgia, 1976.

Atkinson, L.P., Models of Gulf Stream intrusions into the South Atlantic Bight shelf water, *Geophys. Res. Letters*, *7*, 583-586, 1977.

Atkinson, L.P., G.A. Paffenhofer, and W.M. Dunstan, Chemical and Biological Effect of a Gulf-Stream Intrusion Off St-Augustine, Florida, *Bulletin of Marine Science*, *28* (4), 667-679, 1978.

Bane, J.M., Initial Observations of the Subsurface Structure and Short-Term Variability of the Seaward Deflection of the Gulf-Stream Off Charleston, South-Carolina, *Journal of Geophysical Research-Oceans and Atmospheres*, *88* (NC8), 4673-4684, 1983.

Bane, J.M., Results from the Genesis of Atlantic Lows Experiment physical oceanographic studies: Introduction, *J, Geophys. Res.*, *94* (C8), 10,685, 1989.

Bane, J.M., and D.A. Brooks, Gulf-Stream Meanders Along the Continental-Margin from the Florida Straits to Cape Hatteras, *Geophysical Research Letters*, *6* (4), 280-282, 1979.

Bishop, S.S., J.A. Yoder, and G.A. Paffenhofer, Phytoplankton and Nutrient Variability Along a Cross-Shelf Transect Off Savannah, Georgia, USA, *Estuarine and Coastal Marine Science*, *11* (4), 359-368, 1980.

Blanton, J.O., J.A. Amft, D.K. Lee, and A. Riordan, Wind Stress and Heat Fluxes Observed During Winter and Spring 1986, *Journal of Geophysical Research-Oceans*, *94* (C8), 10686-10698, 1989.

Blanton, J.O., and L.P. Atkinson, Transport and Fate of River Discharge on the Continental-Shelf of the Southeastern United-States, *Journal of Geophysical Research-Oceans and Atmospheres*, *88* (NC8), 4730-4738, 1983.

Blanton, J.O., L.P. Atkinson, L.J. Pietrafesa, and T.N. Lee, The Intrusion of Gulf-Stream Water across the Continental-Shelf Due to Topographically-

Induced Upwelling, *Deep-Sea Research Part a-Oceanographic Research Papers*, *28* (4), 393-405, 1981.
Blanton, J.O., F.B. Schwing, A.H. Weber, L.J. Pietrafesa, and D.W. Hayes, Wind Stress Climatology in the South Atlantic Bight, in *Oceanography of the Southeastern United States Continental Shelf*, edited by D.W.M. L. P. Atkinson, and K. A. Bush, pp. 10-22, Washington D. C., 1985.
Boudra, D.B., R. Bleck, and F. Schott, A Numerical-Model of Instabilities in the Florida Current, *Journal of Marine Research*, *46* (4), 715-751, 1988.
Chao, S.Y., and G.S. Janowitz, Effect of a Localized Topographic Irregularity on the Flow of a Boundary Current Along the Continental-Margin, *Journal of Physical Oceanography*, *9* (5), 900-910, 1979.
Chen, C., A Modeling Study of the Episodic Cross-Frontal Water Transport over the Inner Shelf of the South Atlantic Bight, *Journal of Physical Oceanography*, *30* (7), 1722-1742, 2000.
DuMouchel, W., and F. O'Brien, Integrating a robust option into a multiple regression computing environment, in *Computing Science and Statistics: Proceedings of the 21st Symposium on the Interface*, edited by K. Berk, and L. Malone, pp. 297-301, American Statistical Association, Alexandria, VA, 1989.
Dunstan, W.M., and L.P. Atkinson, Sources of new nitrogen for the South Atlantic Bight, in *Estuarine Processes*, edited by M. Wiley, pp. 69-78, Academic Press, New York, 1976.
Garver, S.A., and D.A. Siegel, Inherent optical property inversion of ocean color spectra and its biogeochemical interpretation .1. Time series from the Sargasso Sea, *Journal of Geophysical Research-Oceans*, *102* (C8), 18607-18625, 1997.
Grinsted, A., J.C. Moore, and S. Jevrejeva, Application of the cross wavelet transform and wavelet coherence to geophysical time series, *Nonlinear Processes in Geophysics*, *11* (5-6), 561-566, 2004.
Hanson, R.B., C.Y. Robertson, J.A. Yoder, P.G. Verity, and S.S. Bishop, Nitrogen Recycling in Coastal Waters of Southeastern United-States During Summer 1986, *Journal of Marine Research*, *48* (3), 641-660, 1990.
Jacobsen, T.R., L.R. Pomeroy, and J.O. Blanton, Autotrophic and Heterotrophic Abundance and Activity Associated with a Nearshore Front Off the Georgia Coast, USA, *Estuarine Coastal and Shelf Science*, *17* (5), 509-520, 1983.
Jahnke, R., M. Richards, J. Nelson, C. Robertson, A. Rao, and D. Jahnke, Organic matter remineralization and porewater exchange rates in permeable South Atlantic Bight continental shelf sediments, *Continental Shelf Research*, *25* (12-13), 1433-1452, 2005.
Janowitz, G.S., and L.J. Pietrafesa, The effects of allongshore variation in bottom topography on a boundary current - (topographycally induced upwelling), *Cont. Shelf Res.*, *1* (2), 123-141, 1982.
Johns, W.E., and F. Schott, Meandering and Transport Variations of the Florida Current, *Journal of Physical Oceanography*, *17* (8), 1128-1147, 1987.

Kourafalou, V.H., T.N. Lee, L.Y. Oey, and J.D. Wang, The fate of river discharge on the continental shelf .2. Transport of coastal low-salinity waters under realistic wind and tidal forcing, *Journal of Geophysical Research-Oceans*, *101* (C2), 3435-3455, 1996.

Kowalczuk, P., W.J. Cooper, R.F. Whitehead, M.J. Durako, and W. Sheldon, Characterization of CDOM in an organic-rich river and surrounding coastal ocean in the South Atlantic Bight, *Aquatic Sciences*, *65* (4), 384-401, 2003.

Larsen, J.C., and T.B. Sanford, Florida Current Volume Transports from Voltage Measurements, *Science*, *227* (4684), 302-304, 1985.

Lee, T.N., and L.P. Atkinson, Low frequency current and temperature variability from Gulf Stream frontal eddies and atmospheric forcing along the U. S. outer continental shelf, *J. Geophys. Res.*, *88*, 4541-4567, 1983.

Lee, T.N., L.P. Atkinson, and R. Legeckis, Observations of a Gulf Stream frontal eddy on the Georgia continental shelf, April 1977, *Deep-Sea Research*, *28*, 347-378, 1981.

Lee, T.N., and L.J. Pietrafesa, Summer upwelling on the southeastern continental shelf of the U.S.A. during 1981, *Progress in Oceanography*, *19*, 276-312, 1987.

Lee, T.N., and E. Williams, Wind-Forced Transport Fluctuations of the Florida Current, *Journal of Physical Oceanography*, *18* (7), 937-946, 1988.

Lee, T.N., J.A. Yoder, and L.P. Atkinson, Gulf-Stream Frontal Eddy Influence on Productivity of the Southeast United-States Continental-Shelf, *Journal of Geophysical Research-Oceans*, *96* (C12), 22191-22205, 1991.

Legeckis, R.V., Satellite-Observations of the Influence of Bottom Topography on the Seaward Deflection of the Gulf-Stream Off Charleston, South-Carolina, *Journal of Physical Oceanography*, *9* (3), 483-497, 1979.

Levitus, S., and T.P. Boyer, World Ocean Atlas 1994 Volume 4: Temperature, pp. 117, NOAA, 1994.

Levitus, S., R. Burgett, and T.P. Boyer, World Ocean Atlas 1994 Volume 3: Salinity, pp. 99, NOAA, 1994.

Li, C.Y., J.R. Nelson, and J.V. Koziana, Cross-shelf passage of coastal water transport at the South Atlantic Bight observed with MODIS Ocean Color/SST, *Geophysical Research Letters*, *30* (5), 2003.

Lorenzzetti, J.A., J.D. Wang, and T.N. Lee, Summer upwelling on the southeastern continental shelf of the U.S.A. during 1981: circulation modeling, *Progress in Oceanography*, *19*, 313-327, 1987.

Maritorena, S., D.A. Siegel, and A.R. Peterson, Optimization of a semianalytical ocean color model for global-scale applications, *Applied Optics*, *41* (15), 2705-2714, 2002.

Martins, A.M., and J.L. Pelegri, CZCS chlorophyll patterns in the South Atlantic Bight during low vertical stratification conditions, *Cont. Shelf Res.*, *26*, 429-457, 2006.

McClain, C.R., Correction, *Journal of Geophysical Research-Oceans*, *90* (NC6), 2015-2018, 1985.

McClain, C.R., and L.P. Atkinson, A Note on the Charleston Gyre, *Journal of Geophysical Research-Oceans*, *90* (NC6), 1857-&, 1985.
McClain, C.R., and J. Firestone, An Investigation of Ekman Upwelling in the North-Atlantic, *Journal of Geophysical Research-Oceans*, *98* (C7), 12327-12339, 1993.
McClain, C.R., J. Ishizaka, and E.E. Hofmann, Estimation of the Processes Controlling Variability in Phytoplankton Pigment Distributions on the Southeastern United-States Continental-Shelf, *Journal of Geophysical Research-Oceans*, *95* (C11), 20213-20235, 1990.
McClain, C.R., L.J. Pietrafesa, and J.A. Yoder, Observations of Gulf-Stream Induced and Wind-Driven Upwelling in the Georgia Bight Using Ocean Color and Infrared Imagery, *Journal of Geophysical Research-Oceans*, *89* (NC3), 3705-3723, 1984.
McClain, C.R., S.R. Signorini, and J.R. Christian, Subtropical gyre variability observed by ocean-color satellites, *Deep-Sea Research Part Ii-Topical Studies in Oceanography*, *51* (1-3), 281-301, 2004.
McClain, C.R., J.A. Yoder, L.P. Atkinson, J.O. Blanton, T.N. Lee, J.J. Singer, and F. Mullerkarger, Variability of Surface Pigment Concentrations in the South-Atlantic Bight, *Journal of Geophysical Research-Oceans*, *93* (C9), 10675-10697, 1988.
McLellan, H.J., *Elements of Physical Oceanography*, 151 pp., Pergamon Press, New York, 1968.
Menzel, D.W., Ocean Processes: U. S. Southeast Continental Shelf. A summary of research conducted in the South Atlantic Bight under the auspices of the U. S. Department of Energy, pp. 112, U. S. Department of Energy, Savannah, 1993.
Miller, J.L., Fluctuations of Gulf-Stream Frontal Position between Cape-Hatteras and the Straits of Florida, *Journal of Geophysical Research-Oceans*, *99* (C3), 5057-5064, 1994.
Nelson, J.R., J.E. Eckman, C.Y. Robertson, R.L. Marinelli, and R.A. Jahnke, Benthic microalgal biomass and irradiance at the sea floor on the continental shelf of the South Atlantic Bight: Spatial and temporal variability and storm effects, *Continental Shelf Research*, *19* (4), 477-505, 1999.
Nelson, J.R., and S. Guarda, Particulate and Dissolved Spectral Absorption on the Continental-Shelf of the Southeastern United-States, *Journal of Geophysical Research-Oceans*, *100* (C5), 8715-8732, 1995.
Neumann, G., and W.J. Pierson, Jr., *Principles of Physical Oceanography*, 545 pp., Prentice Hall, Englewood Cliffs, N.J., 1966.
Oey, L.Y., A Model of Gulf-Stream Frontal Instabilities, Meanders and Eddies Along the Continental-Slope, *Journal of Physical Oceanography*, *18* (2), 211-229, 1988.
Oey, L.-Y., The Formation and Maintenance of Density Fronts on the U.S. Southeastern Continental Shelf during Winter, *Journal of Physical Oceanography*, *16* (6), 1121-1135, 1986.

Oey, L.Y., L.P. Atkinson, and J.O. Blanton, Shoreward Intrusion of Upper Gulf-Stream Water onto the United-States Southeastern Continental-Shelf, *Journal of Physical Oceanography*, *17* (12), 2318-2333, 1987.

Olson, D.B., O.B. Brown, and S.R. Emmerson, Gulf-Stream Frontal Statistics from Florida Straits to Cape Hatteras Derived from Satellite and Historical Data, *Journal of Geophysical Research-Oceans and Atmospheres*, *88* (NC8), 4569-4577, 1983.

Paffenhofer, G.A., L.P. Atkinson, J.O. Blanton, T.N. Lee, L.R. Pomeroy, and J.A. Yoder, Summer Upwelling on the Southeastern Continental-Shelf of the USA During 1981 - Summary and Conclusions, *Progress in Oceanography*, *19* (3-4), 437-441, 1987.

Pietrafesa, L.J., J.O. Blanton, J.D. Wang, V.H. Kourafalou, and T.N. Lee, The Tidal Regime in the South Atlantic Bight, in *Oceanography of the Southeastern United States Continental Shelf*, edited by D.W.M. L. P. Atkinson, and K. A. Bush, pp. 63-76, American Geophysical Union, Washington D. C., 1985.

Pomeroy, L.R., L.P. Atkinson, J.O. Blanton, W.B. Campbell, T.R. Jacobsen, K.H. Kerrick, and A.M. Wood, Microbial Distribution and Abundance in Response to Physical and Biological Processes on the Continental-Shelf of Southeastern USA, *Continental Shelf Research*, *2* (1), 1-20, 1983.

Rio, M.-H., and F. Hernandez, A mean dynamic topography computed over the world ocean from altimetry, in situ measurements, and a geoid model, *J, Geophys. Res.*, *109* (C12032), 2004.

Rio, M.-H., P. Schaeffer, J.-M. Lemoine, and F. Hernandez, Estimation of the ocean mean dynamic topography through the combination of altimetric data, in-situ measurements and GRACE geoid: From global to regional studies, in *GOCINA International Workshop*, Luxembourg, 2005.

Signorini, S.R., and C.R. McClain, Report on Ocean Color and Carbon Study for the South Atlantic Bight and Chesapeake Bay Regions, pp. 45, NASA Goddard Space Flight Center, Greenbelt, 2005.

Singer, J.J., L. Atkinson, J.O. Blanton, and J.A. Yoder, Cape Romain and the Charleston Bump: historical and recent hydrographic observations, *J, Geophys. Res.*, *88* (C8), 4685-4697, 1983.

Steinberg, D.K., C.A. Carlson, N.R. Bates, R.J. Johnson, A.F. Michaels, and A.H. Knap, Overview of the US JGOFS Bermuda Atlantic Time-series Study (BATS): a decade-scale look at ocean biology and biogeochemistry, *Deep-Sea Research Part Ii-Topical Studies in Oceanography*, *48* (8-9), 1405-1447, 2001.

Yoder, J.A., *Environmental control of phytoplankton production on the Southeastern U.S. Continental Shelf, in Oceanography of the southeastern U.S. continental shelf, Coastal and Estuarine Sci.*, American Geophysical Union, Washington, D. C., 1985.

Yoder, J.A., L.P. Atkinson, S.S. Bishop, J.O. Blanton, T.N. Lee, and L.J. Pietrafesa, Phytoplankton Dynamics within Gulf-Stream Intrusions on the Southeastern United-States Continental-Shelf During Summer 1981, *Continental Shelf Research*, *4* (6), 611-635, 1985.

Yoder, J.A., L.P. Atkinson, S.S. Bishop, E.E. Hofmann, and T.N. Lee, Effect of upwelling on phytoplankton productivity on the outer southeastern U.S. continental shelf, *Cont. Shelf Res.*, *1*, 385-404, 1983.

Yoder, J.A., L.P. Atkinson, J.O. Blanton, D.R. Deibel, D.W. Menzel, and G.A. Paffenhofer, Plankton Productivity and the Distribution of Fishes on the Southeastern United-States Continental-Shelf, *Science*, *214* (4518), 352-353, 1981a.

Yoder, J.A., L.P. Atkinson, T.N. Lee, H.H. Kim, and C.R. McClain, Role of Gulf-Stream Frontal Eddies in Forming Phytoplankton Patches on the Outer Southeastern Shelf, *Limnology and Oceanography*, *26* (6), 1103-1110, 1981b.

Yoder, J.A., C.R. McClain, J.O. Blanton, and L.Y. Oey, Spatial Scales in Czcs-Chlorophyll Imagery of the Southeastern United-States Continental-Shelf, *Limnology and Oceanography*, *32* (4), 929-941, 1987.

Yoder, J.A., J.E. O'Reilly, A.H. Barnard, T.S. Moore, and C.M. Ruhsam, Variability in coastal zone color scanner (CZCS) Chlorophyll imagery of ocean margin waters off the US East Coast, *Continental Shelf Research*, *21* (11-12), 1191-1218, 2001.

Zantopp, R.J., K.D. Leaman, and T.N. Lee, Florida Current Meanders - a Close Look in June July 1984, *Journal of Physical Oceanography*, *17* (5), 584-595, 1987.

REPORT DOCUMENTATION PAGE

Form Approved
OMB No. 0704-0188

1. REPORT DATE *(DD-MM-YYYY)*	2. REPORT TYPE	3. DATES COVERED *(From - To)*
29-12-2006	Technical Memorandum	

4. TITLE AND SUBTITLE

Remote Versus Local Forcing of Chlorophyll Variability in the South Atlantic Bight

5a. CONTRACT NUMBER

5b. GRANT NUMBER

5c. PROGRAM ELEMENT NUMBER

6. AUTHOR(S)

Sergio Signorini and Charles McClain

5d. PROJECT NUMBER

5e. TASK NUMBER

5f. WORK UNIT NUMBER

7. PERFORMING ORGANIZATION NAME(S) AND ADDRESS(ES)

National Aeronautics and Space Administration
Washington, DC 20546-0001

8. PERFORMING ORGANIZATION REPORT NUMBER

2007-00229-0

9. SPONSORING/MONITORING AGENCY NAME(S) AND ADDRESS(ES)

National Aeronautics and Space Administration
Washington, DC 20546-0001

10. SPONSORING/MONITOR'S ACRONYM(S)

11. SPONSORING/MONITORING REPORT NUMBER

TM-2006-214145

12. DISTRIBUTION/AVAILABILITY STATEMENT

Unclassified-Unlimited, Subject Category: 48
Report available from the NASA Center for Aerospace Information, 7115 Standard Drive, Hanover, MD 21076. (301)621-0390

13. SUPPLEMENTARY NOTES

S. Signorini: Science Applications International Corp., Beltsville, MD

14. ABSTRACT

This TM documents results of analyses addressing the local versus remote forcing of chlorophyll variability on the shelf and slope regions of the South Atlantic Bight (SAB) based on satellite-derived products and a limited amount of in situ data. This study is part of a larger multi-disciplinary, multi-institutional effort to study the Eastern U.S. Continental Shelf carbon budget (U.S. Eastern Continental Shelf Carbon Budget: Modeling, Data Assimiliation, and Analysis, U.S. ECoS), a project funded by the NASA Earth System Enterprise Interdisciplinary Science Program that started in the summer of 2004.

15. SUBJECT TERMS

Ocean Color, South Atlantic Bight, SeaWiFS, Chesapeake Bay, Carbon Budget

16. SECURITY CLASSIFICATION OF:			17. LIMITATION OF ABSTRACT	18. NUMBER OF PAGES	19b. NAME OF RESPONSIBLE PERSON
a. REPORT	b. ABSTRACT	c. THIS PAGE			Charles R. McClain
Unclassified	Unclassified	Unclassified	Unclassified	63	19b. TELEPHONE NUMBER *(Include area code)* (301) 286-5377